Technische Universität Graz

Institut für Chemische Verfahrenstechnik und Umwelttechnik

Influence of biogas trace compounds on hydrogen production via Chemical Looping

Dalvai Ragnoli Martin

Graz, Februar 2019

► www.icvt.tugraz.at

Chemical Engineering and Environmental Technology

Dalvai Ragnoli Martin, BSc

Influence of biogas trace compounds on hydrogen production via Chemical Looping

Masterarbeit

zur Erlangung des akademischen Grades eines

Diplom-Ingenieur

Verfahrenstechnik

eingereicht an der

Technischen Universität Graz

BetreuerIn:

Assoc.Prof. Dipl.-Ing. Dr.techn. Viktor Hacker

Institut für Chemische Verfahrenstechnik und Umwelttechnik

Graz, 08. February 2019

Acknowledgements

At this point I would like to thank all to people who supported me during my studies and made these last couple of years so special and joyful.

First of all, I want to express my gratitude to Assoc. Prof. Dipl.-Ing. Dr.techn. Viktor Hacker for giving me the opportunity to generate this master thesis.

A special thanks goes also to the whole fuel cell system group for an inspiring and dynamic working atmosphere. Here I would like to single out Dipl.-Ing. Sebastian Bock for supervising my work, being always helpful with some problem-solving pieces of advice and for the assistance during this whole period.

Furthermore I would like thank all the friends and colleges I met over all these years. I consider myself really happy to have so many special people in my life. Thanks for all the laughs, diversions and distractions from university.

Last but not least I want to thank my family, especially my mother Ruth, to render my whole education possible and for all the support and care I received my entire life.

All of you are the reason I managed to reach this point and to become the person I am today.

Deutsche Fassung:
Beschluss der Curricula-Kommission für Bachelor-, Master- und Diplomstudien vom 10.11.2008
Genehmigung des Senates am 1.12.2008

EIDESSTATTLICHE ERKLÄRUNG

Ich erkläre an Eides statt, dass ich die vorliegende Arbeit selbstständig verfasst, andere als die angegebenen Quellen/Hilfsmittel nicht benutzt, und die den benutzten Quellen wörtlich und inhaltlich entnommenen Stellen als solche kenntlich gemacht habe.

Graz, am …… ……
(Unterschrift)

Englische Fassung:

STATUTORY DECLARATION

I declare that I have authored this thesis independently, that I have not used other than the declared sources / resources, and that I have explicitly marked all material which has been quoted either literally or by content from the used sources.

Graz, …… ……
date (signature)

Kurzfassung

Der Reformer Eisen Dampf Prozess (Reformer Steam Iron Cycle, RESC) bietet die Möglichkeit Wasserstoff bei Bedarf dezentral aus erneuerbaren Ressourcen zu produzieren. Das Verfahren basiert auf der zyklischen Reduktion und Oxidation einer metallischen Kontaktmasse. In einem Festbettreaktor wird das eingesetzte Metalloxid durch ein Synthesegas reduziert. Im nachfolgenden Prozessschritt oxidiert Wasserdampf die Kontaktmasse wobei Wasserstoff entsteht. Die, in Form von reduziertem Metalloxid, gespeicherte chemische Energie kann im RESC sicher und verlustfrei gespeichert und bei Bedarf als Hochdruckwasserstoff mit sehr hoher Reinheit freigesetzt werden.

Im Rahmen der Diplomarbeit wurde der Einsatz von vergaster Biomasse und von Biogas zur Wasserstofferzeugung untersucht. Es wurden Modellkomponenten, welche charakteristische Verunreinigungen von Biogas repräsentieren, dem Reduktionsgas zu dosiert und die Auswirkungen auf die Produktgasreinheit evaluiert. Methan und Propan wurden stellvertretend für azyklische Kohlenwasserstoffe, Ethanol für organische Alkohole und Toluol repräsentativ für Aromaten verwendet.

Kohlenwasserstoffe, Kohlenmonoxid und Kohlendioxid wurden als Verunreinigungen im produzierten Wasserstoff detektiert. Das Auftreten von Kohlenwasserstoffen wurde auf das unzureichende Spülen des Reaktors nach der Reduktionsphase zurückgeführt. Längeres Spülen sowie die Evakuierung des Reaktors hatten eine deutliche Senkung der Kohlenwasserstoffverunreinigungen im Produktgas zur Folge. Kohlenmonoxid und Kohlendioxid bilden sich durch die Oxidation von elementarem Kohlenstoff, der sich während der Reduktionsphase ablagert. Eine Akkumulation von Kohlenstoffablagerungen durch gasförmige Modellkomponenten wurde nicht beobachtet. Die Beimengung von Ethanol und Toluol hatte eine deutliche Akkumulation von Kohlenstoff und eine Verschlechterung der Wasserstoffqualität zur Folge. Die Oxidation mit Luft als Aufreinigungsschritt verhindert die Akkumulation von Kohlenstoff und gewährleistet eine konstante Wasserstoffqualität.

Abstract

The Reformer Steam Iron Cycle (RESC) is suitable for decentralised medium scale hydrogen production from a broad range of renewables. An iron based oxygen carrier is cyclically reduced by syngas and reoxidised by steam. During the oxidation phase the oxygen atoms of the steam bond within the metal lattice and hydrogen is released.

The use of various syngases from renewable energy carriers was investigated. Model compounds, which represent typical trace gases from biogas or gasified biomass, were fed with the reductive gas in the reaction system. Methane and propane are selected as model compounds for acyclic hydrocarbons, ethanol is to be substitutional for organic alcohols and toluene to represent cyclic hydrocarbons.

Hydrogen production during oxidation phase behaved like a 'bell shape curve'. Carbon oxides as well as hydrocarbons were detected during oxidation. Hydrocarbons were attributed to incomplete reactor purging as they are not expected to form under given conditions. Carbon oxide impurities were attributed to reoxidation of elemental carbon depositions formed during reduction. Reactor evacuation and extended reactor purging had positive effects on the quality of the produced hydrogen. An increase of impurities with ongoing number of cycles related to carbon accumulation was not observed for gaseous trace compounds. The addition of ethanol and toluene to the reductive gas did result in a progressive decrease of the hydrogen quality as carbon was accumulated with ongoing number of cycles. Intermediate air oxidation did prevent accumulation of carbon and allowed a constant hydrogen quality.

Table of Content

1 Introduction

Global energy demand is constantly increasing. Even assuming that we will increase the energy-efficiency, analyses forecast that in 2050 our energy demand will be 30-40% higher than today's. [1]

Up to now, we depend on fossils resources to produce most of our energy, whereby carbon dioxide and other greenhouse gases are released. Environmental impacts such as global warming and climate change result as a direct consequence of the elevated amount of those greenhouse gases in the atmosphere. Furthermore, fossil resources are finite and limited in availability. To cover future energy demand and to reduce harmful emissions at the same time, a transition towards a more sustainable energy production is needed.

For the decarbonisation of energy various technologies will be needed in tandem. The transition from fossil-based to renewable energy will pose a big challenge for politics, society and technology in equal measure and the complexity of future energy systems will increase. The solution partly lies in the use of renewable energy, which can provide net-zero carbon energy production. A drawback of renewables such as wind and solar power is that they cannot be produced continuously, as the primary energy source is available only temporarily. Therefore, they require large-scale energy storage to compensate the production fluctuations. [2]

The energy carrier hydrogen offers a long term solution and contributes to the reduction of global and local emissions. Hydrogen is versatile and has a wide range of potential use, including fuel for transportation and as energy storage. It can be produced in times of surplus energy via electrolysis, stored and reconverted into electricity by a carbon-free reaction emitting only water.

Hydrogen with a share of approximately 90% is the most common element in the universe. However, due to its low weight and high reactivity, hydrogen is rarely present in its gaseous form on earth and therefore it has to be gained from a primary energy source. Hydrogen is almost exclusively present in bounded form, as water, in minerals, hydrocarbons (HC) or in organisms. [3]

Although only water is produced when hydrogen is combusted, its environmental impact is directly related to the primary energy source used for its production as secondary energy carrier. Hydrogen is only as clean as the primary energy source used for its production.

1.1 Properties of Hydrogen

Consisting only of one proton and one electron hydrogen is the lightest element. At ambient conditions, two hydrogen atoms form a stable diatomic molecule, which is a colourless, odourless, tasteless and nontoxic gas. [4]

Hydrogen has the smallest gas density and the highest diffusivity. The low density results in a very high energy density by mass compared to other fuels (see Table 1-1). On the other hand, the volumetric energy density is very low (H_2: 0.0107 MJ L^{-1} at ambient pressure versus petrol: 34.2 MJ L^{-1}). For transport and storage a high energy density is of major importance. Therefore, hydrogen has to be pressurized or liquefied in order to store more energy per volume. Approximately 7% of the hydrogen energy content is necessary to compress hydrogen from 1 to 200 bar [5]. Although some of that energy could be recovered during expansion, it is clear that this highly energy consuming processes significantly lowers the overall efficiency. [4] [6]

Table 1-1: Gravimetric and volumetric energy density of common fuels [6]

Fuel	**Energy density by Mass** **MJ kg^{-1}**	**Energy Density by Volume** **MJ L^{-1}**
Hydrogen (liquid)	143	10.1
Hydrogen (at 700 bar)	143	5.6
Hydrogen (ambient pressure)	143	0.0107
Methane (ambient pressure)	55.6	0.0348
Natural gas (liquid)	53.6	22.2
Natural Gas (at 250 bar)	53.6	9
Natural gas (ambient pressure)	53.6	0.0364
LPG propane	49.6	25.3
LPG butane	49.1	27.7
Petrol	46.4	34.2
Biodiesel oil	42.2	33
Diesel	45.4	34.6

1.2 Hydrogen utilization

Hydrogen is widely accepted as a promising energy carrier to replace fossil fuels. Nevertheless, today's hydrogen consumption does not reflect this scenario. The chemical and petrochemical industries are the world largest hydrogen consumers with an estimated global consumption of approximately 8 EJ per year [7]. It is reported that 2% of the global primary energy demand is used for hydrogen production. [8] Figure 1-1 illustrates the share of hydrogen consumption: it is used for the production of chemical intermediates like ammonia (51%) and methanol

(10%), but also for other chemicals like polymers or fatty acids. Approx. 31% is used for hydrogen refining by the petrochemical industry. Impurities are removed in hydrotreating operations and hydrocracking operations, including the saturation of hydrocarbons and the upgrade of heavy oil fractions to lighter products [9] [10]. Hydrogen also finds application in other industries like metallurgic processing, welding and annealing of metals, in electronic industry and in glass production. Automotive industry uses hydrogen as fuel for fuel cell driven vehicles and H_2 is used as fuel in space shuttles. [7]

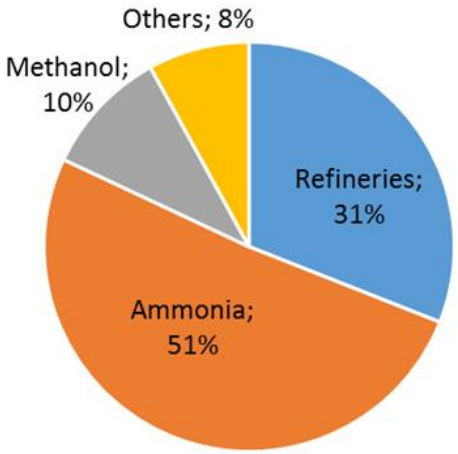

Figure 1-1: Global consumption of hydrogen [7]

1.2.1 Fuel cells for mobility applications

Transport is identified as the second largest sector to emit CO_2, being responsible for 23% of total global emissions. Since demand for transportation is unlikely to decrease in the near future, emissions related to this sector have to be lowered significantly. Hydrogen is one promising solution to replace fossil fuels as energy carrier. [11]

In 2014 Toyota reached a milestone by releasing the Toyota MIRAI as the first fuel cell electric vehicle (FCEV) available for consumers. In FCEVs electricity is supplied from a fuel cell stack. The fuel cell is an electrochemical cell that produces electricity by converting the chemical energy of a fuel, e.g. hydrogen, through electrochemical reactions. It consists of two electrodes, an electrolyte, a separator and an external electrical circuit. Hydrogen is supplied to the negative electrode, the anode, and chemically oxidized. The products from this reaction are electrons and H^+ cations (Equation (1-1)). Latter ones are transported through the electrolyte to the positively charged cathode where they are reduced (Equation (1-2)). Oxygen from the air serves as oxidizing agent in most cases. This process can be considered as environmental friendly, since only water vapour and heat are emitted (Equation (1-3)). [12] [13]

Anode: $$H_2 \rightarrow 2\,H^+ + 2\,e^-$$ (1-1)

Cathode: $$2\,H^+ + \frac{1}{2}O_2 + 2\,e^- \rightarrow H_2O$$ (1-2)

Total: $$H_2(g) + \frac{1}{2}O_2\,(g) \rightarrow H_2O(l) \qquad \Delta\mathrm{H} = 286\,\frac{\mathrm{kJ}}{\mathrm{mol}}$$ (1-3)

To ensure a long lifetime of the FC very pure hydrogen fuel is required. Impurities cause degradations of the cell and even small amounts can result in a high voltage loss. Carbon monoxide in the hydrogen fuel is poisoning the catalyst by adsorbing and bounding on the platinum surface. Carbon dioxide may react to carbon monoxide when the water gas-shift reaction is reversed at high potentials or by catalytic reduction at the platinum surface. Sulphuric compounds such as hydrogen sulphide also tend to poison the catalyst, while ammonia, which can be formed within the fuel cell if nitrogen is present, blocks proton exchange in the membrane of the fuel cell. [14] Table 1-2 shows the hydrogen purity requirements for different applications.

Table 1-2: Hydrogen purity requirements for various hydrogen users in the energy and transport sector [11]

Application	**H_2 purity (min) / %**	**Impurity limits (max) / ppm**
Refining	95	S: low levels
Ammonia	23 -25	CO_2, CO, H_2O and S: low levels
PEFC (for automotive purposes)	99.97	H_2O:5, HC:2, O_2:5, He:300, N_2+Ar:100; CO_2:2, CO:0.2, S:0.004, NH_3:0.1
PEFC (for stationary purposes)	Cat. 1 :50 Cat. 2: 50 Cat. 3: 99.9	HC:10, O_2:200, He+N_2+Ar:50%; CO:10, S:0.004 HC:2, O_2:200, He+N_2+Ar:50%; CO:10, S:0.004 HC:2, O_2:500, He+N_2+Ar:0.1%; CO:2, S:0.004
Gas Turbines	Low	Limited amount of Na, K, V and S
Industrial fuel	99.90	H_2O: NC, HC: NC, O_2:100, N_2:400, S:10

NC = no to be condensed, HC = hydrocarbons on methane basis

1.3 Challenges for a Hydrogen based economy

Because of a pollutant free combustion, hydrogen will play a crucial role in mobility applications, to drive stationary power generation and as energy storage in the near future. To fulfil high expectations and become a suitable renewable secondary energy carrier hydrogen has to be produced in high quantities at low production costs and with low greenhouse gas emissions. In addition, the stringent purity requirements for all different applications have to be met. [3]

The main challenges for fully developed hydrogen driven transport system are improvements in hydrogen storage and distribution, the current status is not acceptable technically and economically. [6][9] Decentralised safe and user-friendly refilling stations are required. Therefore, hydrogen must be produced on site or efficiently transported. [5] In long-term, a shift towards a sustainable hydrogen based economy will additionally face the challenge to outperform inexpensive production from fossils.

Centralized hydrogen production in large-scale plants as performed today allows hydrogen production at high efficiencies. Nevertheless, an infrastructure is required to deliver the hydrogen to the decentralised consumers. Transportation by pipelines, trucks or rail transportation requires high investment costs for pipeline and container material resistant to hydrogen embrittlement. The need of compressing hydrogen additionally lowers the transportation efficiency. On the other hand, decentralised production potentially has higher production costs and lower efficiencies. [9]

2 State of the Art Hydrogen Production and novel technologies

As hydrogen does not appear as free molecule on earth in high quantity, it has to be gained from hydrogen containing matter as water or hydrocarbons in form of fossil resources or biomass. Either way it is an energy consuming process and energy in form of electricity, heat or radiation/light has to be supplied. [2] Ambitions to produce hydrogen through an economical and environmental sustainable path are key objectives for future supply. [15]

2.1 Current situation

As society tends to shift to a fossil fuel - free economy also hydrogen as sustainable energy carrier has to be produced in a CO_2 neutral way. Crucial for the lifecycle greenhouse gas emissions of hydrogen is the primary energy source used for its production.

Today 96% of the hydrogen is produced from fossil fuels by thermochemical processes. Currently most hydrogen is produced from natural gas (48%), oil refining (30%) and coal gasification (18%). Only 4% is electrolytic hydrogen produced electrochemically. [3] [16]

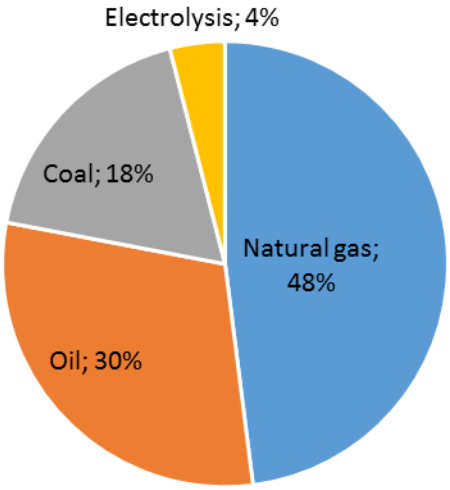

Figure 2-1: Sources of hydrogen [16]

An alternative environmental friendly way to produce renewable H_2 is the use of biomass as feedstock material, especially if organic waste is used. Biomass can be converted into a gaseous intermediate, which can be further used for hydrogen production. Main conversion technologies for solid biomass are gasification and pyrolysis. Liquids, like effluents from pulp and paper industry, manure slurry or wastewater, can be used for hydrogen production by microbial biomass conversion. Hereby microbes break down organic matter in fermentation processes to produce hydrogen. [8] [22]

Novel technologies, which are still in early stages of research, use water in combination with sunlight to produce hydrogen. Photo-electrochemical water splitting technologies use the conductivity of semiconductor materials to convert radiation energy into chemical energy by

dissociating water molecules into hydrogen and oxygen. In photo-biological processes micro-organisms, such as green algae or bacteria, are used. Some of the major challenges related to these technologies are the low hydrogen conversion rate and the poisoning of hydrogen by oxygen as by-product. [22] Furthermore, a slow production rate caused by low mass transfer rates and slow kinetics are a great economical drawback for biological reactors. [23]

2.2 Hydrogen production from hydrocarbons

Technologies for hydrogen production from fossils are fully developed, technically mature, offer high efficiencies an in addition the feedstock is available at low costs. [3] Steam reforming is performed based on a wide range of hydrocarbons, nevertheless, steam methane reforming (SMR) is the most applied and least expensive. [9]

In SMR, methane and steam react to hydrogen and carbon monoxide typically on a nickel based catalyst (Equation (2-1)). The reaction is highly endothermic and equilibrium limited. Operating conditions are temperatures between 500-1000°C and pressures greater than 20 bar. High conversion towards H_2 is favoured at high temperatures, low pressure and high S/C ratio. From an energy efficiency view, a low S/C ratio is preferred as evaporation is an energy intensive process. Process parameters are further constrained by risk of carbon formation on the catalyst bed. By using S/C ratios of 2.5 to 3 conventional plants achieve thermal efficiencies up to 85%. [3]

During partial oxidation (POX), a fossil feedstock is burned with substoichometric oxygen to carbon ratio (O/C). By this method, a variety of heavy hydrocarbons like coal or residual oil can be processed. The reaction is exothermic, wherefore no external heating is required. Equation (2-2) shows the general reaction mechanism for the POX of hydrocarbons. [3]

A technology combining steam reforming and POX is autothermal reforming. By incorporating both mechanisms in one reactor unit an overall reaction enthalpy close to zero can be obtained. Heat for the endothermic reforming step is provided by the POX zone. [3]

The product gas of reforming, partial oxidation or gasification consist of CO and H_2. To increase the hydrogen yield the gas is further reacted with steam to produce CO_2 and additional hydrogen. In the water gas shift (WGS) reaction (Equation (2-3) the gas composition is shifted towards H_2 and CO_2 in the expense of CO and water. [11]

$$CH_4 + H_2O \leftrightarrow CO + 3H_2 \qquad \Delta H = 206.2 \frac{kJ}{mol} \qquad (2\text{-}1)$$

$$C_mH_n + \frac{1}{2}O_2 \rightarrow m\,CO + \frac{1}{2}n\,H_2 \qquad \Delta H \leq 0 \frac{kJ}{mol} \qquad (2\text{-}2)$$

$$CO + H_2O \leftrightarrow H_2 + CO_2 \qquad \Delta H = -41.2 \frac{kJ}{mol} \qquad (2\text{-}3)$$

2.3 Hydrogen from Biomass

Biomass is the only sustainable carbon containing resource and a strategic primary energy source for renewable energy and commodity chemicals. Biogas and Biosyngas are expected to be key intermediates for renewable fuels and chemicals produced from biomass [10]. As industrial interest in biomass utilisation increases there is a variety of different conversion technologies. At industrial scale none seems to emerge. Instead it is more likely that a range of advanced technologies will contribute to an extended use of biomass residues and organic waste. [17]

2.3.1.1 Gasification of Biomass

Gasification is a key conversion technology when using biomass for energy production, as fuel replacement or to gain chemical valuable compounds. The gasification process consists of a complete thermal breakdown of a feedstock at high temperatures using oxygen, air, steam or mixtures of these as gasifying agents. The products are a combustible gas, volatiles, chars and ash. The gasification process, reactor configuration, gasification agent and most off all the gasification temperature influence the composition of the syngas as the main product. [10] [17]

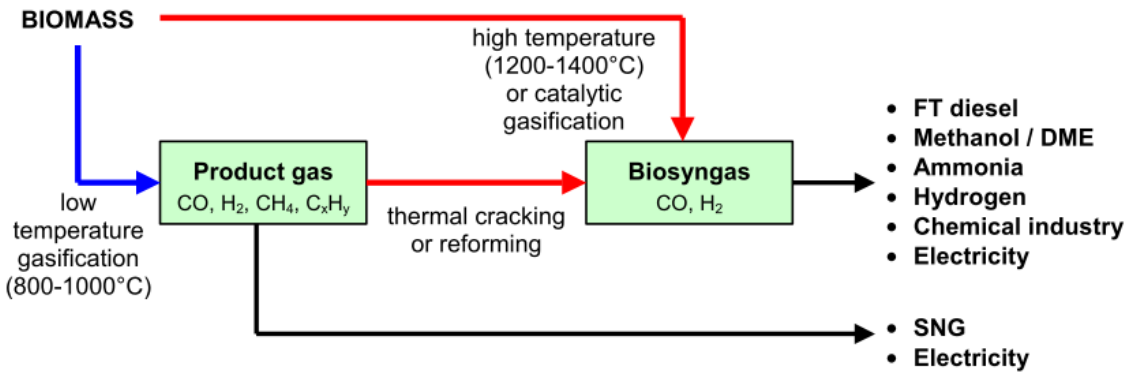

Figure 2-2: Gasification routes for biomass [10]

Since at lower gasification temperatures (100-800°C) not all biomass is completely converted, the product gas still contains methane, higher hydrocarbons or tars in form of aromatic compounds like benzene and toluene. Syngas produced at temperatures higher than 1200°C is chemically similar to syngas from fossil resources. Typically, the gaseous fraction from steam gasification is composed of 30-50 vol% of H_2, 25-40 vol% of CO, 8-20 vol% of CO_2 and 6-15 vol% of CH_4. Therefore, syngas from biomass gasification can be seen as possible source to replace its fossil derived counterpart. [10] [18]

2.3.1.2 Fermentation of Biomass

Biogas is formed by biological anaerobic degradation of organic material. It is produced from various sources intentionally or by natural decomposition and can originate e.g. from landfills,

wastewater treatment plants and waste digesters. Typically, methane and carbon dioxide as well as low amounts of steam, oxygen and nitrogen are the major components of biogas. However, biogas has a complex gas matrix containing also a large number of different trace components. Although the amount of those trace components is low compared to bulk gases, they exert a disproportionate impact on the utilisation. They affect process feasibility and contribute to material corrosion, impose health risks, negatively influence exhaust gas quality and have a negative environmental impact contributing on stratospheric ozone depletion and the greenhouse effect. [19]

A significant influence on the trace components in biogas is attributed to the feedstock material. In addition, different biomass feed (heterogeneous waste, agricultural waste, sludge's, sewage etc.), production methods (digesters, landfill etc.) and process parameters (moisture, temperature, pH etc.) on top of seasonal fluctuations and influences of the age and the state of degradation of the decomposed material make an overall biogas specification difficult to assess. Therefore, more than 200 compounds can be detected in biogas samples and about 10 chemical families are reported. Among those are saturated and unsaturated hydrocarbons, aromatic hydrocarbons, terpenes, oxygen-organic compounds (e.g. ketones, esters, furans, aldehydes, and alcohols), sulphur-and nitrogen- organic compounds, silicon compounds and halogenated compounds. [20]

Despite of all differences in the gas composition, the dry biogas matrix can be divided into incondensable gases (main gases such as CH_4, CO_2 and N_2), inorganic compounds (H_2S, NH_3) and volatile organic compounds (VOCs). [2]

If biogas is combusted in gas engines or in turbines impurities causing material corrosion, need to be removed. Sulphur is present in all biological materials. Most of the sulphur in biogas is present as hydrogen sulphide, originating from anaerobic sulphide reducing microbes. In addition, varying concentrations of carbonyl sulphide (COS), mercaptans (thiols) and disulphides are found in biogases. Siloxanes are linear or cyclic organic silicon compounds. The most common siloxanes present in biogas are L2-L5 and D3-D6 siloxanes. Linear compounds are designated with the letter L and cyclic compounds with the letter D. The number following the letter refers to the quantity of siloxanes in the molecule. Siloxanes are widely used in industry as waxes detergents or anti-foam agents and in consumer hygiene products such as shampoos and cosmetics. The use of siloxanes is continuously increasing, having the drawback that if burned, they form hard abrasive silicon oxides which damage the equipment. [21]

Halogens are widely used in the chemical industry and reach problematic levels mainly in chemical industrial landfills. The halogen compounds are directly released from the waste. During combustion the molecules break down and the halogens form acidic and corrosive hydrogen halides in an aqueous solution. [3]

2.4 Hydrogen production from water

Technologies, which produce hydrogen directly from water, offer an interesting pathway since they often result in a low - to zero net carbon emission.

In Power-to-Hydrogen (PtH_2) concepts hydrogen is used as an intermediate energy storage. The concept includes power generation from renewables, electrolysis and centralised or decentralised hydrogen storage. The use of electricity from renewable sources results in a net-zero greenhouse gas emission. Due to locally and temporarily fluctuating availability of renewables an efficient energy storage has crucial importance for a shift towards a renewable energy economy. A solution is to produce hydrogen as intermediate energy storage in times of surplus electricity via electrolysis. By reconversion to electricity in fuel cells, the gap between availability and demand of energy can be bridged. [3]

Electrolysis is an electrochemical technology where water is split into hydrogen and oxygen using direct current. The electrolyser consists of two electrodes, an anode and a cathode which are separated by an ion conductive electrolyte. In an acidic electrolyser, oxygen and hydrogen ions are generated at the anode side of the reaction (Equation (2-4)). The hydrogen ions migrate to the cathode side of the electrolytic cell where they recombine with electrons from an external electric circuit (Equation (2-5)).

Anodic reaction:
$$H_2O \leftrightarrow \frac{1}{2}O_2 + 2\,H^+ + 2e^- \qquad (2\text{-}4)$$

Cathodic reaction:
$$2H^+ + 2e^- \rightarrow H_2 \qquad (2\text{-}5)$$

Overall reaction:
$$H_2O \rightarrow H_2 + \frac{1}{2}O_2 \qquad (2\text{-}6)$$

Costs of hydrogen produced by electrolysis directly depends on electricity costs. Therefore the PtH_2 concept is only cost-effective if electricity cannot be directly used [2].

2.5 Hydrogen Upgrade technologies

Purification techniques include catalytic processes, absorption, cryogenic separation, adsorption and membrane separation techniques.

Adsorption is a physical separation technique where the different affinity of the gaseous compounds to certain materials is used to separate gas streams. Through this phenomenon certain molecules adsorb on the surface of the adsorbents while others are not or less affected. By using various layers of different adsorbents all different types of impurities are adsorbed while hydrogen has only limited interaction with the solid material. Most common adsorbents in hydrogen purification are silica gel, alumina, activated carbon and zeolite. [11] As new adsorbent material also Metal-Organic- Frameworks (MOF's) are studied. Depending on synthesis

method and post-treatment, those materials can have a very high inner surface and high performance especially for CO_2 capture. [24]

For the purpose of hydrogen purification most commonly pressure swing adsorption (PSA) is used. A semi continuous process including several time-shifted columns yields a high purity hydrogen stream, where purities up to 99.9999 mol% of hydrogen can be achieved. Other existing adsorption processes are temperature swing adsorption (TSA), electric swing adsorption (ESA) or vacuum swing adsorption (VSA).

Cryogenic separation processes are used to separate gas streams based on the different boiling points of their chemical components. By cooling the gas mixture to cryogenic temperatures, contaminant gases are condensed while hydrogen remains in gas phase due to the very low boiling point (-252.85°C [9]) [11].

In membrane reactors hydrogen production by steam reforming and product purification can be combined in one single device. A membrane inside of the reactor acts as a barrier. Hydrogen can permeate this barrier, while other molecules are hindered. This results in a shift of the thermodynamic equilibrium towards the product side allowing to overcome conversion rates of an equivalent conventional reactor. For hydrogen separation/purification composite membranes consisting of a porous support material coated with an expensive dense metallic palladium layer are used. [3] [25]

3 Chemical looping for hydrogen production

With high potential to reduce greenhouse gas emissions chemical looping technology recently experienced a boost of interest in research. Generally, a solid oxygen carrier (OC) completes a cyclic loop of two or more sub-reactions in a reaction-regeneration cycle. [26]

Chemical Looping Combustion (CLC) uses that principle to avoid direct contact between fuel and air in a combustion reaction by using two separate reactors or reactor sections: an air reactor (AR) and a fuel reactor (FR). Fuel is burned in the FR, where the oxygen for the combustion is supplied by a metal oxide which is thereby reduced. To regenerate the depleted oxygen the reduced metal is reoxidized with air in the AR. With respect to Hess' law, that states, that the enthalpy of a chemical process is independent from the reaction path, total heat production in the CLC remains the same as in a conventional combustion [27]. The main advantage of the CLC process is the inherent separation of the combustion products CO_2 and steam from the flue gases of the oxidation. After steam is condensed, almost pure CO_2 is obtained for storage [28]. Additionally, no NO_x is formed as nitrogen is not present during combustion. Figure 3-1 shows process scheme for the CLC process.

As reactor configuration fixed bed reactors as well as fluidized bed reactors are reported. By switching operation gases, the fixed bed reactor design is operated in batch mode. The system is characterised by a low degree of complexity and no moving parts. In the fluidized bed reactor system the oxygen carrier is circulated between two reactors, thus enabling a continuous operation mode. [26][29]

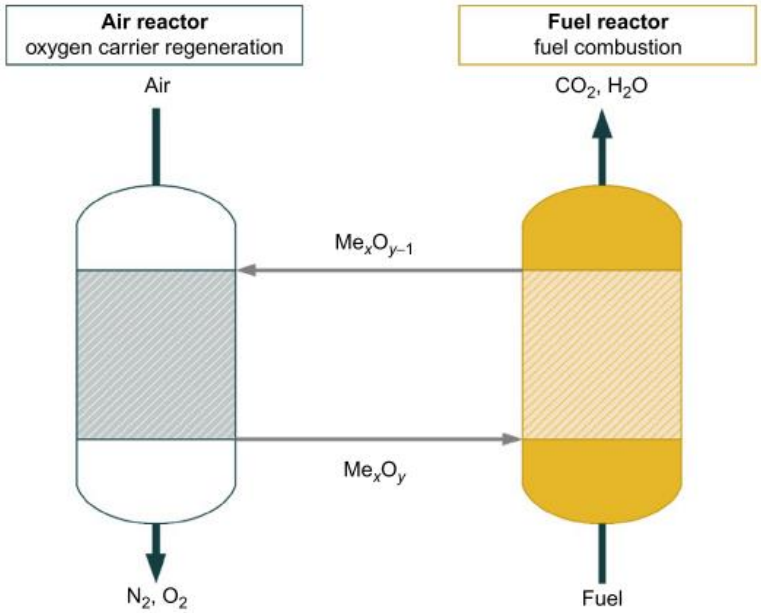

Figure 3-1: Schematic working principle of the CLC process [3]

When the regeneration of the oxygen carrier is performed with steam instead of air as oxidizing agent, hydrogen can be produced. This method is referred as Chemical Looping Hydrogen (CLH) and offers the opportunity to use renewable, carbon neutral resources for hydrogen production, in addition to efficient CO_2 sequestration. [29] Literature reports the successful use of several oxygen carrier as Ni, Cu or Ce, but the most common used is iron. [3]

Analogous to the CLC the CLH process is divided into two consecutive steps, which are cyclically repeated one after another (see Figure 3-2). The first step involves the reduction of an iron oxide to iron with a reductive gas. During the second step steam reconverts the OC to iron oxide producing hydrogen. The water is hereby thermally split into oxygen and hydrogen. The oxygen binds to the iron forming an iron oxide and hydrogen is released. [3] [30]

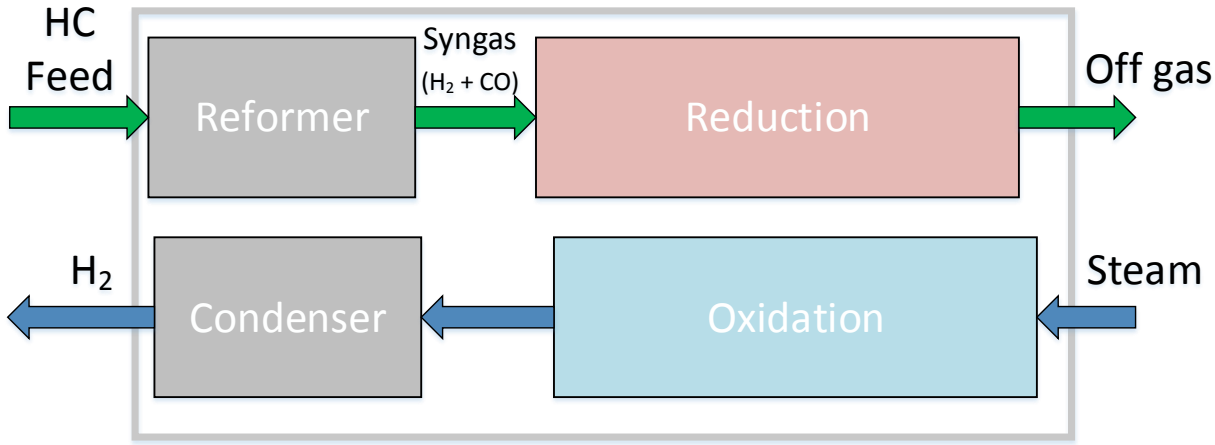

Figure 3-2: Process scheme for the CLH process

At Graz University of Technology Hacker et al. first published the *Sponge Iron Reactor (SIR)* [31][32] and the *Reformer Sponge Iron Cycle (RESC)* [33], which later was named Reformer Steam Iron Cycle (RESC). The process offers an interesting method to produce pressurized hydrogen in decentralised plants. It allows hydrogen production, purification and storage in a single compact unit. It is based on the historic *Steam Iron Process* developed by Messerschmitt in the late 19th/early 20th century. Messerschmitt produced hydrogen in a thermochemical cycle process oxidising hot iron with steam and reducing the obtained iron oxide with a lean reduction gas from coal gasification.

To produce the reductive gas in the RESC process, a reformer unit is pre-set, where methane, biogas or higher hydrocarbons are catalytically reformed. According to Equation (3-1) a syngas rich in CO and H_2 is obtained. This syngas in turn is used for the stepwise reduction of the iron based OC. Haematite (Fe_2O_3) is reduced to magnetite (Fe_3O_4) and subsequently to wüstite (FeO) and elemental iron (Equation (3-2)-(3-4)). Since the reduction is performed at the same temperature as the reforming reaction no heat exchanger between reformer section and reduction section is necessary. This allows the realisation of a very simple and compact unit [34].

After the reduction step the iron is reoxidised with steam. Here the oxygen atoms from the steam bond within the metal lattice and hydrogen is released according to Equation (3-5) and (3-6). To regenerate magnetite to haematite an additional oxidation step using pure oxygen or air can be performed (Equation (3-7)). Air oxidation can be used supplementary to reach the highest oxide state which cannot be achieved by oxidation with steam and as a cleaning step to remove carbon deposition. Otherwise the following reduction phase starts with magnetite.

As long as solid carbon formation during the reduction step is avoided, pure hydrogen can be obtained after condensation of the surplus steam from the oxidation off gas. Impurities are formed by oxidation of solid carbon (following Equation (3-8) and (3-9)). Solid carbon deposits on low temperature areas following the Boudouard reaction (Equation (3-10)) or direct methane decomposition (Eq. (3-11)) during the reduction step.

$$C_xH_y + xH_2O \rightarrow \left(x + \frac{y}{2}\right) H_2 + xCO \quad (3\text{-}1)$$

$$3\ Fe_2O_3 + H_2/CO \rightarrow 2\ Fe_3O_4 + \ H_2O/CO_2 \quad (3\text{-}2)$$

$$Fe_3O_4 + H_2/CO \ \rightarrow 3\ FeO + \ H_2O/CO_2 \quad (3\text{-}3)$$

$$3\ FeO + 3H_2/CO \ \rightarrow 3\ Fe + \ 3\ H_2O/CO_2 \quad (3\text{-}4)$$

$$3\ Fe + 3\ H_2O \ \rightarrow 3\ FeO + 3H_2 \quad (3\text{-}5)$$

$$3\ FeO + H_2O \ \rightarrow Fe_3O_4 + H_2 \quad (3\text{-}6)$$

$$2\ Fe_3O_4 + \frac{1}{2} O_2 \rightarrow 3\ Fe_2O_3 \quad (3\text{-}7)$$

$$C_S + H_2O \ \rightarrow CO + H_2 \quad (3\text{-}8)$$

$$C_S + 2\ H_2O \ \rightarrow CO_2 + 2\ H_2 \quad (3\text{-}9)$$

$$2\ CO \ \leftrightarrow CO_2 + C_S \quad (3\text{-}10)$$

$$CH_4 \leftrightarrow C_S + 2\ H_2 \quad (3\text{-}11)$$

To identify the reduction stage of iron and iron oxides under given conditions the Baur-Glaessner diagram is used (Figure 3-3). In this diagram the thermodynamic phase equilibrium of iron oxides can be depicted at given temperatures and gas phase composition. The diagram is separated in three regions by the equilibrium lines which represent the transition between the oxidation states of iron. Hematite (Fe_2O_3) is not present in the diagram as it is not stable in a reductive environment. The dashed line shows the equilibrium concentration for the reduction with hydrogen, whereas equilibrium lines based on the CO gas ratio are shown as solid lines. The gas ratio on the horizontal axis is defined by the volume content of H_2/CO within the reductive gas and calculation is shown by Equation (3-12) and (3-13). If reduction

is performed with a gas containing both, H_2 and CO, the equilibrium lines merge into one and an arithmetic average of the two reductive curves form the combined equilibrium curve. [35]

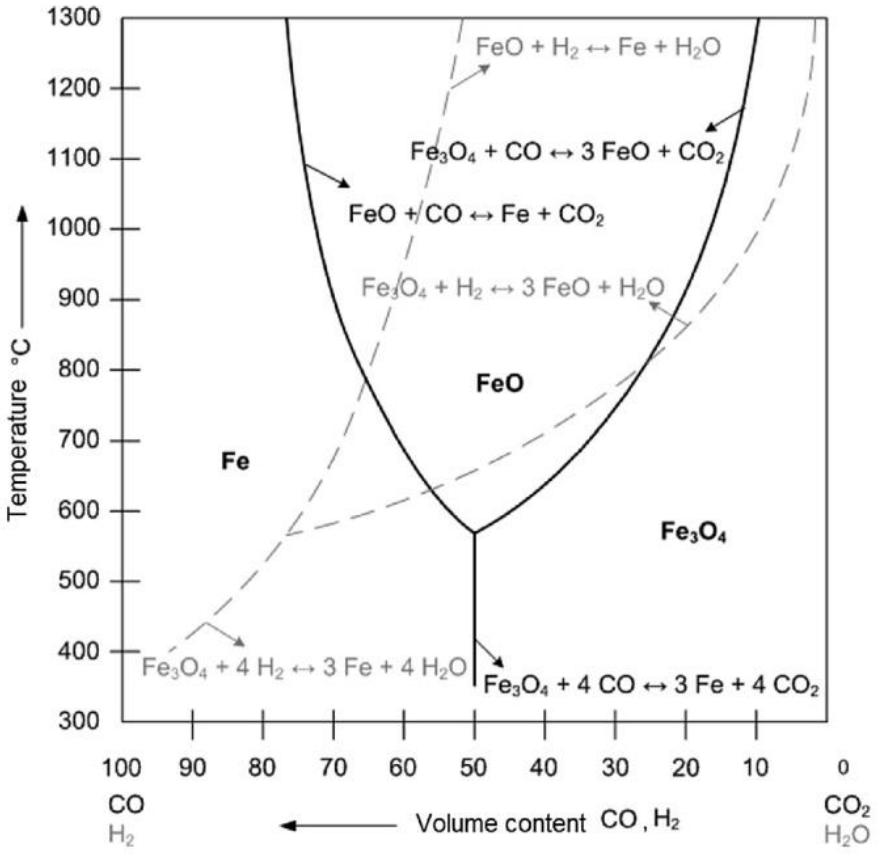

Figure 3-3: Baur-Glaessner diagram [35]

SMR is performed with an excess of steam in order to reach high methane conversion. Literature recommends a molar steam-to-carbon ratio (Equation (3-14)) of 1.2 to 1.6 [34]. As a direct consequence of excessive steam is the volume content of H_2 and CO in the reductive gas lower. On the other hand, high H_2/CO content does result in a greater distance to the equilibrium line, wherefore the concentration gradient as driving force for reduction is greater for small S/C ratios. [36]

$$Y_{H2} = \frac{H_2}{H_2 + H_2O} \tag{3-12}$$

$$Y_{CO} = \frac{CO}{CO + CO_2} \tag{3-13}$$

$$\frac{S}{C} = \frac{n_{H_2O}}{n_{CH_4}} = \frac{\frac{m_{H_2O}}{MM_{H_2O}}}{\frac{m_{CH_4}}{MM_{CH_4}}} \tag{3-14}$$

Most chemical looping plants operate with a reactor configuration of two interconnected fluidized bed reactors. At Graz University of Technology a fixed bed reactor system is chosen. Such reactor configuration appears to be more advantageous for small and medium scale decentralised hydrogen production. [34][37] In one compact unit syngas production, reduction and oxidation can be performed if gas streams are switched between reduction and oxidation. In addition, no moving parts in the reactor system are required. For continuous hydrogen production multiple reactors can be operated periodically.

The presence of two-time independent reaction stages gives the opportunity to store hydrogen chemically as iron by keeping the oxygen carrier in reduced state. In addition, it allows higher flexibility for on-demand hydrogen production and to reduce the OC anytime syngas is available. For cycles proceeding from magnetite to iron a mass based storage density of 4.8 wt% is possible [38]. Another advantage of the periodical operation is the production of pressurized hydrogen without an additional gas compression step. By increasing the liquid water pressure before evaporating steam the oxidation pressure can be increased equally. As hydrogen compression is a major cost factor and pumping liquid water to elevated pressure consumes energy to a lower extent than compressing a gas, the process efficiency can be increased. [34] Voitic et. al. [39] performed steam oxidation at different pressure levels up to 50 bar and found no significant negative effect of system pressure on hydrogen purity.

4 Experimental

For decentralized on-demand hydrogen production the use of syngas from all different types of renewables (e.g. biogas, gasified biomass) as reductive gas is investigated. Since the composition of biogas or gasified biomass varies heavily based on the feedstock material, production method and season, a high flexibility of the process is required. Besides the main components methane, carbon dioxide and nitrogen, biogas has a high amount of various trace compounds. Those include several volatile organic impurities as tars, which are a mixture of condensable organics (mostly aromatic hydrocarbons like benzene and toluene [40]), hydrogen sulphide and halogenated compounds as well as siloxanes, alcohols, ethers and organic acids. [19][41][42]

Table 4-1 gives an overview of different biogas trace compounds and their quantitative amount from literature. Gas from different sources is distinguished: from municipal solid waste (MSW) landfills, from agricultural waste (AW) digesters as well as from sewage digesters.

Studying the influence of those trace compounds on the hydrogen purity when using biogas in a chemical looping process is of crucial importance for the overall process feasibility. Hence model compounds are fed with the reductive gas in the reaction system during the reduction step. Methane and propane are selected as model compounds for acyclic hydrocarbons, ethanol is to be substitutional for organic alcohols and toluene to represent cyclic hydrocarbons.

Natural gas and biogas contain methane as bulk gas. Therefore, independently if syngas origins from SMR, biomass gasification or biogas reforming it will always contain unconverted methane, which makes methane the most common trace component.

Propane was selected to represent higher hydrocarbons as it was easily available. Additionally, it is delivered as pressurised gas, simplifying dosage to the feed without the necessity of experimental setup modifications.

Ethanol was chosen to substitute organic alcohols. It was available at high purity and is less toxic than methanol. Furthermore, ethanol steam reforming is widely studied and reported in literature. It is soluble in water which allows to control S/C ratio by introducing a pre-defined ethanol-water mixture.

Typical model compounds chosen to represent tars are one- and two ring aromatic hydrocarbons as benzene, toluene and naphthalene [40]. As benzene is carcinogen and naphthalene is a crystalline solid, toluene was chosen to be substitutional for cyclic hydrocarbons. It is less toxic than benzene and still in liquid state, which allows an easy feed dosage.

Table 4-1: Summary of biogas trace compounds from literature

		[19]	[20]			[41]			[43]
Bulk gases		**MSW Landfill**	**MSW Landfill**	**Sewage Digester**	**AW Digester**	**MSW Landfill**	**Sewage Digester**	**AW Digester**	**MSW Landfill**
CH_4	vol%	37-65				47-57	61-65	55-58	
CO_2	vol%	24-42				37-41	36-38	37-38	
O_2	vol%	<1				<1	<1	<1	
N_2	vol%					<1-17	<2	<1-2	
Trace compounds									
Total Alkanes	mg m^{-3}	302-1543	0-1400	0-60	n.d				302-503
C_2-C_5 Alkanes	mg m^{-3}	62-553							
C_6-C_{12} Alkanes	mg m^{-3}	122-1415							
Total cycloalkanes	mg m^{-3}	80-487	100-16000	0-400	0-300				
Total terpenes	mg m^{-3}	35-652	0-4200	0-40	0-450				74-152
Total aromatics	mg m^{-3}	36-1906							94-330
Benzene	mg m^{-3}	<0.1-7				0.6-2.3	0.1-0.3	0.7-1.3	
Toluene	mg m^{-3}	10-287				1.7-5.1	2.8-11.8	0.2-0.7	
Oxygenates	mg m^{-3}	-	100-300	0-100	n.d				
Total alcohols	mg m^{-3}	<0.1-1418							6-147
Ethanol	mg m^{-3}	<0.1-262							
Total halocarbons	mg m^{-3}	264-1239	0-300	n.d	n.d				224-739
Chlorinated compounds	mg m^{-3}	259-1239							
Siloxanes	mg m^{-3}	-	0-1300	0-210	0-20				
H_2S	mg m^{-3}					50-160	BDL	44-236	

4.1 Experimental setup

The experimental setup was designed and constructed within the framework of this master thesis. A fixed bed reactor with cyclic alternation between oxidation media and reduction gas is chosen. An image and the process scheme of the experimental setup is presented in Figure 4-1.

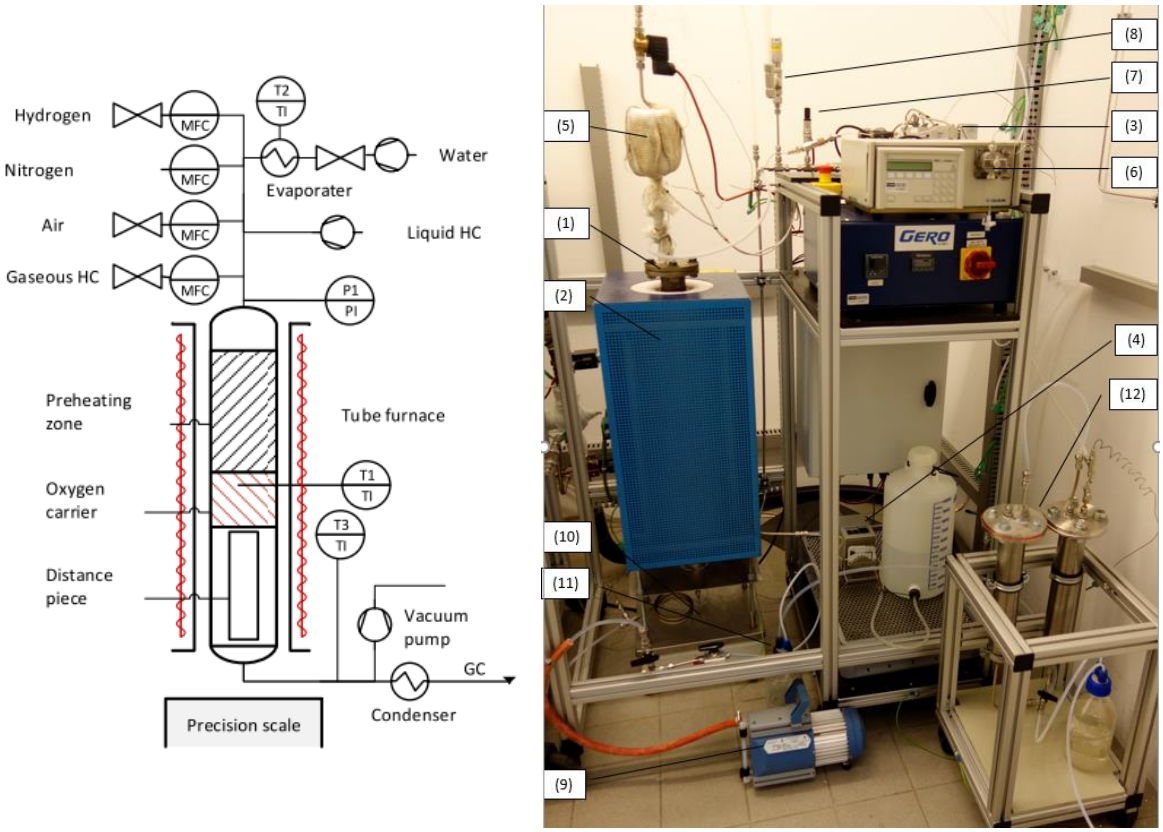

Figure 4-1: Flowsheet of experimental setup (left) and picture of experimental setup (right)

The reactor (1) consists of a stainless-steel tube from material 1.4876 a nickel iron chrome alloy (Alloy 800). The material is resistant against oxidation and carbonization at high temperatures as well as corrosion resistant against aqueous solutions. The reactor has an inner diameter of 50 mm and a length of 800 mm.

Reaction temperature is set to 850 °C by an electrical furnace (2) resulting in idle temperature of 830°C within the reactor bed. This temperature range was chosen by the working group based on previous experiments [30] as reformer and OC exhibit good conversion rates. To avoid heat losses, the furnace is equipped with an insulation.

The tubing is made from steel 316L or PTFE with an inner diameter of 4 or 6 mm and wall thicknesses of 1mm. An exception is made at the off gas tubes which have an inner diameter of 10 mm.

To directly measure the reaction temperature, one thermocouple is positioned in the centre of the oxygen carrier bed and several others allow to control the temperature at different key positions of the reaction system. Those include a measurement of the preheater temperature at the water inlet, a measurement of the off gas temperature to prevent tube damaging and control of the temperature after the cooling system to guarantee a dry gas for gas analysis.

Inside the reactor a distance piece (Alloy 800) ensures that the OC is embedded in the centre of the reactor. Above the oxygen carrier a layer of inert material is filled as a preheating zone for the inlet fluids. The inlets for gases are regulated by thermal mass flow controllers (Bronkhorst) to guarantee exact feed composition (3). Water is supplied by a peristaltic pump from Ismatec Reglo (4) and evaporated in a preheater (5). In case of further liquid media supply an additional inlet with an inner tube diameter of 1mm is joined. The liquid is conveyed by a Gilson 307 piston pump (6). Furthermore, all inlets are equipped with normally-closed magnetic valves for safety reasons which shut down in case of malfunction.

The reaction takes place at ambient pressure. Nevertheless, the media supply backpressure is constantly measured by a manometer (7) and a pressure relief valve is integrated (8) to release overpressure to the off gas section in case of reactor plugging. A vacuum pump (9) can be joint to evacuate the reactor. The vacuum pump has to be operated manually. As the chemical looping process comes with a weight alteration between the cyclic repeated steps the weight can be used to evaluate the progress of the momentarily performed phase. For this reason a precision scale (10) constantly monitors the reactor weigh. Outlet gases pass through a condensate system consisting of a wet scrubber (11), a water-cooled condenser and a demister unit (12). The dry flue gas is analysed with a Micro GC gas analytic system.

The GC system (Inficon Fusion) consist of two separate gas chromatographs (GC) which can detect molecules based on their retention time in the fixed phase (column). The first one houses two independent modules which work on different separation principles. One is equipped with a 10 m Rt-Molsieve column which separates the molecules based on their size and detects N_2, H_2, O_2, CO and CH_4. Detection limit for CO and CH_4 of this column is 1000 ppm. The second is equipped with a 12 m long Rt-Q-Bond column and separates molecules based on their polarity. It detects carbon dioxide and hydrocarbons like ethane, ethine, ethene, propane and butane. The programmable temperature ramping reduces the analysis time for higher hydrocarbons significantly. The second GC has only one module with a 12m Rt-Q-Bond column and can detect methane and carbon dioxide in single digit ppm concentration. Every module is equipped with a thermal conductivity detector (TCD) to determine the retention time of the molecules. As carrier gases argon and helium are used.

The GC's were calibrated with eight defined gas mixtures. From previous use of the GC is was known that calibration behaves linearly. The concentration for each component of those gas mixtures varied. Maximal and minimal concentration of the gas mixtures as well as lowest

detected value during experiments are listed in Table 4-2. Propane and butane were calibrated only for one concentration. Calibration lines for all components can be found in the appendix.

Table 4-2: Maximal and minimal concentration of calibration gases for GC and lowest detected value during experiments

Component	Maximal calibration concentration	Minimal calibration concentration	Lowest detected concentration
N_2	97%	1.9%	4.5%
H_2	98%	30%	0.01 %
CO_2	30%	5 ppm	5 ppm
CO	12%	5 ppm	2 ppm
CH_4	15%	5 ppm	2 ppm
C_2H_2/C_2H_4	10%	2%	1 ppm
C_2H_6	5%	1%	1ppm

The experimental setup is monitored and operated with LabVIEW software. Output data from the manometer, precision scale and all thermocouples are monitored and stored. Additionally, the MFCs, the magnetic valve and the water pump can be addressed.

The experimental setup is placed in a laboratory box at the Institute of Chemical Engineering and Environmental Technology at Graz University of Technology. To guarantee personal safety the box is equipped with gas sensors for H_2, CH_4, CO and CO_2 at the upper part and the bottom of the box respectively as well with an aeration system with a ventilation number β =20. In case of gas alarm the gas inlets as well as electricity are shut off ant the aeration systems is turned on to β =60. Furthermore, the box is built with fire resistant material and a smoke detector connects the box to the fire alarm.

4.1.1 Modifications

For experiments with selected biogas trace compounds the experimental setup is adapted to fulfil particular needs. Previous described setup is further referred as experimental setup version 1.

• The first adaptation was replacing the topmost layer of inert material with spheres of alumina oxide. The spheres are less porous than the inert material pellets. This setup was chosen to potentially reduce the inaccuracy of trace gases by adsorption on the high-porous inert material by Alfa-Aesar. (Experimental setup version 2)

• In experimental setup version 3 the condenser configuration is optimized. A ball valve to uncouple the demister unit is integrated. This adaptation reduced measurement inaccuracy due to gas retention in dead zones of the experimental setup.

4.1.2 Inputs for further improvements

Below some improvements for the experimental setup are listed which should be considered for future experiments in order to ensure more accurate analysis and operation mode:

For a more precise analysis and to reduce time lag between system and gas analysis the off gas tubing to the gas sample should be shortened. Thereby dead zones are reduced and measurement time coincides more accurately to the time of the reaction phases. It may be beneficial to take a small representative gas sample directly after the reactor. Cooling and condensation of excess steam would still be required before analysis.

To obtain a higher quality of measurements during oxidation it should be considered to reduce analysis time of the GC system or to lower steam feed during oxidation. Less steam would result in a longer oxidation phase and therefore more measuring points.

For further experiments the inlet for liquid model compounds during reduction should be upgraded. First, liquid feed should be preheated before entering the reactor. Additionally, it should be ensured that no liquid is evaporated from the pipe to avoid model components entering the system during oxidation phase. Evaporation during oxidation was noticed by a pressure drop of the piston pump. By placing a one-way valve close to the pipe outlet the pressure drop and therefore so evaporation could be prevented.

To be able to address all components and operate the system fully automatically the piston pump further be integrated in the LabVIEW software.

4.2 Experimental procedure

The experimental prearrangement starts by inserting the distance piece and positioning the thermocouple in the reactor. Afterwards, the reactor has to be placed in the furnace without touching the surrounding insulation tube to assure minimal influences on the gravimetric measurements. At this point, the reactor is filled with a first layer consisting of 1-2 cm of inert material pellets. Then 500g of oxygen carrier material is filled in. The thermocouple has to be in the middle of this OC layer. The topmost layer consists of inert material. The weight and height of each layer has to be notated.

After the reactor flange is tightened and all tubing’s are connected, a leakage test is performed. The valve before the condenser section is closed and the reactor is filled with nitrogen to an overpressure of approximately 2 bar(a). All connections are checked with leakage spray and retightened if necessary. The overpressure has to be kept for at least an hour. Pressure difference should not be higher than 0.01 bar. Additionally, a vacuum leak test is performed. A vacuum of approx. 0.1 bar(a) is generated with the vacuum pump. Again a pressure loss not greater than 0.01 bar should be reached.

To heat up the system, the furnace temperature is increased stepwise by 100°C h^{-1} until a reactor temperature of 850° is reached. To start the reaction, gas taps in the laboratory box and gas bottles are opened, pumps and preheater are turned on and cooling water is supplied. For the flue gas analysis the Micro GC system is started with the respective analysis method. Programming of the cycles is done previously in the LabVIEW interface, there also the reaction progress is monitored.

Reduction time is fixed to 60 minutes for 500g OC with regard to previous measuring series in a similar test stand. Hydrogen flow is set to 15 NL min^{-1}. If hydrocarbon feed is applied, the S/C ratio is fixed at 1.4. Literature recommends a S/C ratio of 1.2-1.6 for favourable thermodynamics and high syngas conversion [34]. After reduction the reactor system is purged with 5.9 NL min^{-1} of nitrogen for 15 minutes followed by one additional minute of holding time where the weight is taken and defined as final reduction state. During oxidation steam is supplied to the reactor system with the peristaltic pump. Amount was varied between experiments in order to prolong oxidation time and is specified for each cycle. Analogous purging and holding procedure with 5 minutes purging time is preformed after the oxidation. Nitrogen is used as internal standard within all experiments (0.89 NL min^{-1}).

Figure 4-2 shows the mass change of the whole reactor system and the OC bed temperature during one cycle. Reduction phase is coloured in red, steam oxidation in blue and air oxidation is dyed green. During reduction mass decreases and temperature drops as the oxygen carrier loses oxygen atoms and energy is consumed by the reduction reaction. If hydrocarbons were added in the reductive gas the temperature drop is intensified by the endothermic reformation reactions. The mass gain during oxidation with steam can be directly correlated to the amount of produced hydrogen. During oxidation with air a further mass increase can be observed as magnetite is oxidised to haematite. The exothermic nature of both oxidation reactions results in an abrupt temperature increase.

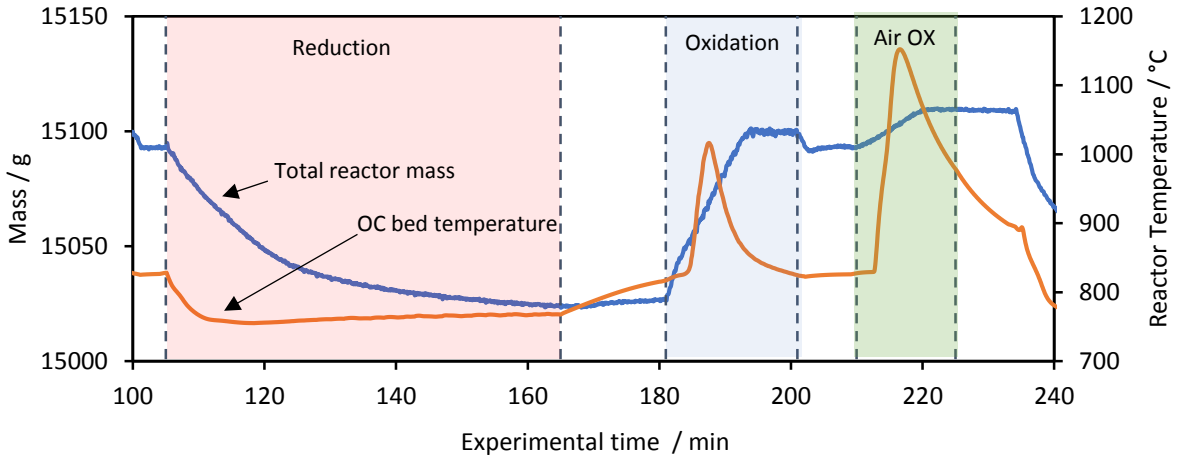

Figure 4-2: Reactor mass and OC bed temperature during cycle 17 of experiments with methane

Within the experiments evacuation of the reactor was investigated to exclude gaseous impurities from reduction. Before evacuation the reactor is purged for 7.5 minutes with a nitrogen flow of 5.9 NL min^{-1} for safety reasons. Subsequently the reactor is evacuated three times within 5 minutes to an absolute pressure of approximately 0.1 bar (a) and refilled with nitrogen. To reach the normally applied 15 minutes of reactor purging the reactor is further purged with nitrogen for 7.5 minutes after evacuation. During evacuation the ball valve before the condensate bottle is closed and the valve to the vacuum pump opened.

If air oxidation is performed after steam oxidation the reactor is purged with nitrogen for 15 minutes beforehand to avoid an explosive atmosphere. Air oxidation is performed for 15 minutes with an air flow of 5.9 NL min^{-1}.

During experiments one has to assure that:
• Condensate bottles are regularly emptied
• Temperature after the condensate system does not exceed 25°C
• High purity water is always present in the water feed tank
• No leakage occurs, wherefore tubing and reaction system are regularly checked with the hydrogen detector.

4.3 Oxygen carrier characterisation

The chemical reduction reaction from a metal oxide to the respective metal and the reoxidation with steam allow hydrogen to be stored chemically as reduced metal and steam. The number of oxygen atoms bond by one metal atom in its oxidised state defines the amount of hydrogen which can be stored. [38]

Some of the major advances of iron based oxygen carrier materials for hydrogen production and storage with chemical looping are:

- Price and availability
- Environmental friendly characteristics
- A high reactivity and favourable thermodynamics regarding syngas reduction
- Low risk of carbon formation
- High stability during the redox cycles
- A high steam-to-hydrogen conversion and high oxygen exchange capacity
- High resistance to attrition, agglomeration and sintering

Different authors [13] [38] [44] have reported that Fe_2O_3 is the most favourable metal oxygen carrier regarding different properties including cost, toxicity, oxygen carrying capacity, thermodynamic properties, reaction kinetics, physical strength, melting point and environmental effects.

Inert support materials are added to the metal oxides to avoid iron oxide sintering after only a few cycles. This would result in a reduction of the active surface area, limiting mass transport and hence decreasing reaction kinetics [38].

The oxygen carrier used for these experiments consist of 80 wt% of Fe_2O_3 and 20 wt% Al_2O_3 and is produced in house. The powders (from Alfa Aesar) are dry mixed with an intensive mixer (type Eirich El 1) and pelletized with water as binder. After palletisation they are calcined in air at 900 °C for 6h. Oxygen carrier characterisation was done and published by Bock and Zacharias [30]. After the first cycles a conversion of 74% is reported with a further decrease of stability of 0.14% in average per cycle starting from cycle 7.

Grain size distribution of the calcined pellets was analysed with an image scanner and the imageJ software and is illustrated in Figure 4-3. On the left hand side one can see the density distribution by number (q_0) and by mass (q_3). It can be seen that the highest share of particles is, as desired, in a narrow range between 1 mm and 2.5 mm. On the left hand side the cumulative distribution of the analysed particles is shown.

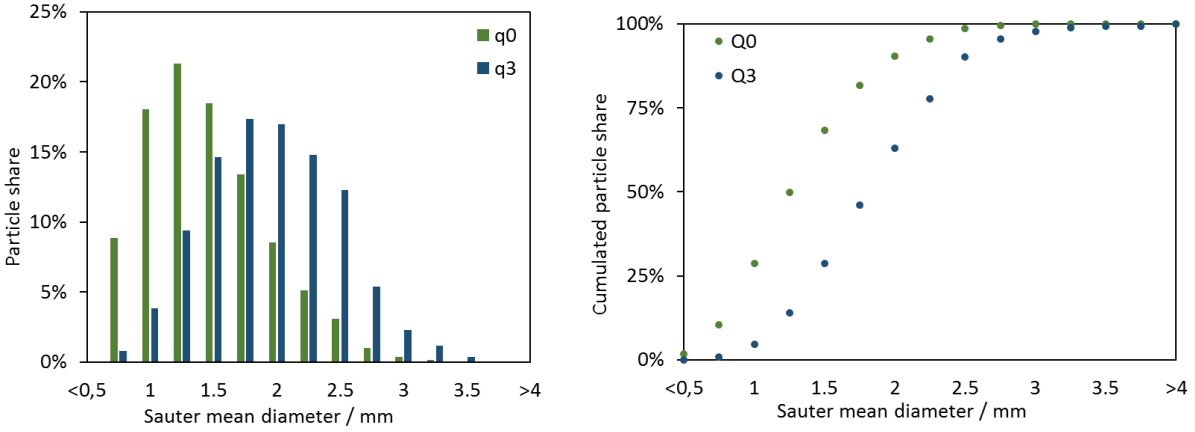

Figure 4-3: Particle size distribution (PSD) of the pelletised OC, left: density distribution, right: cumulative distribution

Voitic et al. [45] investigated the effects of oxidation at elevated pressure for pressurized hydrogen production on an oxygen carrier based on Fe_2O_3-Al_2O_3 (90+10 wt%). They performed experiments in a fixed bed reactor system at pressure levels of 7-22 bar (a) at temperatures of 750°C. They point out that the elevated system pressure did not reduce conversion efficiency. The decrease in stability of the oxygen carrier can be related to sintering effects inducted by the high reaction temperatures.

To determine the structure of the oxygen carrier material, single pellets were analysed with both light microscopy (LM) and scanning electron microscopy (SEM). Images are presented in Figure 4-4. The calcined sample showed a homogeneous compact surface. No pores were visible at 1 kx magnification (a) and even with 5 kx magnification (b) the surface appeared dense

and homogeneous. After performing 40 cycles of reduction and oxidation in the test stand some pellets were oxidised in air in a furnace at 800°C. The oxidised pellets featured the typical reddish colour for iron (III) oxides, while all reduced pellets appeared in a dark black colour. Analysis via LM revealed mayor differences in the surface structure between the reduced and oxidizes sample at 250 x magnification. The reduced sample (c) displayed some larger particles which were surrounded by pulverulent matter, whereas the oxidised sample presented itself more homogenously. Analysis of the same samples was done with SEM to gain a more detailed view of aforesaid phenomenon. At 1 kx magnification the reduced sample (e) revealed clearly visible pores and a cluster of matter while the pores in oxidised state (f) are minor. These can be attributed to the volume change from elemental iron to iron oxide. In reduced state the oxygen carrier loses volume and encircles the support material. When oxidized, the oxygen carrier lattice expands and closes the pores between the different clusters. Due to repeated volume change, macroscopic porosity of the cycled samples is higher. In microscopic range the calcined pellets do exhibit higher porosity. That coincides with results reported from Bock et. al. [30], who determined the surface area of sample pellets with Brunauer-Emmett-Teller (BET) method. The pellets were produced analogously to those used in these experiments. They report BET surface area of 2.90 m^2 g^{-1} for samples after calcination. Already after 20 cycles in a lab-scale reactor the surface area decreased to 0.43 m^2 g^{-1}.

(a) (b)

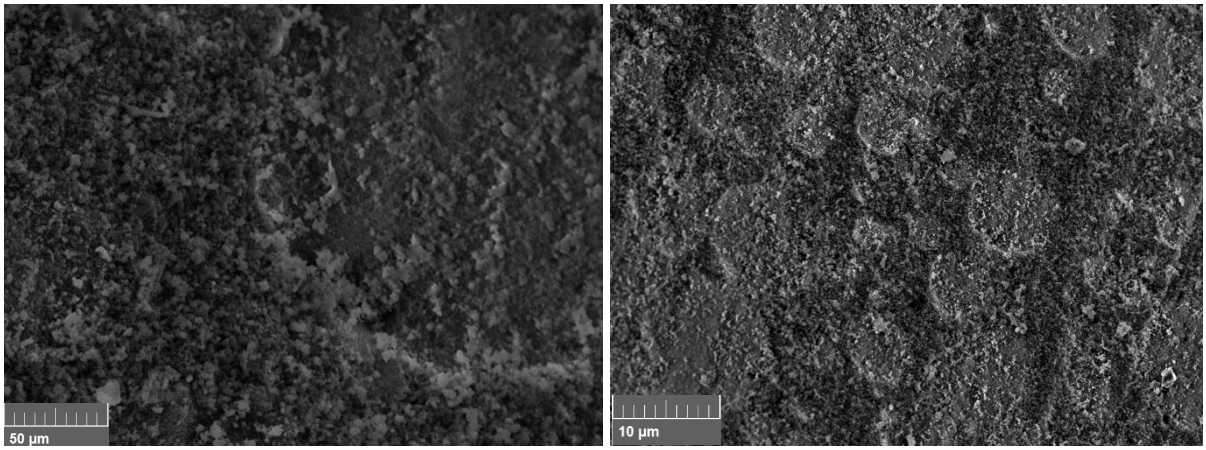

(c) (d)

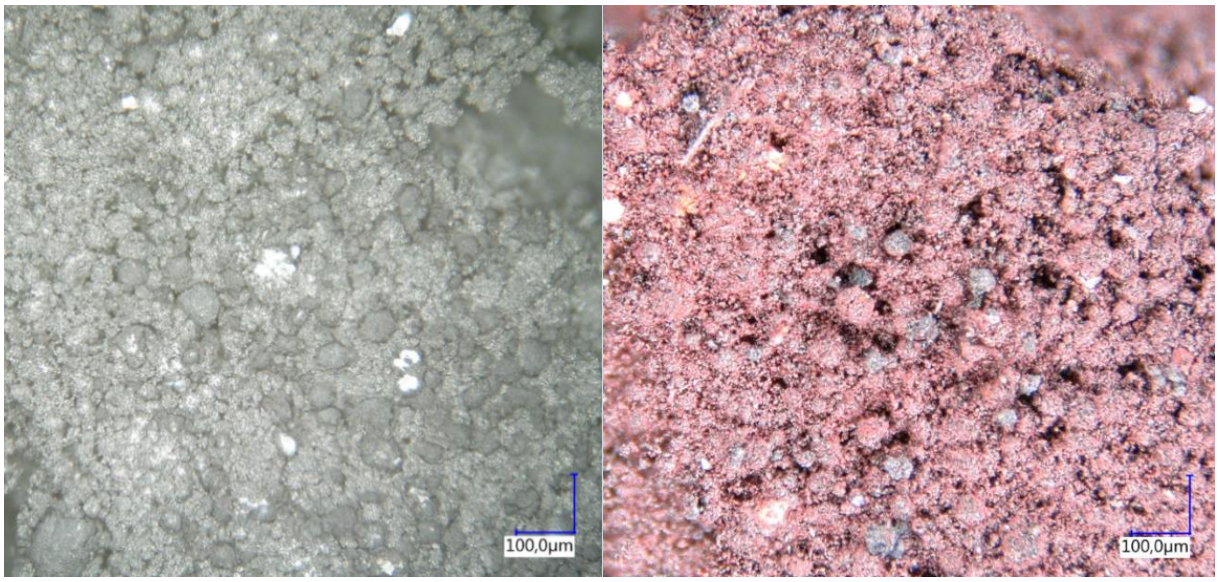

(e) (f)

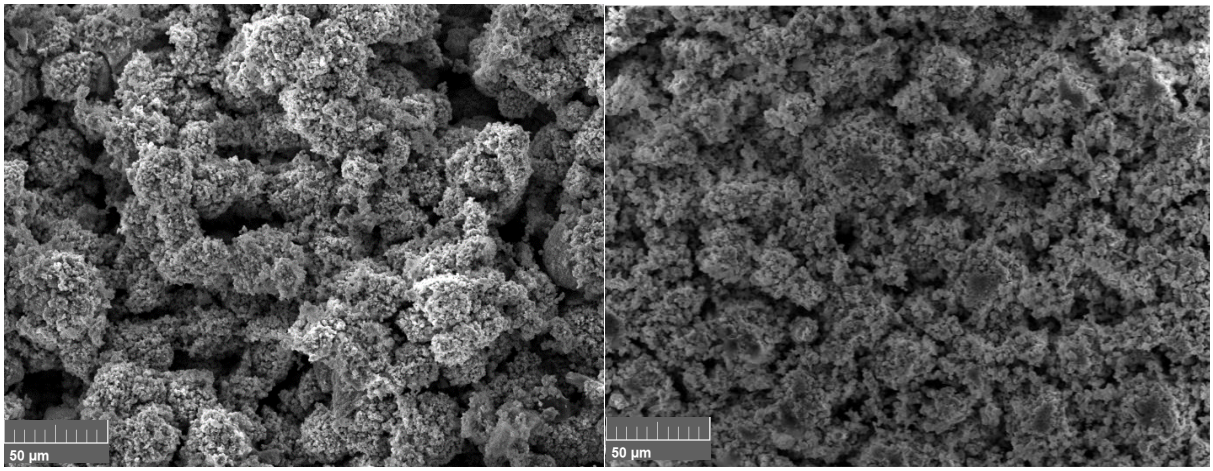

Figure 4-4: SEM image of calcined pellet at 1kx (a) and 5 kx (b), LM image (250 x) of cycled sample (40 cycles) reduced (c) and oxidized state (d) and SEM image of cycled sample (40 cycles) at 1kx magnification in reduced (e) and oxidized state (f).

5 Results for addition of C_1 compounds to the reductive gas – model compound: Methane

Methane is the simplest alkane consisting of one carbon atom which has four equivalent C-H bonds. At room temperature and standard pressure methane is gaseous. Literature reports methane can reduce magnetite at temperatures higher than 700 K in an endothermic reaction (Equation (5-1)). [46]

$$Fe_3O_4 + CH_4 \leftrightarrow 3\,Fe + CO_2 + 2\,(H_2O)_g \qquad \Delta H_{800} = 295.26\,kJ\,mol^{-1} \qquad (5\text{-}1)$$

Experiments with methane in the reductive gas were carried out with experimental setup version 1.

5.1 Methane operation points

As previously reported the syngas of biomass gasification usually contains 6-15% of CH_4. To simulate incomplete CH_4 conversion in the reformer section of the RESC process the first OP is chosen with a low amount of methane (2 vol%). To investigate the influence of direct utilisation of syngas from biomass gasification as reductive gas for the chemical looping process, the consecutive OP contain 10 vol% of CH_4. H_2 flow of the 2nd CH_4 OP was reduced to check for heat expansion with increased gas throughput, as the PTFE tubing should not be overheated. H_2 flow of the 3rd CH_4 OP was set to 15 NL min^{-1} with 10 vol% of CH_4. The water flow was adjusted to ensure a constant steam to carbon ratio of 1.4. Oxidation was performed with 9.6 g min^{-1} of steam and oxidation time was adjusted to achieve full oxidation at each methane OP. Parameters for all CH_4 OP are listed in Table 5-1.

Table 5-1: Overview of investigated methane operation points

	H_2	CH_4		Water	S/C	Ox time	Relative OC conversion
	NL min^{-1}	NL min^{-1}	vol%	g min^{-1}	mol $_{H2O}$ mol$_C^{-1}$	min	%
1st CH_4 OP	15	0.32	2	0.35	1.4	15	54
2nd CH_4 OP	10.5	1.38	10	1.57	1.4	20	41
3rd CH_4 OP	15	1.97	10	2.26	1.4	20	42

Table 5-1 gives an overview of the methane operation points, their gas and water flows, and the real conversion compared to ideal complete conversion of the metal oxygen carrier. It can be seen that the rate of conversion of the oxygen carrier diminished with an increasing methane/steam content. This can be easily explained when looking at the Baur-Glaessner diagram already discussed in chapter 3. An increase of steam results in a lower $H_2/(H_2+H_2O)$ rate. Therefore, the distance to the equilibrium line, which is directly related to the driving force for reduction, is smaller, wherefore the oxygen carrier conversion is lower.

Throughout the experiments with methane a total of 44 cycles were performed and the mass difference of those is shown in Figure 5-1. The dots represent a mean value of the mass difference of reduction and oxidation phase. An exception was made for cycles with air oxidation, where only the mass difference of the steam oxidation was considered in order to correctly represent the mass increase of the OC carrier. In the beginning the oxygen carrier has to undergo a few cycles to reach stable mass difference as already discussed in chapter 4.3. Cycles were an oxidation with air was performed after steam oxidation are marked with a red cross, cycles where methane content corresponded to 2 vol% of the feed gas during reduction are encircled in green and where methane content corresponded to 10 vol% are encircled in blue. Ideal calculated mass change for every cycle is marked with a black dashed line. The mass change for the first reduction would have been 120 g for complete conversion of the oxygen carrier and for all following cycles it would have been 106.9 g. Calculation was based on the total amount of oxygen carrier and can be found in the appendix together with a summary of all cycles, their operation points and investigated methods to eliminate impurities (Table 11-3).

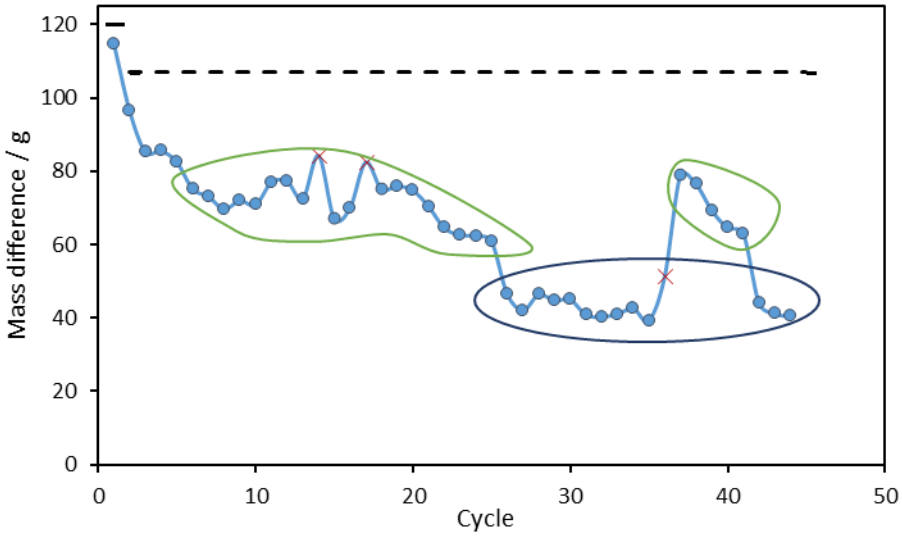

Figure 5-1: Absolute mass difference during cycles of methane experiments (mean value of reduction and oxidation, with except for cycles with air oxidation - where only the mass difference during steam oxidation is considered)

5.2 Reduction

In the reduction phase methane was added to the reducing gas stream and the off gas composition was measured. Besides excess H_2, N_2 as internal standard and unconverted CH_4, CO and CO_2 were detected. The latter two origin from methane reforming and WGS reaction (see Equation (2-1), (2-3)). Based on the methane in- and outflow, CH_4 conversion for each OP was calculated.

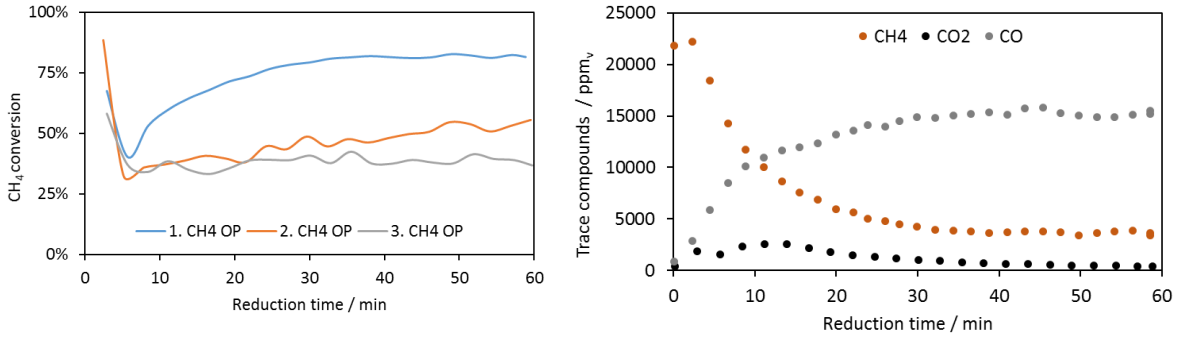

Figure 5-2: Methane conversion during reduction (left) and off gas analysis during reduction of 1st CH_4 OP (right). Average of cycle 22-25.

On the left hand side in Figure 5-2 the methane conversion for each OP over time is plotted and on the right the concentration of CO, CO_2 and CH_4 in the off gas for the first CH_4 OP. At the beginning of each reduction the methane conversion was high and after a steep decrease reached a minimum for all three OP at approximately 5 minutes. Afterwards conversion levelled at a constant value of about 80% for 2 vol% of CH_4 in the feed and of 40 to 50% for operation points with 10 vol% of CH_4 in the feed. The initially high methane conversion could be a result of the time lag between system and gas analysis, as reduction off-gas may not have reached the point of analysis sampling the first 5 minutes. As methane content in the off gas decreased the CO content rose towards a stable level. The CO_2 concentration level was small compared to the other two gases. Input flow was compared to the output flow for the first methane OP in Figure 5-3. Hydrogen was consumed with a higher extent at the beginning of the reduction and the outflow converged towards the input flow with ongoing reduction time. The outflow of all three carbon containing gases matched the carbon input after approximately 5 minutes of reduction time. This discrepancy of the carbon balance within the first minutes may be a further hint for a time lag between the system and the gas analysis and was not accounted for the further calculation. The difference of the total carbon balance for the 1st CH_4 OP accounted for 5% with a standard deviation of 0.006 between the measurement data. Similar behaviour was observed for the 2nd and 3rd CH_4 OP although with a larger difference in the carbon balance (23± 0.016 and 25 ± 0.023% respectively).

Reactor temperature decreased constantly during reduction as a result of the endothermic methane reforming reaction. Lowest recorded reactor temperatures were 745 °C for the 1st and 2nd CH_4 OP and 730°C for the 3rd CH_4 OP.

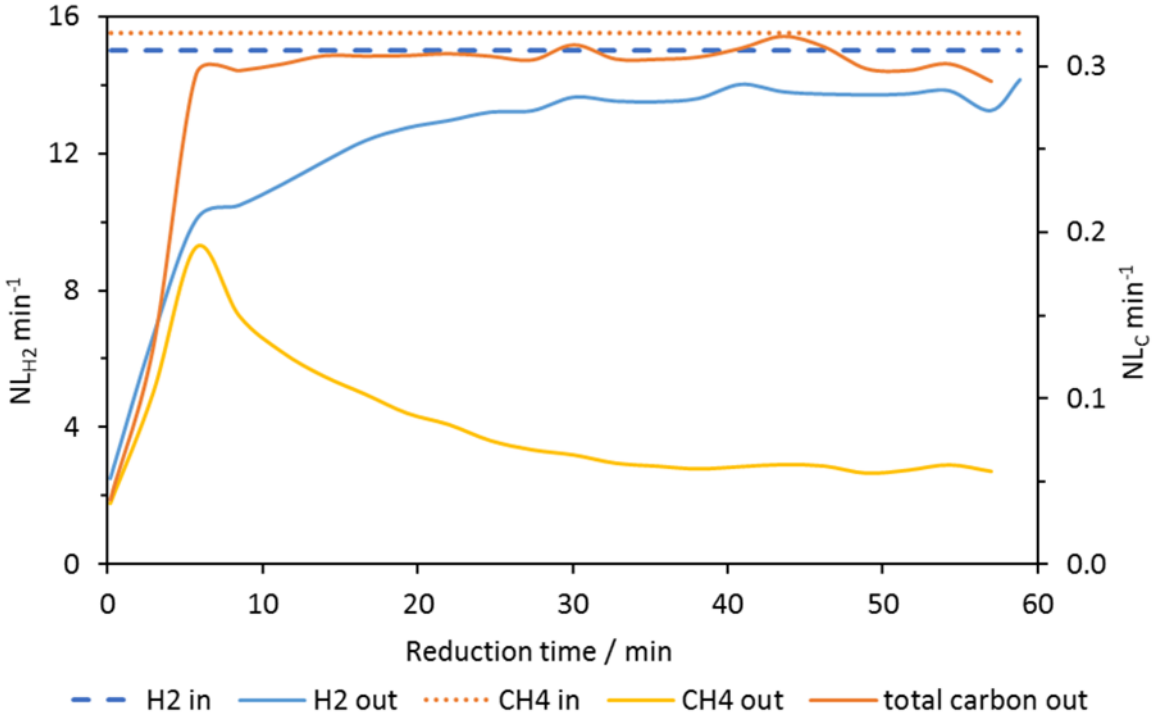

Figure 5-3: Exemplary outgoing gas flow of hydrogen and carbon-containing gases at 1st CH_4 OP

5.3 Steam Oxidation

Hydrogen production during oxidation behaved like a 'bell shape curve' with an initial increasing hydrogen flow to a stable flow of approx. 7 NL min^{-1} in every oxidation phase. The amount of produced hydrogen heavily depended on the degree of reduction which in turn was influenced by the amount of steam during reduction phase. As illustrated in Figure 5-4, CO, CO_2 and CH_4 impurities appeared during oxidation. Impurities were calculated in ppm in relation to the momentary produced hydrogen amount. Impurities exhibited a noticeable U-curve, as the impurity concentration per amount of produced H_2 was high at the beginning and the end of oxidation where no or only little hydrogen was produced. As methane is not expected to form at given conditions incomplete purging of the reactor system can be source of arising of methane during oxidation. Carbon monoxide and carbon dioxide can partly origin from incomplete purging as well as from reoxidation of carbon deposition according to Eq.(3-8) and (3-9).

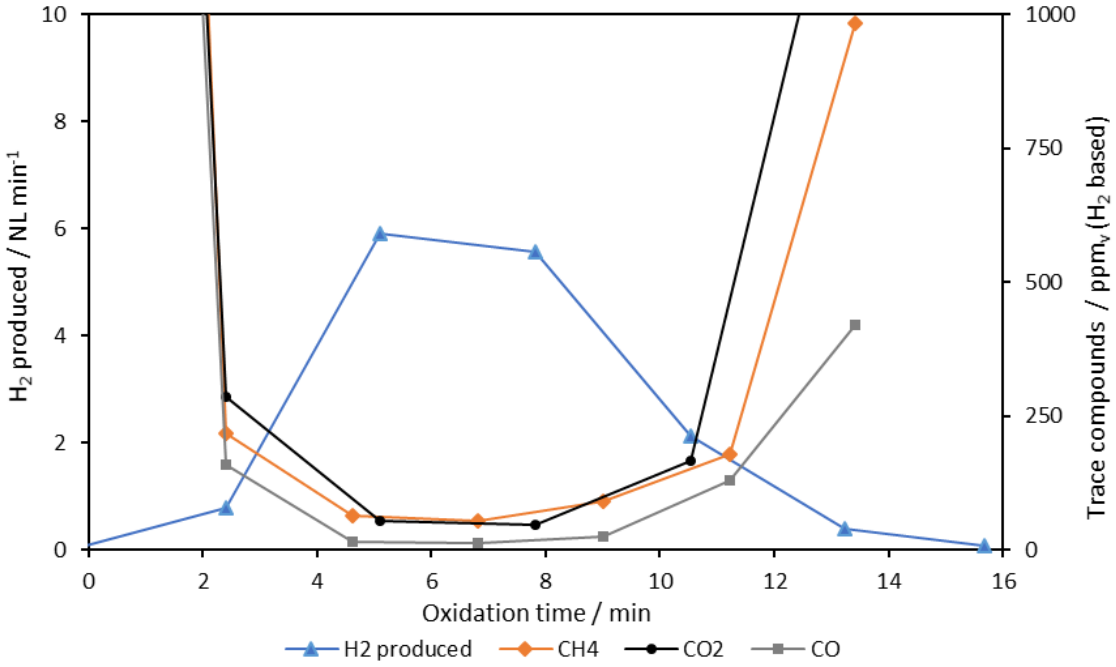

Figure 5-4: H_2 production and impurities during oxidation, 3rd CH_4 OP, average for cycles 30-33

Increasing the amount of methane in the reductive gas resulted in higher amounts of impurities in oxidation phase. So did the increase from 2 to 10 vol% of methane result in an increase of the hydrogen contamination from 100 to approximately 300 ppm_v. In Table 5-2 average values of the total carbon impurities in proportion to produced H_2 amount of four cycles for each OP are shown.

Table 5-2: Total carbon impurities based on produced H_2 for all CH_4 OP

1st CH_4 OP*		**2nd CH_4 OP****		**3rd CH_4 OP*****	
Time min	**Total carbon impurities ppm_v (H_2 based)**	**Time min**	**Total carbon impurities ppm_v (H_2 based)**	**Time min**	**Total carbon impurities ppm_v (H_2 based)**
2.4	124	1.6	549	2.4	956
5.1	102	4.3	189	5.1	234
7.8	83	7.0	182	7.8	180
10.5	77	9.7	196	10.5	195
13.2	80	12.4	224	13.2	235
15.9	84			15.7	293
18.6	92				
21.2	104				
*	Average of cycle 22-25	**	Average of cycle 26-29	***	Average of cycle 30-33

5.4 Reactor evacuation before steam oxidation

In order to exclude gas remains from the reduction gas the reactor was evacuated between reduction and oxidation phase. Three evacuations to an absolute pressure of approximately 0.1 bar(a) were performed within 5 minutes and in between the reactor was refilled with nitrogen. Hence approximately one thousandth of the original reduction gas should remain in the reactor after evacuation. Holding time of the applied vacuum varied within the single experiments as evacuation had to be performed manually.

During the holding time of the vacuum gas is expected to desorb from the pores of the solid materials. Desorption of trace compounds is enhanced by filling the reactor with nitrogen after every evacuation as the partial pressure of all other compounds than nitrogen is decreased. Therefore, it can be assumed that after evacuation most gases from the reductive phase were desorbed from the pores of the oxygen carrier and the inert material and no reductive gas remains were left in the reactor system. During oxidation arising carbon-oxide impurities can hence be allocated to reoxidation of elemental carbon settled in the reactor system.

The effect of evacuation on the hydrogen purity was investigated for the 1st and 3rd CH_4 OP. For both OP similar effects were observed and total volumetric amount of impurities based on the total amount of produced hydrogen during the oxidation phase as well as the percentage of removal due to evacuation can be found in Table 5-3. Total carbonaceous impurities could be lowered roughly 50% for both OP. The greatest effect of evacuation was observed on methane. At the OP with 2 vol% of CH_4 in the reductive gas, methane could be removed completely from the oxidation phase. This strengthens the aforesaid fact, that no methane is expected to be formed during oxidation. At the 3rd CH4 OP roughly 90% of methane could be removed by evacuating the reactor. The remaining methane may be result from incomplete purging and gas retention in dead zones of the experimental setup

Carbon oxide impurities were less affected by evacuation. This is a hint for carbon deposition, as remaining impurities can be attributed to reoxidation of elemental carbon. Those carbon settlements, formed during the reduction phase, cannot be eliminated by evacuation and result in contamination of the hydrogen produced during the oxidation phase.

Table 5-3: Influence of reactor evacuation for 1st and 3rd CH_4 OP

		1st CH_4 OP			**3rd CH_4 OP**		
			evacuation			**evacuation**	
Average cycles		22-25	39-41	compound removal	30-33	42-44	compound removal
CO_2	ppm_v (H_2 based)	53	37	30 %	174	114	34 %
CO	ppm_v (H_2 based)	27	13	54 %	34	8	76 %
CH_4	ppm_v (H_2 based)	24	0	100 %	86	11	88%
total	ppm_v (H_2 based)	104	49	52 %	293	133	55 %

Figure 5-5 shows the hydrogen production during the 3rd CH_4 OP as well as the CH_4 and CO_2 impurities. Cycles without evacuation are presented in dotted lines and empty dots and cycles performed after evacuation are presented in continuous lines and filled dots. The effects of evacuation are clearly visible. Evacuation resulted in a much lower CH_4 concentration, whereas CO_2 concentration could not be lowered significantly. Although not shown in Figure 5-5 CO impurities were, with analogy to CO_2, only little affected by evacuation of the system.

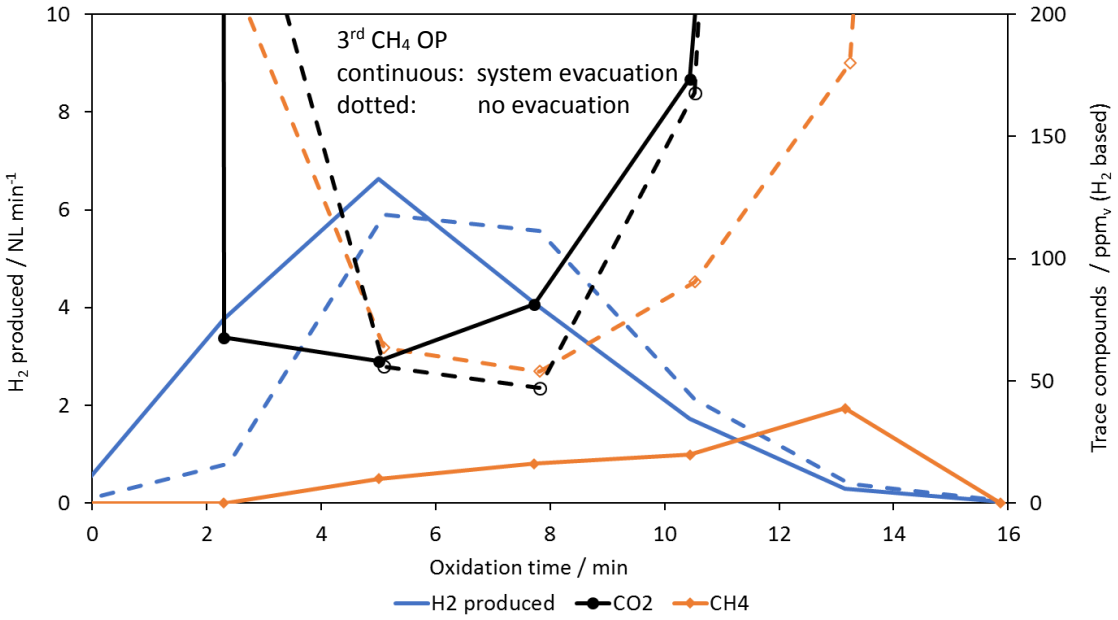

Figure 5-5: Influence of evacuation on CH_4 and CO_2 impurities for the 3rd CH_4 OP (average for cycles 42-44) and without evacuation (average for cycles 30-33).

5.5 Air Oxidation

Air oxidation can be performed after steam oxidation to reach haematite as highest iron oxide state and deposited carbon is oxidised. By these means carbon depositions can be eliminated and an accumulation with ongoing number of cycles is prevented. Procedure for air oxidation was already described in chapter 4.2.

Before investigating the influence of air oxidation, two cycles were performed for conditioning the system. To investigate the influence of air oxidation two cycles were compared: One without previous air oxidation and one with an air oxidation before the reduction. A sum of arising impurities in relation the produced hydrogen amount and the removal rate of impurities due to air oxidation are listed in Table 5-4.

Methane content is roughly 50% lower after air oxidation for the regarded cycle. Air oxidation is not expected to influence methane concentration in the subsequent cycle, as it is performed after steam oxidation to eliminate elemental carbon not reoxidised by the steam. Therefore, methane impurities are left aside in the present case.

Values of impurity concentration for carbon oxides were not lowered significantly by air oxidation. It can be deviated that no accumulation of carbon in the reactor system took place when methane was present during the reduction, wherefore air oxidation does not bring any advantage in terms of impurity elimination in the present case.

Table 5-4: Arising impurities during oxidation phase with and without air oxidation, cycles 14 and 15

		no Air Ox	Air Ox	
Cycles		14	15	compound removal
CO_2	ppm_v (H_2 based)	104	99	5%
CO	ppm_v (H_2 based)	29	27	7%
CH_4	ppm_v (H_2 based)	34	18	47%
total	ppm_v (H_2 based)	166	143	14%

The regeneration of magnetite to haematite during air oxidation and the associated temperature rise as result of the exothermic reaction could be observed (see Figure 4-2). Calculated mass change resulted in an ideal mass difference of 13 g based on the filled amount of oxygen carrier for the methane experiments. Three oxidation with air were performed independently. Mass change varied between 10 and 15 g and temperature reached a maximum value of 1150°C. From the achieved mass difference of the single air oxidation it can be deduced that full oxidation to the respective oxide state is achieved by steam and air oxidation.

5.6 Extended storage of reactor in reduced state

To simulate the chemical storage of hydrogen with chemical looping hydrogen technology when reduction takes place with a syngas from biogas or gasified biomass, the reaction system was kept in reduced state after reduction with CH_4 in the feed gas for approx. 68 hours before oxidising it with steam. As always after reduction the reactor was purged for 15 minutes with 5.9 NL min^{-1} of nitrogen for safety reasons. During the 68 hours of storage no gas flow went through the reactor and reactor temperature was kept constant at 850°C. Before reoxidising the reactor was purged for 5 minutes with 5.9 NL min^{-1} of nitrogen.

To investigate the effect of long time storage in the reductive atmosphere the oxidation after 68h storage was compared with three oxidation phases without storage. The hydrogen based impurities for all considered cycles are listed in Table 5-5. All investigated cycles were performed according to the 1st CH_4 OP. Cycles without storage were not performed consecutively. Nevertheless, are impurities comparable as the standard deviations for all compounds to the average value are small.

After extended storage time in the reductive atmosphere no methane was detected during the subsequent oxidation phase. CO impurities were reduced by roughly 50%, whereas CO_2 impurities increased by 95% compared to cycles without storage time.

Table 5-5: Influence of reactor storage for 68 hours after reduction at 1st CH_4 OP

		no storage					after 68h storage	
Cycles		7	9	10	Std dev	average	8	compound removal
CO_2	ppm_v (H_2 based)	30	22	26	2.5	22	43	-95%
CO	ppm_v (H_2 based)	21	28	18	4.0	22	11	52%
CH_4	ppm_v (H_2 based)	37	29	31	3.8	32	0	100%
total	ppm_v (H_2 based)	88	78	74	1.6	76	54	29%

The effects of the storage in reduced state are also shown in Figure 5-6, where the produced hydrogen and the carbon-oxide impurities are illustrated. The average for the oxidation of cycles without storage is presented in dotted lines and empty dots. The oxidation phase after 68h of storage time is presented in continuous lines and filled dots.

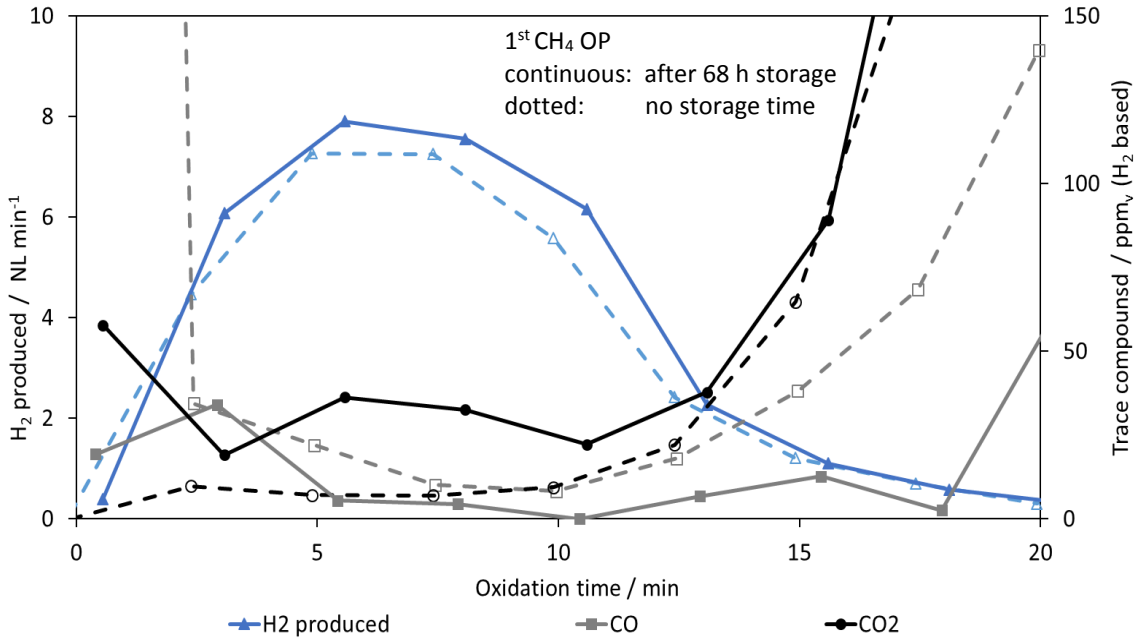

Figure 5-6: Influence of long time storage on impurities for the 1st CH_4 OP. Oxidation after 68h storage (cycle 8) and without storage (average for cycles 7, 9, 10).

The increase amount of CO_2 and the contemporaneous decrease of CO and CH_4 for reactor storage at reduced state can be explained by two different effects which may occur simultaneously.

During the storage time, a chemical equilibrium can establish within the reactor. As already hinted by previous results is the reductive gas not completely flushed out of the reactor during the applied 15 minutes of purging after reduction. Therefore, the gas atmosphere in the reactor during storage contained gas remains from the reductive gas, including CH_4, CO, CO_2 and steam. Temperature was kept constant during storage, providing energy for

thermochemical reformation of methane. The decrease of methane can therefore be explained by thermal breakdown of methane by SMR or direct methane decomposition resulting in carbon settlements. Previous results suggest, that elemental carbon formed by the direct methane decomposition tend to be reoxidised by steam into CO_2 rather than CO, which explains the increase of CO_2 after storage.

On the other hand, physical adsorption does explain the decrease of total amounts of impurities during the oxidation phase after storage. Due to the purging of the reactor with nitrogen the partial pressure of nitrogen is higher than during reduction. Consequently the partial pressure for all other compounds is lower and they tend to desorb from the pores of the solid materials within the reactor. Therefore, the combination of reactor storage and reactor purging before steam oxidation can result in flushing out a disproportionally high amount of gaseous impurities.

5.7 Extended reduction

The reactor was reduced for 5 hours to analyse the oxygen carrier for carbon deposition. The first hour of reduction was conducted as in previous reductions according to the 3rd CH_4 OP. Afterwards feed gas was halved while all parameters (10 vol% CH_4, S/C=1.4) were kept constant. Due to longer reduction time a greater mass change was achieved than during one-hour reduction (54% in relation to ideal reduction compared to 42% when reducing for one hour at 3rd CH_4 OP).

5.7.1 Analysis of the Oxygen carrier

Samples of the oxygen carrier were taken from the outer border towards the reactor wall (position A) and from middle of the oxygen carrier bed (position B). SEM analysis showed mayor differences in the structure of the sample depending on the sample position (Figure 5-7). Sample from position A (a) close to the reactor wall showed similar results as samples discussed previously in chapter 4.3. The reduced iron oxide clustered around aluminium oxide particles resulting holes between the distinct inert spheres. A complete different structure was revealed at the sample from position B (b, c, d) where a coating layer was found to cover all oxygen carrier surface. The particle was cracked open to gain an insight in the particle inner structure. The outer structure featured a shell-like morphology (c). The inner part of the sample bared a denser matrix with some single distinguishable grains. If pictures (a) and (b) with 500 x magnification are compared directly it is clearly visible that the particle from position B was much denser and less porous. To gain more information's about the chemical composition of the different regions, sample position (d) was analysed with energy dispersive X-ray spectroscopy (EDX) at 1kx. The result of the EDX analysis is shown in (e). Iron is pigmented in red, alumina in blue and oxygen is died green. While iron was detected to be all over the sample image alumina and oxygen appeared always in combination as result of the Al_2O_3 which is used as support material within the oxygen carrier. Remarkably no Al_2O_3 did appear in the

outer layer which completely covers the sample. It can be deduced that the outer layer consisted completely of iron and that increasing number of cycles resulted in an accumulation of Al_2O_3 particles towards the centre of the oxygen carrier and therefore a gradual de-mixing occurred. The above mentioned grains in the inner part of the sample seemed to be made completely of Al_2O_3. Differences of the sample in position A and B could be attributed to a greater temperature gradient within the oxygen carrier material layer, as the particles in the middle of the bed did suffer a greater temperature change during the cycles as result of the strong exothermic oxidation reaction. Therefore, it is worth mentioning that the position of sampling is of mayor importance and further studies regarding this phenomenon should be conducted.

(a) (b)

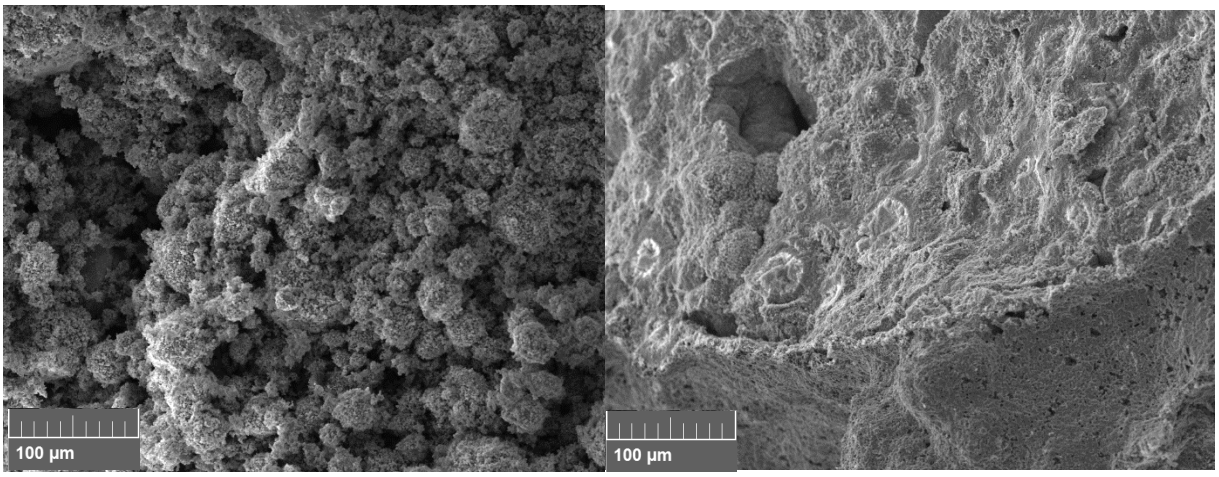

(c) (d)

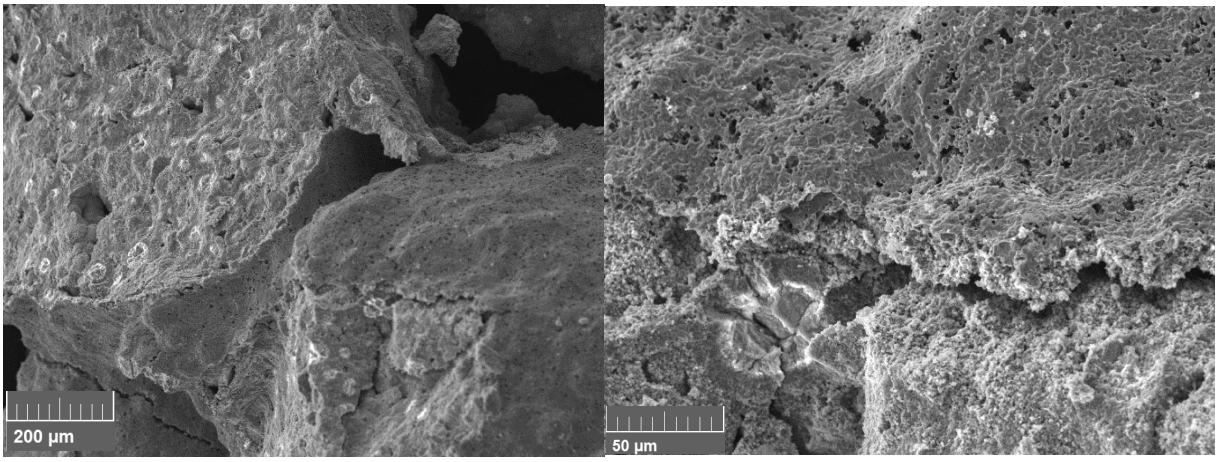

(e)

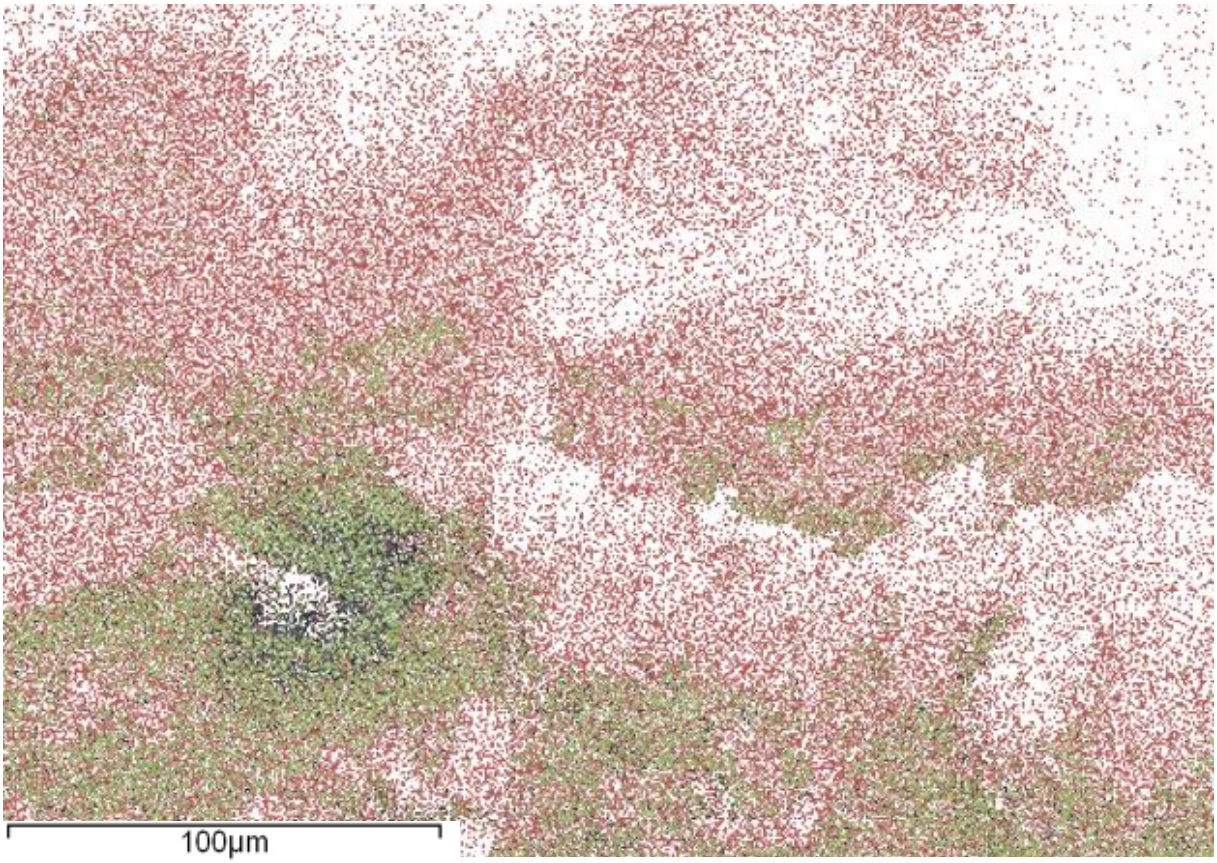

Figure 5-7: SEM images of oxygen carrier from position A at 500 x magnification (a) and from position B: 500 x (b), 200 x (c) and 1000 x (d) and EDX image of (d) (e)

5.7.2 Analysis of the inert material of the preheating zone

The inert material of the preheating zone was analysed and examined for carbon deposition. Visually it appeared clear and clean after reduction with methane. However blackish depositions were found on the particles facing the reactor wall (see Figure 5-8). A single pellet was analysed by SEM and EDX. An image of the depositions at 1kx magnification is presented in Figure 5-8 manifesting a uniform fissured layer (c). EDX analysis revealed peaks of alumina and oxygen but also traces of iron, manganese, nickel and chrome (d).

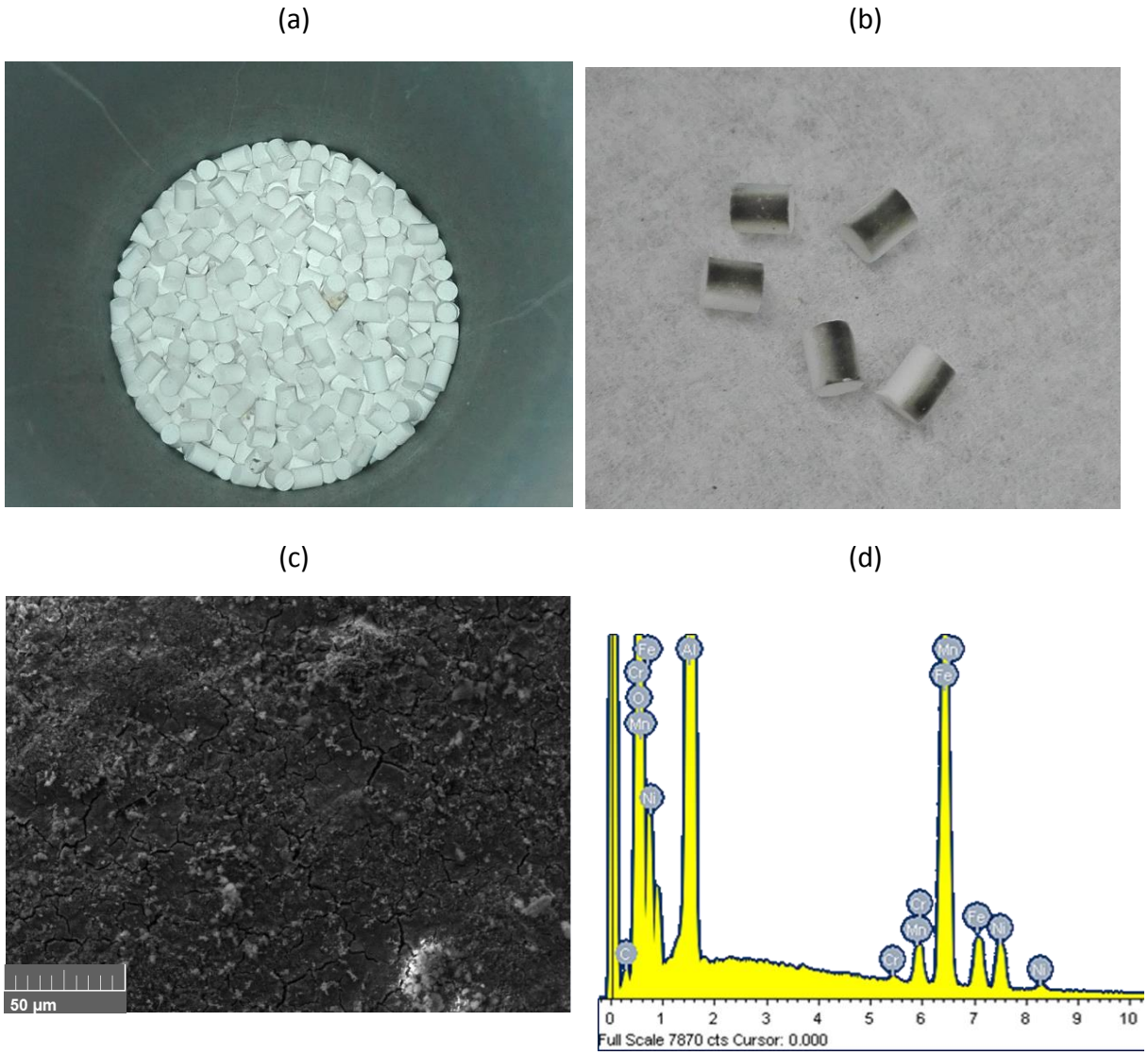

Figure 5-8: Inert material of the preheating zone: topmost layer (a) and selected particles with blackish depositions (b). SEM image at 1kx magnification of straining (c) and EDX spectrum (d)

As the latter three elements did only appear in the experimental setup as alloys for the reactor material, their arising is attributed to metal dusting. Metal dusting is referred as the disintegration of metals and metal alloys to fine dust of graphite and metal particles in a carburizing atmosphere. It occurs in processes involving reforming of methane or natural gas and direct iron-ore reduction. Increase of process efficiency by a reduction of the S/C ratio as well as a high CO/CO_2 ratio results in an increase of the carbon activity of the syngas, which makes metal dusting more likely to occur. The presence of CO and/or HC in the gaseous phase leads to tendency for graphite formation and hence carbon activity of the gaseous phase is greater than one (a_C >1). Carbon dissolves into the metal lattice and carbon accumulations grow resulting in pits and grooves in the material. Critical temperature range for metal dusting is reported to be from 400 to 750°C [47] which coincides with the temperature during reduction in the preheating zone for given experimental setup. [48][49]

6 Results for addition of C_x compounds to the reductive gas – model compound: Propane

Propane is of the group of liquefied petroleum gases. It has the chemical formula C_3H_8 and is a gas at standard temperature and pressure.

Experiments with propane in the reductive gas were carried out with experimental setup version 1. Propane was delivered as pressurised gas, wherefore the gas bottle of methane had simply to be substituted by propane and the fluid conversion factor for the MFC taken into account.

6.1 Propane operation points

Propane was introduced as model compound for acyclic hydrocarbons. As shown in Table 4-1 biogas can contain up to 1500 mg of total acyclic HC per cubic meter of biogas. Of those close to 500 mg m^{-3} can be acyclic HC with carbon chain length until C_5.

Table 6-1 gives an overview of the investigated propane OP and their respective parameter. 2.5 and 5 vol% of propane were added to the feed of reductive gas. Those are equivalent to 500 mg m^{-3} of biogas and 1000 mg m^{-3} respectively. Water flow during reduction was adjusted to ensure constant steam to carbon ratio of 1.4. During oxidation 6.96 g min^{-1} of steam were feed and time was adjusted to ensure full oxygen carrier conversion.

Table 6-1: Overview of investigated propane operation points

	H_2	C_3H_8		Water	S/C	Ox time	Relative OC conversion
	NL min^{-1}	NL min^{-1}	vol%	g min^{-1}	mol_S mol_C^{-1}	min	%
1st C_3H_8 OP	15	0.45	2.5	1.57	1.4	25	56%
2nd C_3H_8 OP	11	0.76	5	2.44	1.36	20	46%

Table 6-1 gives and overview of the propane operation points and the consecutive oxygen carrier conversion. Notable is the drop of OC conversion as a result of increasing propane concentration in the reductive gas feed. Analogous to reduction with methane the explanation is given by the high excess steam already discussed in chapter 3. A total of 31 cycles was performed, of which the first eight cycles were performed to reach a stable mass difference of the oxygen carrier. Detail information of every cycle is given in Table 11-4.

6.2 Reduction

Before starting the experiments, the GC system was calibrated to detect higher HC as ethane, propane as well as ethine and ethene in a combined peak. The GC was not calibrated to detect

other C_3 molecules than propane. Figure 6-1 shows the concentration of known detected impurities during the first propane OP. During reduction fractions of carbon monoxide, methane, carbon dioxide, unreacted propane and incompletely reformed C_2 fractions arose in descending quantity. Additionally, the GC system detected a not calibrated peak, which could be allocated to propene. For more detailed information about the appearing C_2 molecules a sample of the off gas was measured externally with a GC 3000 system. Results showed that no ethine was present in the off gas during reduction. Therefore, the combined C_2H_2/C_2H_4 peak can be completely allocated to C_2H_4. To be able to quantitatively analyse the arising C_2H_4 impurities a conversion factor based on the GC 3000 analysis is calculated to relate the peak area of the GC Fusion system to the C_2H_4 quantity. Mentioned calculation can be found in the appendix.

Reactor temperature decreased constantly during reduction as a result of the endothermic hydrocarbon reformation. The lowest recorded temperature was about 680°C after 60 minutes of reduction time at the 2nd C_3H_8 OP and about 710°C for the 1st C_3H_8 OP. Propane conversion of more than 90% for the 1st C_3H_8 OP was calculated based on the relation between input propane flow and propane content in the off gas. For the 2nd C_3H_8 OP conversion was always higher than 80%.

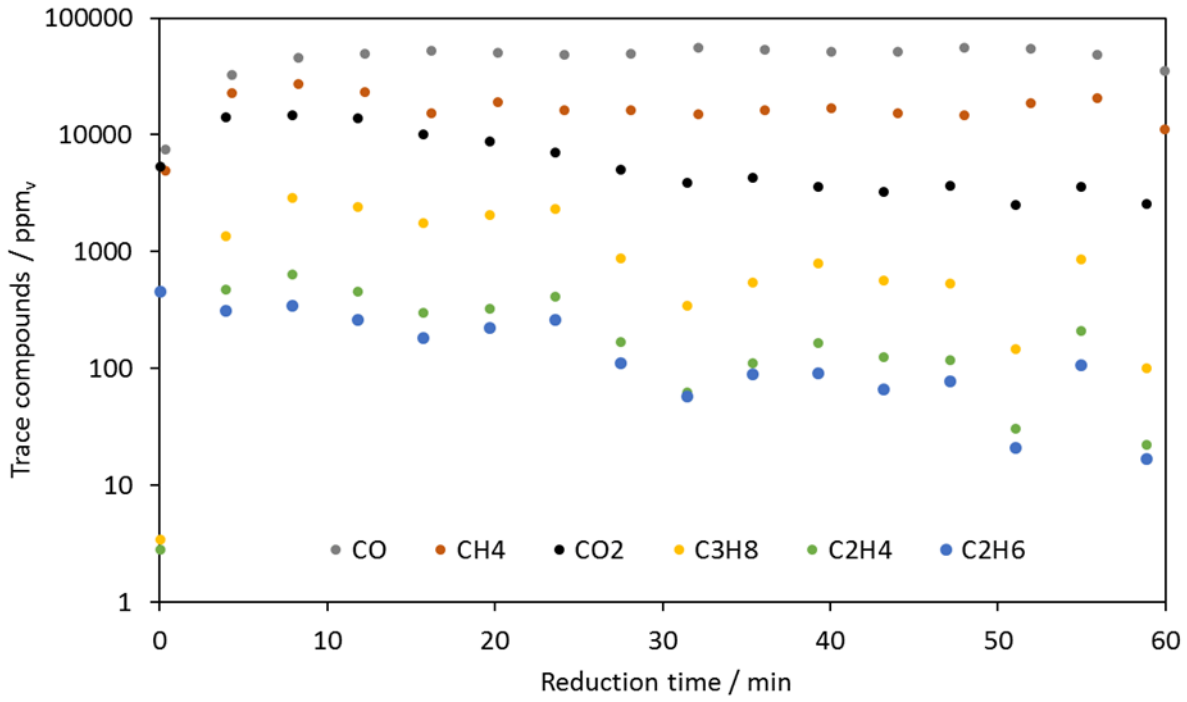

Figure 6-1: Off gas analysis during reduction of 1st C_3H_8 OP, average cycles 9-10

6.3 Steam oxidation

Figure 6-2 illustrates the hydrogen production and impurities during steam oxidation after reducing the oxygen carrier with 2.5 vol% of C_3H_8 in the feed gas. In the oxidation phase arising CO and CO_2 impurities behaved analogously to methane experiments. Again they featured a

U-shape characteristic and relative CO and CO_2 impurities were high at the beginning when H_2 production was low. The level of all other impurities during the remaining oxidation was much lower. Therefore scaling was adjusted in Figure 6-2 (b). While C_2H_6 was never detected during oxidation traces of CH_4, C_2H_4 and C_3H_8 arose at small quantities.

An increase of impurities with ongoing number of cycles related to carbon deposition not observed.

(a)

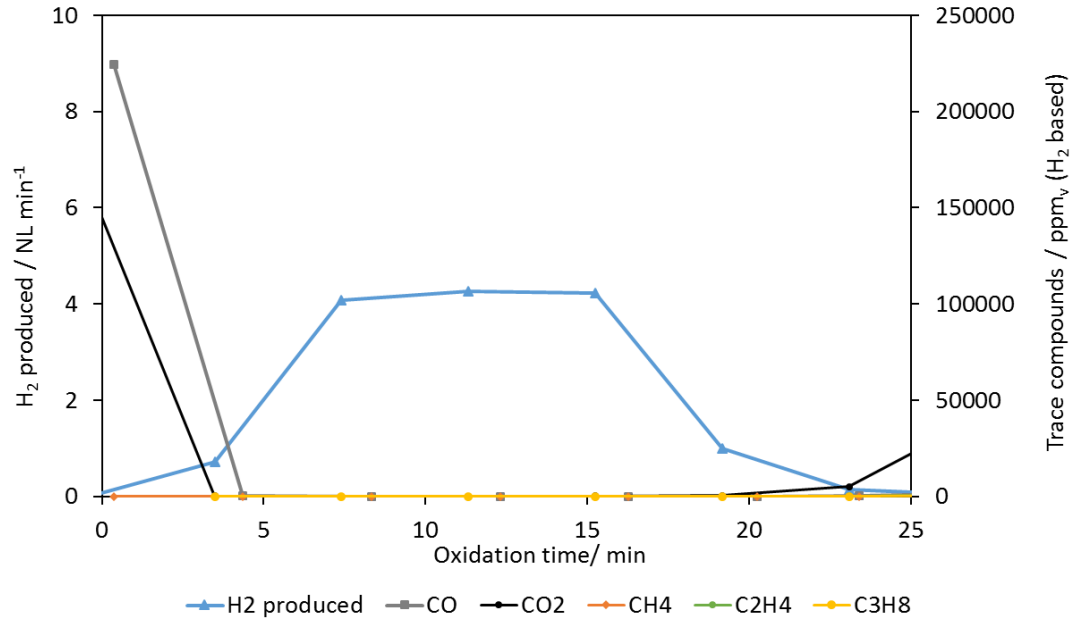

(b)

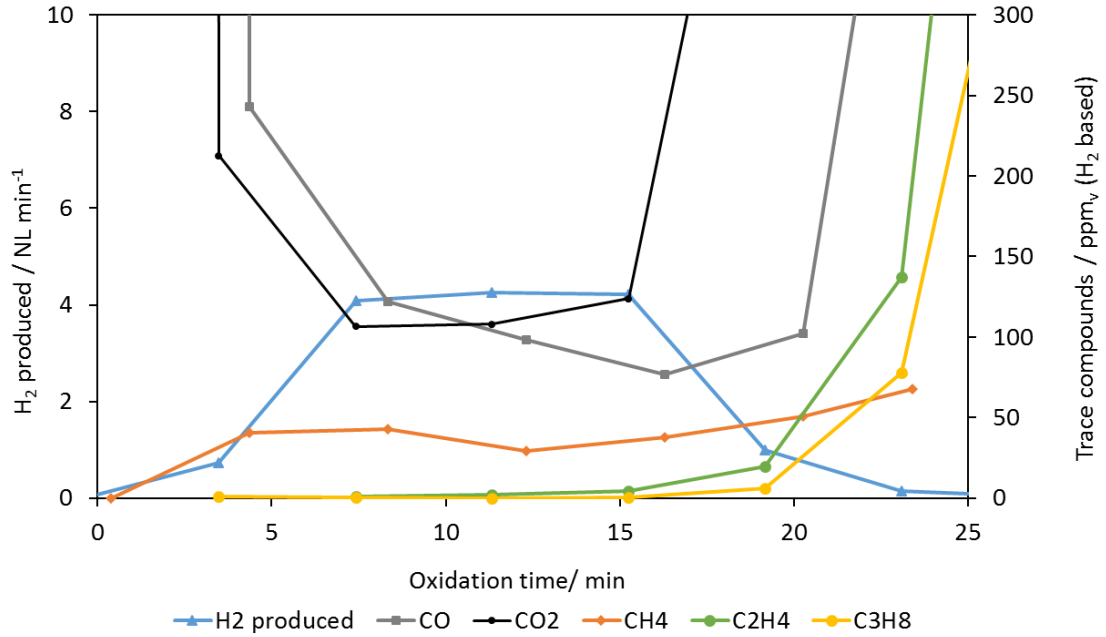

Figure 6-2: H_2 production and impurities during oxidation, 1st C_3H_8 OP, average for cycles 9-10 (a). Identical plot as in image 1 with adjusted scaling (b).

6.4 Reactor evacuation before steam oxidation

In order to eliminate impurities related to incomplete purging the reactor was evacuated after reduction. Evacuation procedure was already described in chapter 4.2.

Effects of evacuation were investigated for the 1st and 2nd C_3H_8 OP and results are shown in

Table 6-2. When reducing with propane in the reductive gas, only 10 to 16 % of total carbonaceous impurities were removed by evacuation. This is way less than for reduction with methane in the feed gas, where roughly 50% were removed. Nevertheless, results obtained by the methane experiments were confirmed by evacuation during the propane experiments. Once again evacuation hat the greatest effect on gaseous hydrocarbons. CH_4, C_2H_4 and C_3H_8 could always be removed by more than 60%. As those compounds are not expected to be formed, their arising was attributed to incomplete purging of the dead zones within the reactor system. Longer holding of the vacuum and a higher number of evacuations as well as longer purging is expected to result in further removal of compounds allocated to gas remains. Again impurities allocated to reoxygenation of carbon settlements could not be lowered significantly. Although the cycles were always performed identically, the total amount of impurity for CO_2 or CO was higher after evacuation. As all other impurity levels were lowered by evacuation these are regarded as runaway values.

Table 6-2: Influence of reactor evacuation for 1st and 2nd C_3H_8 OP

		1st C_3H_8 OP			**2nd C_3H_8 OP**		
			evacuation			**evacuation**	
Average cycles		9-10	13-15	compound removal	16-18	24-26	compound removal
CO_2	ppm_v (H_2 based)	274	252	8%	194	264	-36%
CO	ppm_v (H_2 based)	121	130	-8%	236	150	36%
CH_4	ppm_v (H_2 based)	38	12	68%	37	12	68%
C_2H_4	ppm_v (H_2 based)	7	1	85%	32	1	98%
C_3H_8	ppm_v (H_2 based)	2	1	63%	13	5	59%
total	ppm_v (H_2 based)	442	396	10%	512	432	16%

For the 2nd C_3H_8 OP the effect of evacuation is shown for CO_2 and C_2H_4 exemplarily in Figure 6-3. The average value for cycles 16-18 without evacuation are presented in dotted lines and empty spots and the average cycles 24-26 with reactor evacuation are marked by continuous lines and coloured spots. It can be seen that CO_2 impurities were not affected by reactor evacuation, while C_2H_4 appearance could be lowered significantly. CO impurities showed the same behaviour as CO_2, while CH_4 and C_3H_8 impurities were significantly reduced by evacuation (see Table 6-2).

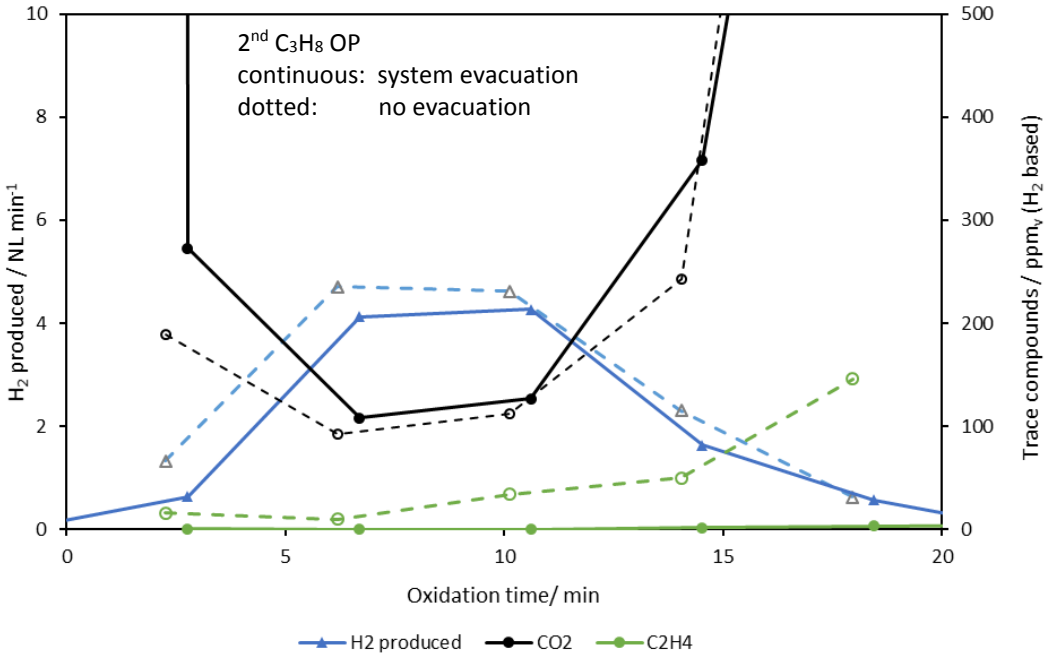

Figure 6-3: Influence of evacuation on C_2H_4 and CO_2 impurities for the 2nd C_3H_8 OP (average for cycles 24-26) and without evacuation (average for cycles 16-18).

6.5 Influence of prolonged reactor purging

In order to eliminate impurities which are allocated to incomplete reactor purging the reactor was purged overnight. Nitrogen flow was set to 0.5 NL_{N2} min^{-1}. To further investigate purging effects the reactor was purged for 30 minutes after reduction at the 2nd C_3H_8 OP. For these cycles nitrogen flow was kept at 5.9 NL_{N2} min^{-1}.Results are shown in Table 6-3.

As a result of overnight purging total amount of impurities of the produced hydrogen could be removed by 60% for both OP. Higher hydrocarbons like CH_4, $C2H_4$ or C_3H_8 were not detected at any point after overnight purging. It is assumed that all trace gases from reduction were completely eliminated. The removal of carbon oxide impurities by 40 to 50% for CO and by roughly 70% for CO_2 by purging are also attributed to removal of reductive gas remains. Remaining carbon oxide impurities can hence be attributed solely to reoxidation of elemental carbon. Further impurity removal due to longer purging is not expected, as purging does not eliminate carbon settlements. The much higher share of CO_2 compared to CO in purged

reactor oxidation is further hint that solid carbon tends for complete reoxidation (Equation (3-9)) at high oxygen abundance.

The outcome for 30 minutes purging time also exhibits the influence of purging, but at a lower extent than overnight purging. CO was reduced, while CO_2 was not significantly affected. The level of hydrocarbons was reduced, but they were not completely eliminated. 30 minutes of purging with a nitrogen flow of 5.9 NL min^{-1} were hence not enough to purge the reactor completely. Total impurities were lowered by 24%. For longer purging and the involved further reduction of total impurities an optimum of regarding purging time, impurity removal and operation costs has to be found.

Table 6-3: Influence of extended reactor purging

		1st C_3H_8 OP			**2nd C_3H_8 OP**				
			overnight purging			**overnight purging**		**30 min purging**	
Average cycles		9-10	12	compound removal	16-18	22	compound removal	27-29	compound removal
CO_2	ppm_v (H_2 based)	274	142	48%	194	114	41%	219	-13%
CO	ppm_v (H_2 based)	121	37	69%	236	59	75%	118	50%
CH_4	ppm_v (H_2 based)	38	0	100%	37	0	100%	35	6%
C_2H_4	ppm_v (H_2 based)	7	0	100%	32	0	100%	8	75%
C_3H_8	ppm_v (H_2 based)	2	0	100%	13	0	100%	7	50%
total	ppm_v (H_2 based)	442	179	60%	512	173	66%	387	24%

6.6 Extended storage of reactor in reduced state

The reactor was stored for an extended time period after reduction with propane in the feed gas to investigate the hydrogen storage with the CLH process. Experimental procedure was carried out analogous to storage investigation for the methane experiments and procedure explanation can be found in chapter 5.6. Measured impurities during the oxidation phase after reducing with propane in the feed gas and subsequent reactor storage are listed in Table 6-4.

After reducing according to the 1st C_3H_8 OP the reactor was stored for 67 hours. Although propane content for the 1st C_3H_8 OP with 2.5 vol% C_3H_8 in the reductive gas was in the same range as methane content for the 1st CH_4 OP (2 vol% of CH_4), the effects of long time storage were not as incisive. 68 hours of storage after methane reduction resulted in complete methane removal during oxidation, whereas approximately 10% of methane were still present when the reactor was stored after reduction with propane in the feed gas. Furthermore, also C_2H_4 and C_3H_8 were detected during the oxidation phase. Methane removal during storage is attributed to thermal breakdown of the molecule. Hence the occurrence of hydrocarbons during the oxidation after storage for the propane experiments is attributed to incomplete hydrocarbon reforming during the storage time.

After reduction according to the 2nd C_3H_8 OP the reactor was stored for 89 hours. Here effects already observed during storage with methane experiments were more distinctively developed. Longer storage resulted in a lower amount of all impurities, with except of CO_2. The increase of CO_2 was already explained in chapter 5.6. The increased removal of hydrocarbons is attributed to a higher reformation rate as result of longer storage time.

Table 6-4: Influence of reactor storage for 68 hours after reduction at 1st and 2nd C_3H_8 OP

		1st C_3H_8 OP			**2nd C_3H_8 OP**		
			after 67 h storage			**after 89 h storage**	
Average cycles		9-10	11	compound removal	16-18	19	compound removal
CO_2	ppm_v (H_2 based)	274	210	23%	194	211	-9%
CO	ppm_v (H_2 based)	121	38	69%	236	53	78%
CH_4	ppm_v (H_2 based)	38	5	87%	37	5	88%
C_2H_4	ppm_v (H_2 based)	7	2	68%	32	3	89%
C_3H_8	ppm_v (H_2 based)	2	1	63%	13	2	89%
total	ppm_v (H_2 based)	442	256	42%	512	273	47%

A higher quality of the produced hydrogen can be expected if the reactor is stored in a hydrocarbon free atmosphere. Longer reactor purging or evacuation of the reactor system before storage are expected to improve the purity of the hydrogen stream and therefore increase storage efficiency with the RESC.

7 Results for addition of organic alcohols to the reductive gas – model compound: Ethanol

Ethanol (EtOH) is found and produced worldwide. As it is universally available, it has a great potential as energy carrier or as fuel of the future. It can either substitute gasoline as fuel, be used as a fuel blend or as a source of H_2 for fuel cells. Favourable are also its attributes like biodegradability, low toxicity and ease of handling in storage and distribution. [50] [23]

Globally over 90% of ethanol is produced via fermentation of sugars. These biological process requires little know-how, is technically mature and universally known. The biomass feedstock for the fermentation can origin from various glucose-rich sources such as corn, wheat, potatoes, sugarcane, etc. Bioethanol produced via fermentation contains about 85% of water. To use it as fuel or fuel additive a further distillation step is required. The balance is produced via hydration of ethylene and used for industrial grade pure ethanol. [51]

Ethanol is also a promising source for H_2 production, wherefore ethanol steam reforming (ESR) is widely studied in literature.

7.1 Theory of ethanol steam reforming

Steam reforming of ethanol is an endothermic process. The overall steam reforming reaction consists of reacting one mole of ethanol with three moles of water (see Equation ((7-1)). Incomplete reforming results in syngas according to Equation (7-2). Depending on the catalyst different reaction pathways can occur. As consequence, a complex reaction network which includes dozens of potential products is characteristic for ethanol reforming. Liquid ethanol is thermochemical broken down into shorter carbonaceous species. A simplified reaction scheme is presented in Figure 7-1. Dehydration (Equation (7-3)) leading to the presence of C_2H_4 has to be avoided since further polymerization reactions lead to coke formation. Dehydrogenation (Equation (7-4)) results in formation of acetaldehyde (C_2H_4O), which in turn reacts to methane (Equation (7-5)) or is further reformed by steam (Equation (7-6)). Methane can result from direct decomposition of ethanol (Equation (7-7)). Rabenstein et.al. [50] reported decomposition into acetone, ethane and acetylene. Additionally the intermediate products water, methane, carbon dioxide and carbon monoxide take part in previously discussed equilibrium reactions like SMR, water gas shift reaction or the Boudouard reaction.

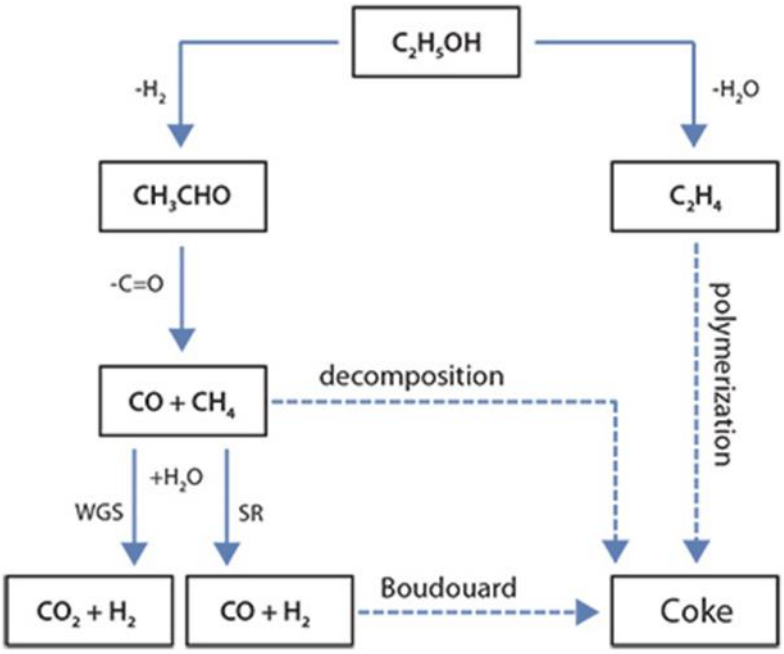

Figure 7-1: Reaction mechanism scheme of ethanol steam reforming [57]

$$C_2H_5OH + 3\,H_2O \rightarrow 2\,CO_2 + 6\,H_2 \qquad \Delta H_r = 347\frac{kJ}{mol} \tag{7-1}$$

$$C_2H_5OH + H_2O \rightarrow 2\,CO + 4\,H_2 \qquad \Delta H_r = 298\frac{kJ}{mol} \tag{7-2}$$

$$C_2H_5OH \rightarrow C_2H_4 + H_2O \tag{7-3}$$

$$C_2H_5OH \rightarrow C_2H_4O + H_2 \tag{7-4}$$

$$C_2H_4OH \rightarrow CH_4 + CO \tag{7-5}$$

$$C_2H_4O + H_2O \rightarrow 3H_2 + CO \tag{7-6}$$

$$C_2H_5OH \rightarrow CH_4 + CO + H_2 \tag{7-7}$$

Rabenstein et. al. [50] calculated thermodynamics of ethanol steam reforming. They report methane and carbon dioxide to be the main products at low temperatures. At higher temperatures CO content increased, which is in accordance with the WGS reaction. They report, that coke formation can only be avoided if steam-to-ethanol (S/E) ratio is higher than 3.

7.2 Ethanol operation points

Ethanol was chosen as model compound for organic alcohols which may be present in biogas. Literature reports biogas to contain up to 1400 mg of alcohols per m^3 and up to 270 mg m^{-3} of ethanol (Table 4-1). Therefore, reduction with different amounts of ethanol in the reductive gas was investigated. Parameters of the OP are listed in Table 7-1. Ethanol amount accounted

for 500, 1000 and 2000 mg of ethanol per m^3 of hydrogen. Ethanol concentration of the 3rd OP is higher than expected alcohol concentration in biogas. It was chosen to gain a better insight of the influence of ethanol on the reduction of the oxygen carrier.

Table 7-1: Overview of investigated ethanol operation points

	H_2	Ethanol			Feed
	NL min^{-1}	$mg_{Ethanol}$ m^{-3}	ppm	mL min^{-1}	mL min^{-1}
1st Ethanol OP	15	500	243	0.0095	0.014
2nd Ethanol OP	15	1000	486	0.019	0.027
3rd Ethanol OP	15	2000	972	0.038	0.054

The GC's did not have matching analysis times during experiments with ethanol. The first GC which was used to detect CO and CH_4 had an analysis time of approx. 2 minutes, while it took the other approximately 4 minutes until measurements were finished. To have time-matching data measurements of CO and CH_4 temporally nearest to the H_2/N_2 measurements were linearly interpolated.

7.3 Alumina oxide spheres as inert material of the preheating zone

To reduce gas adsorption on the inert material, experimental setup 2, with alumina oxide spheres as inert material in the preheating zone, was used for experiments with ethanol.

7.3.1 Reduction

Ethanol was fed in liquid state via the piston pump and the supply pipe was introduced directly in the reactor. The liquid feed was pre-mixed with water and 96% pure Ethanol in order to achieve a constant steam to carbon ratio of 1.4.

To investigate conversion rate for the given experimental conditions samples of the condensate were taken and analysed with a mass spectroscopy coupled gas chromatograph (GC MS). In order to ensure complete condensation, the wet scrubber was situated in an ice bed and the condensate of both reduction and oxidation phase of cycle 21 was collected. During neither phase ethanol was detected and complete conversion was assumed for all cycles. 100% of ethanol conversion over an Al_2O_3 catalyst is also reported by Llorca et. al. [52].

Figure 7-2 shows the gas analysis for the 1st and 3rd ethanol OP. Measurement for the 1st OP are marked by blank dots, while values for the 3rd OP are marked by filled dots. As expected a higher amount of ethanol in the feed results in higher amount of trace compounds. Ethane was only detected at the beginning of reduction of the 3rd ethanol OP. Otherwise no higher hydrocarbons were detected. This can be a hint for dehydration of ethanol to be more likely when the chemical equilibrium is not yet reached, as in the beginning of the reduction phase. Higher hydrocarbons as result of the dehydration pathway can result in coke formation.

The carbonaceous products in the off gas were mainly CH_4, CO and CO_2. Of those CO_2 accounted for the least amount, which is in accordance to thermodynamic calculations for reformation at higher temperatures by Rabestein [50]. The highest share of trace compounds for all three OP was CO.

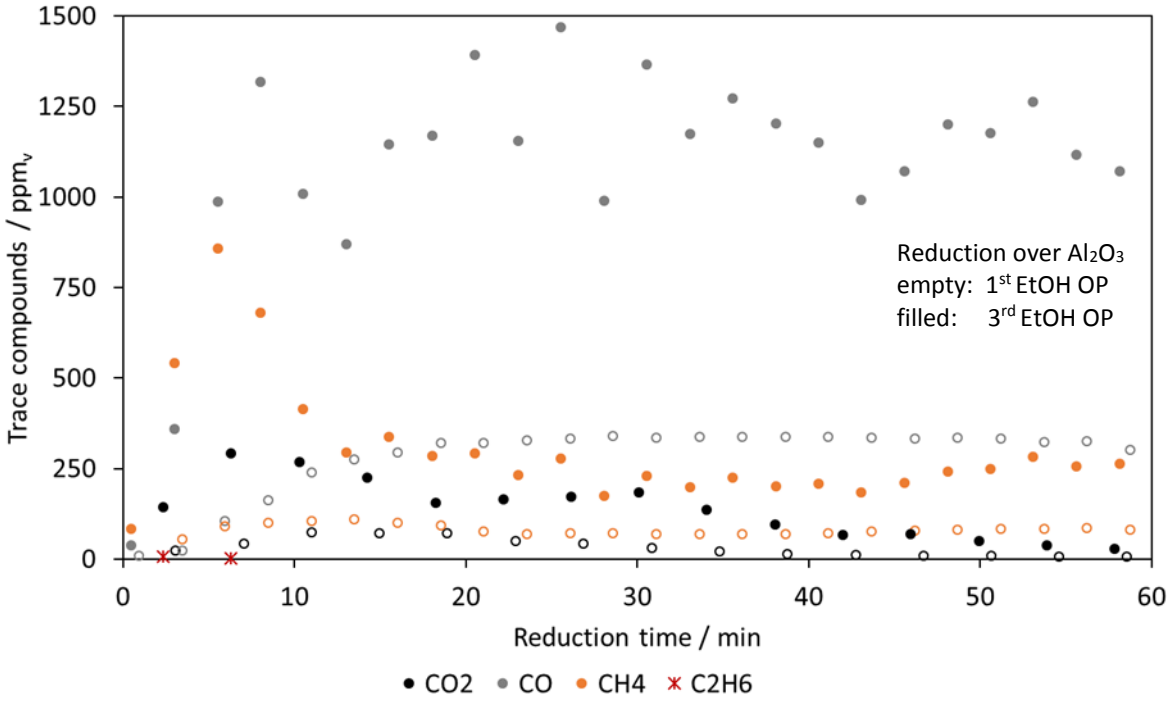

Figure 7-2: Off gas analysis during reduction of 1st and 3rd ethanol OP, average for cycles 13-16 and 31-32

7.3.2 Steam Oxidation

Steam oxidation for the 1st and 2nd ethanol OP was conducted with 9.6 g min^{-1} of water, while water flow was reduced to 6.9 g min^{-1} for the 3rd ethanol OP in order to elongate oxidation time and get additional measurement points for the gas analysis. Carbon oxides were the only arising impurities during oxidation and are attributed to reoxidation of solid carbon. Methane was never detected. Values for trace compounds of every cycle can be found in the appendix (Table 11-6).

Figure 7-3 (a) shows the produced amount of hydrogen and the carbonaceous impurities for the 1st and 2nd ethanol OP. For both an average value of four consecutive cycles is shown. The 1st OP is presented by continuous lines and filled spots and the 2nd OP by dotted lines and empty spots. Whereas the amount of produced hydrogen did not vary, impurities increased none linearly to the increase of ethanol concentration in the feed. Particularly the amount of carbon oxides for the first measurements do exhibit a great discrepancy as they are much higher for the 2nd OP. It is assumed that a higher amount of solid carbon is present, which

would suggest disproportional increase of coke formation at higher ethanol concentrations of the reductive gas.

No change of total amount of impurities was observed with ongoing cycles for the 1st and 2nd OP. However an increase of impurities was evident after every cycle at the 3rd ethanol OP. Image (b) and (c) in Figure 7-3 show CO and CO_2 impurities for succeeding cycles at the 3rd ethanol OP respectively. For both compounds an increase of impurity level was observed with ongoing number of cycles. Primarily at the beginning of the oxidation, when steam started to reach the system, the amount of impurities featured an increasing trend. Carbon accumulation seemed to be more significant the higher the ethanol concentration was, resulting in progressive contamination of the hydrogen stream.

(a)

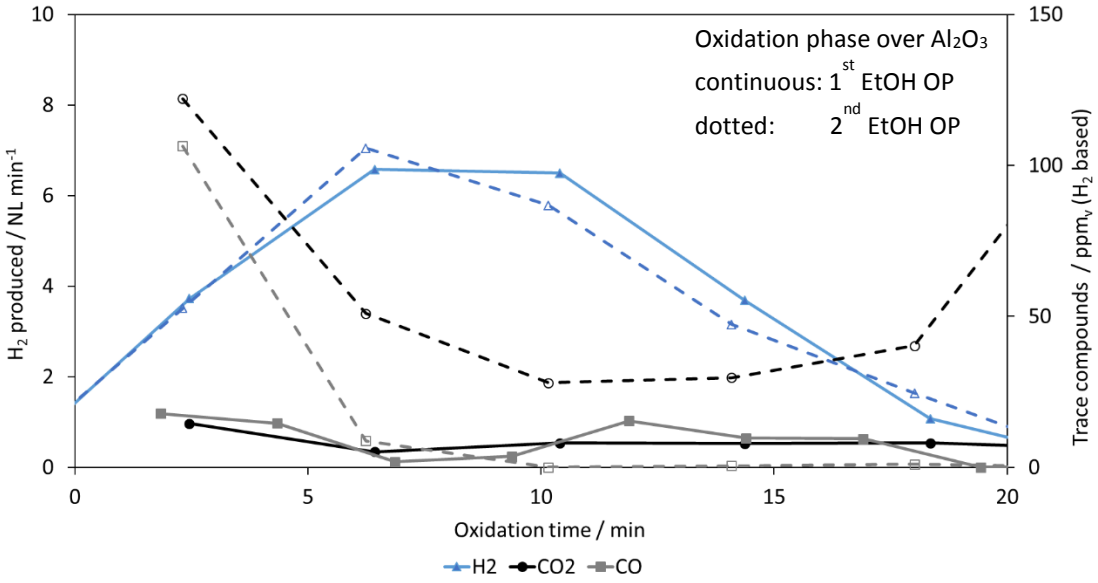

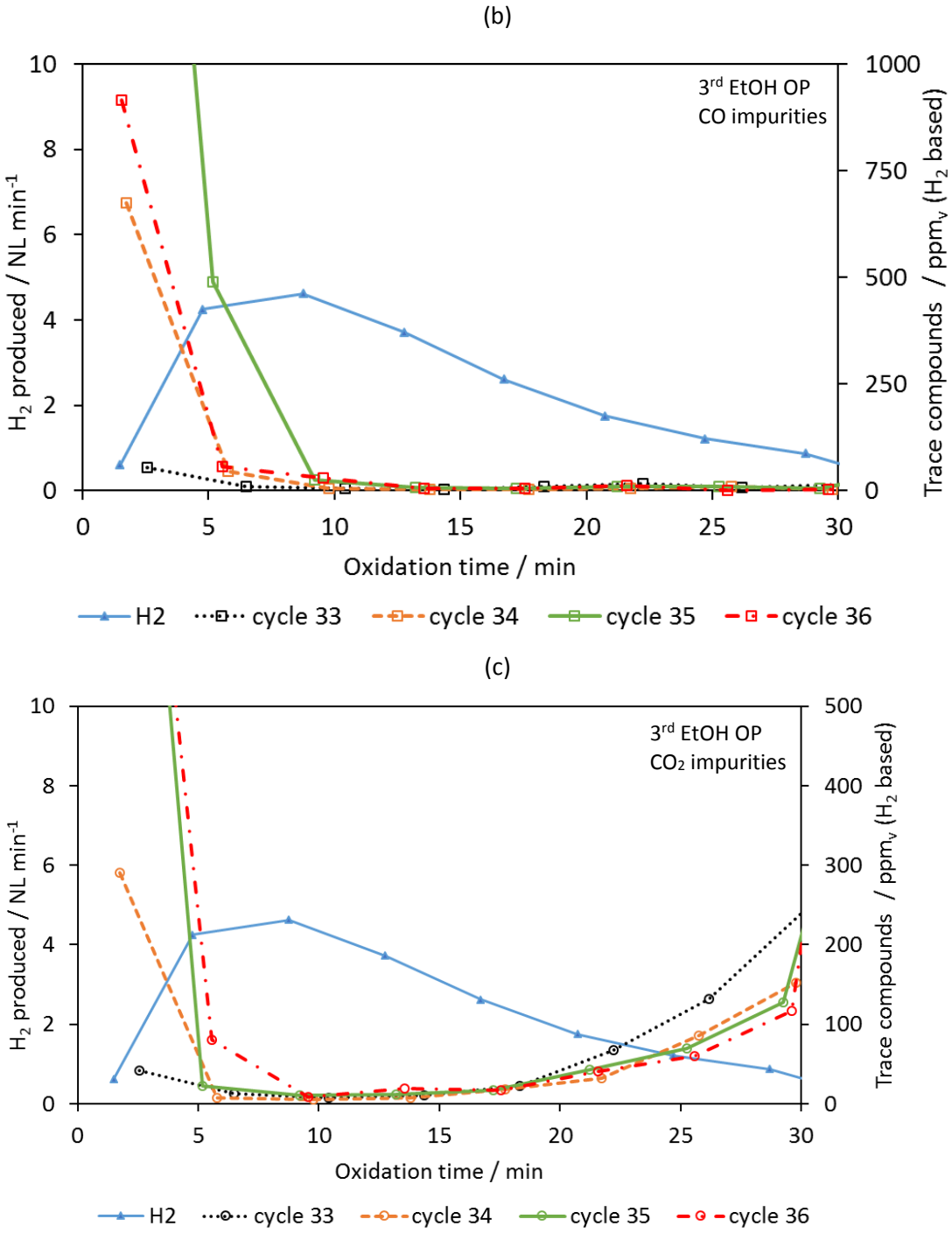

Figure 7-3: Produced H_2 and impurities during oxidation of the 1st ethanol OP (average cycles 13-16) and 2nd ethanol OP (average cycles 23-26) (a). Produced H_2 (average value cycles 33-36) and CO impurities of consecutive cycles of the 3rd ethanol OP (b). Produced H_2 (average value cycles 33-36) and CO_2 impurities of consecutive cycles of the 3rd ethanol OP (c).

7.3.3 Air Oxidation

The effect of air oxidation following the steam oxidation was investigated to show the effect on carbon accumulation. Three consecutive cycles were performed with air oxidation with the 3rd ethanol OP. For the subsequent steam oxidations impurity levels for CO and CO_2 are shown in Figure 7-4. Methane was not detected at any point. The values for produced H_2 amount were averaged from the investigated cycles. As values for impurities did not increase it is concluded that no carbon was accumulated during these cycles. Apparently air oxidation did eliminate all remaining carbon depositions and allowed the production of a constant hydrogen quality.

In Table 7-3 the amount of impurities based on the produced quantity of H_2 for oxidation phases after reduction according to the 3rd ethanol OP are listed. It is clearly visible that the contamination of the produced hydrogen stream increases with ongoing numbers of cycles from cycle 33 to cycle 36. Total impurities increased by 37% after one cycle and by 290% for the 4th consecutive cycle. As already discussed this is attributed to significant carbon depositions when ethanol was present in the reductive gas. After performing an air oxidation the impurity levels were lowered by roughly 50% in average compared to cycle 33. This result suggests that carbon depositions were completely eliminated with air oxidation and hydrogen production with a high purity is achievable if air oxidation is performed always after steam oxidations.

(a)

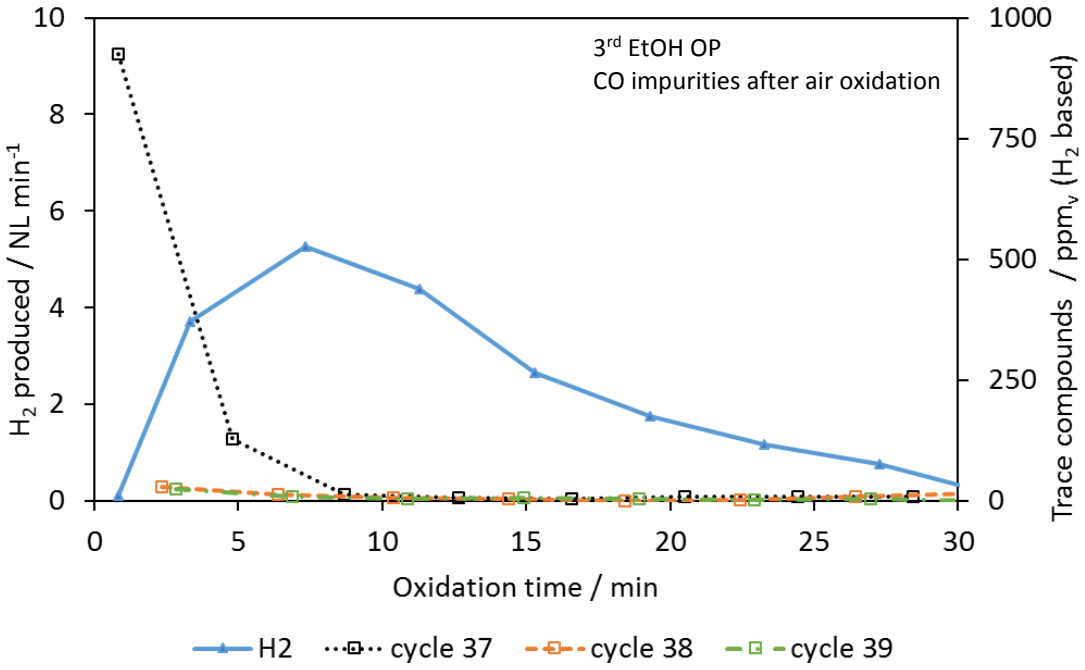

(b)

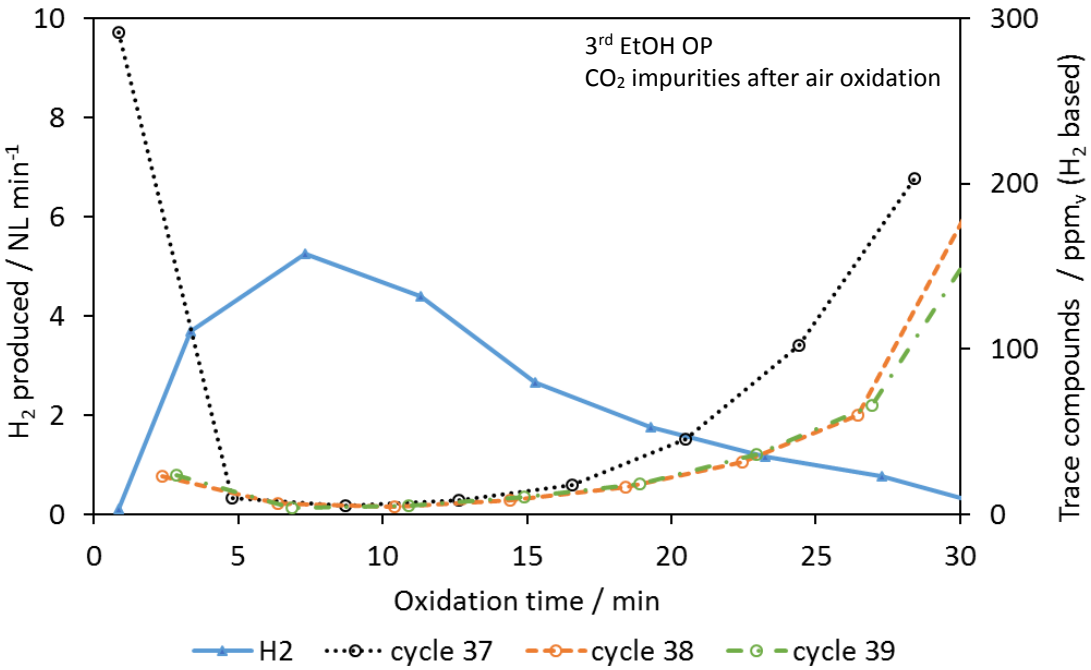

Figure 7-4: Produced H_2 (average value cycles 37-39) and CO impurities of consecutive cycles with air oxidation in between (a). Produced H_2 (average value cycles 37-39) and CO_2 impurities of consecutive cycles with air oxidation in between (b).

Table 7-2: Increase of produced H_2 impurity for consecutive cycles with ethanol in the reductive gas and influence of air oxidation. Reduction according to 3rd ethanol OP

		consecutive cycles			Air oxidation		
Cycles		33	34	36	38	39	average compound removal
CO_2	ppm_v (H_2 based)	34	30	114	16	16	53%
CO	ppm_v (H_2 based)	16	38	80	11	9	37%
total	ppm_v (H_2 based)	50	68	193	28	24	48%

7.3.4 Analysis of the oxygen carrier

To investigate carbonaceous depositions in the system, a prolonged reduction was performed at last. Reduction was performed with the 3rd ethanol OP for the first hour, the following four hours input streams were halved, while all process parameters were kept constant (Ethanol = 2000 mg m_{BG}^{-3}, S/C=1.4).

Samples of the middle of the first layer of oxygen carrier (position A) and from the middle of the oxygen carrier bed, close to the reactor wall (position B), were taken. From both samples a representative pellet was analysed with LM. The pellets were not conditioned and images of the top view with 250 x magnification are presented in Figure 7-5. Differences between the two pellets are easily visible. While the pellet close to the reactor wall (b) featured the typical

characteristics of reduced oxygen carrier (see chapter 4.3), the pellet from position A (a) seem to be covered by a shell-like dense layer. As the pellet in the middle of the reactor did suffer a greater temperature variation, their change of morphology was greater to those in regions with less drastic temperature fluctuations. Coke as a result of carbon formation was not visible on the analysed oxygen carrier samples.

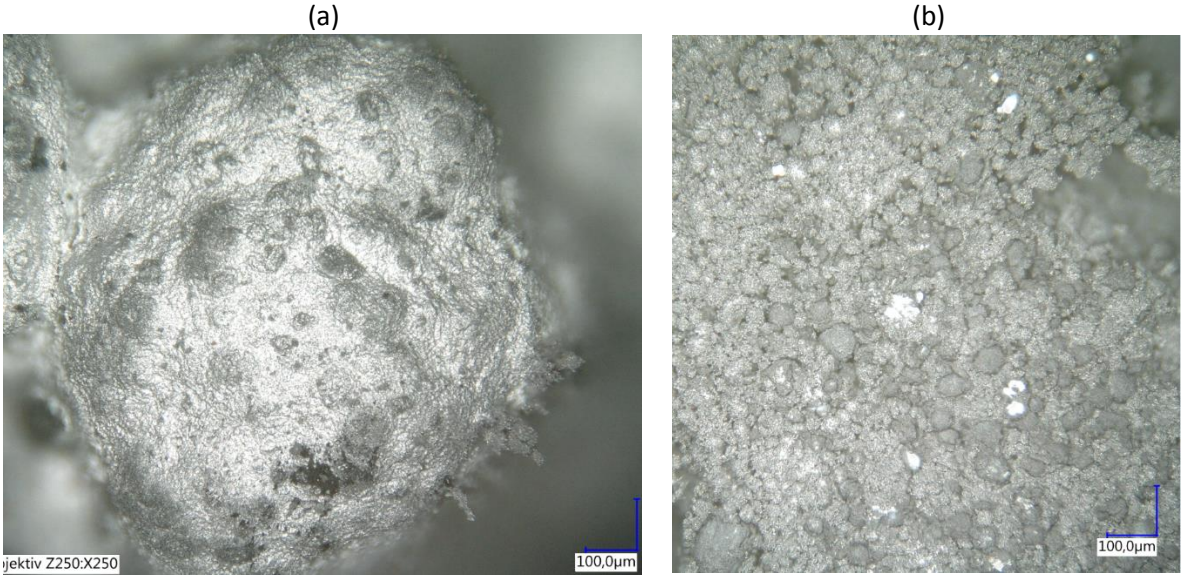

Figure 7-5: LM image (250 x) of cycled sample from position A (a) and B (b)

7.3.5 Analysis of the inert material of the preheating zone

After the tests the alumina oxide spheres from the preheating zone were partly covered by a blackish layer (Figure 7-6 a). The position of the layer could not be allocated to a certain direction nor position of the spheres within the reactor – as shown in (b). A selected particle was analysed with LM, SEM and EDX. Images from LM at 250 x magnification (c) and from SEM at 200 x magnification (d) revealed a closer look of the particle surface. The blackish coating looked to be a layer of scattered matter adhesive to the surface. EDX analysis revealed alumina, oxygen, iron and carbon (e). Amount of carbon on the inert material could not be quantified as peak height in the spectrum is not proportionally to quantity. Nevertheless, carbon seems to settle on the inert material pellet. To further investigate the carbon deposition on the inert material pellets more analysis is required. Alumina and oxygen are components of the inert material spheres and therefore iron the only foreign metal. No alloy elements of the reactor material, which would hint to metal dusting, were found. Image (f) shows the appearance of iron detected by the EDX analysis for image (d). Depositions seen by light microscopy in image (d) coincide with appearance of iron in image (f). The iron could origin from metal dusting or be pulverized oxygen carrier, which agglomerated on the inert material spheres.

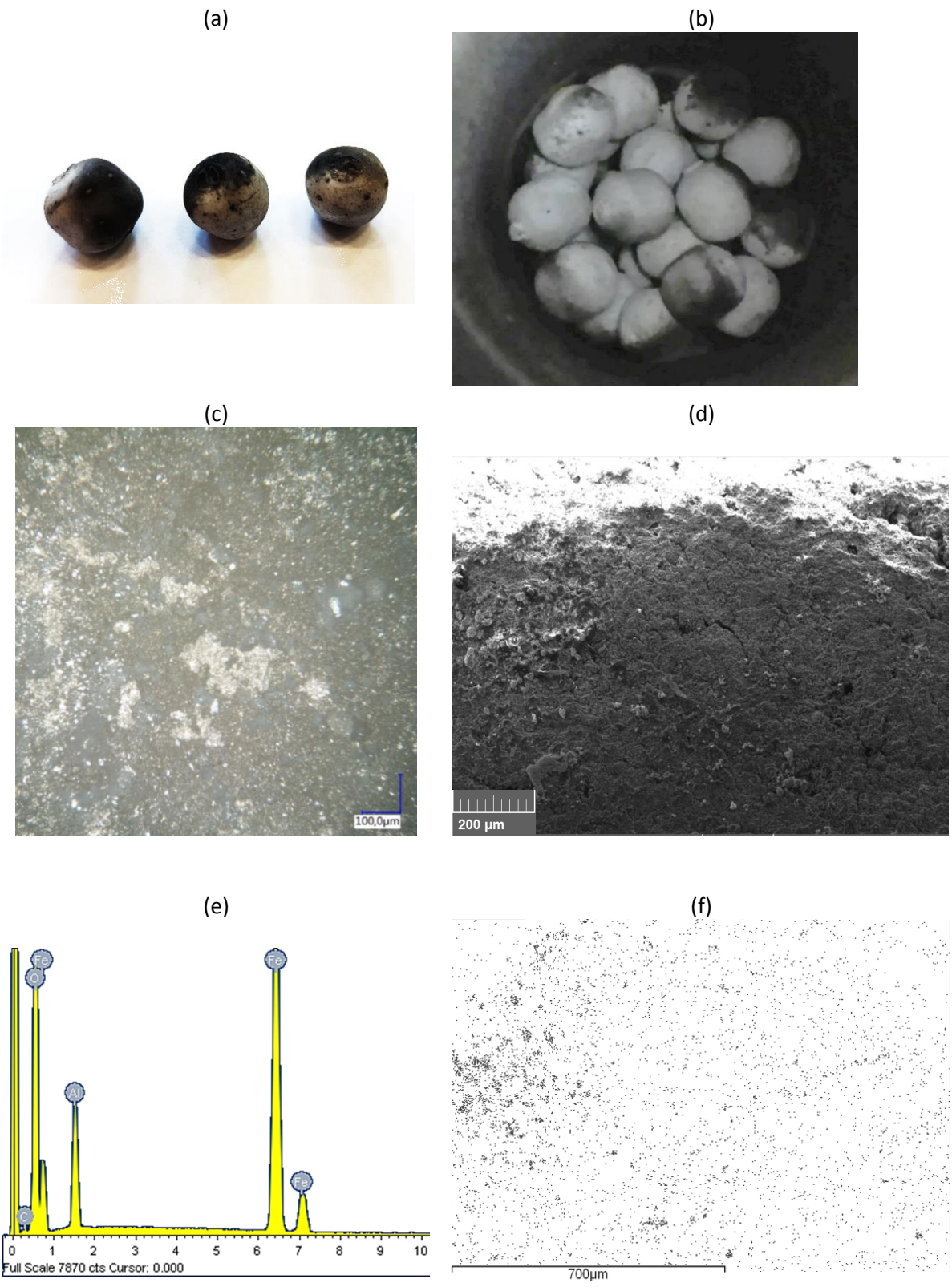

Figure 7-6: Alumina spheres covered by blackish layer (a). First sphere layer of the preheating zone in the open reactor (b). LM image at 250 x magnification (c) and SEM image at 200 x magnification (d). Spectrum of EDX (e) and occurrence of Fe from image d (f).

7.4 Silica oxide pellets as inert material in the preheating zone

Literature [53] states that acidic sites on catalyst surfaces promote coke formation by polymerization reactions. Therefore, the first layer of inert material previously consisting of Al_2O_3 was substituted by SiO_2 for its less acidic nature.

In order to directly compare the influence of SiO_2 to Al_2O_3, the 1st and 3rd ethanol operation points were investigated. Values for trace compounds of every cycle can be found in the appendix (Table 11-7). Condensate from reduction and oxidation phase were analysed with the GC-MS for traces of ethanol. As no ethanol was detected it can be assumed that ethanol is completely reformed.

Experimental setup version 3 was used when SiO_2 was used as inert material in ethanol experiments.

7.4.1 Reduction

Higher hydrocarbons as C_2H_6 or C_2H_2/C_2H_4 were detected only the first few minutes of reduction over both inert materials. While for Al_2O_3 no higher hydrocarbons were detected at the 1st ethanol OP, use of SiO_2 resulted in detection of C_2 compounds. Operation points with a higher amount of ethanol resulted in a greater amount of higher hydrocarbons. Nevertheless, also for the 3rd ethanol OP higher hydrocarbons were detected only the first few minutes. As already discussed this could be due to the fact that equilibria for other compounds were not yet achieved and the dehydration route for ethanol reforming is enhanced. Figure 7-7 illustrate all detected impurities for the 1st (a) and 3rd (b) ethanol OP over Al_2O_3 (blank dots) and SiO_2 (filled dots) respectively. For both OP impurities seemed to trend towards the same equilibrium value independently which inert material was used.

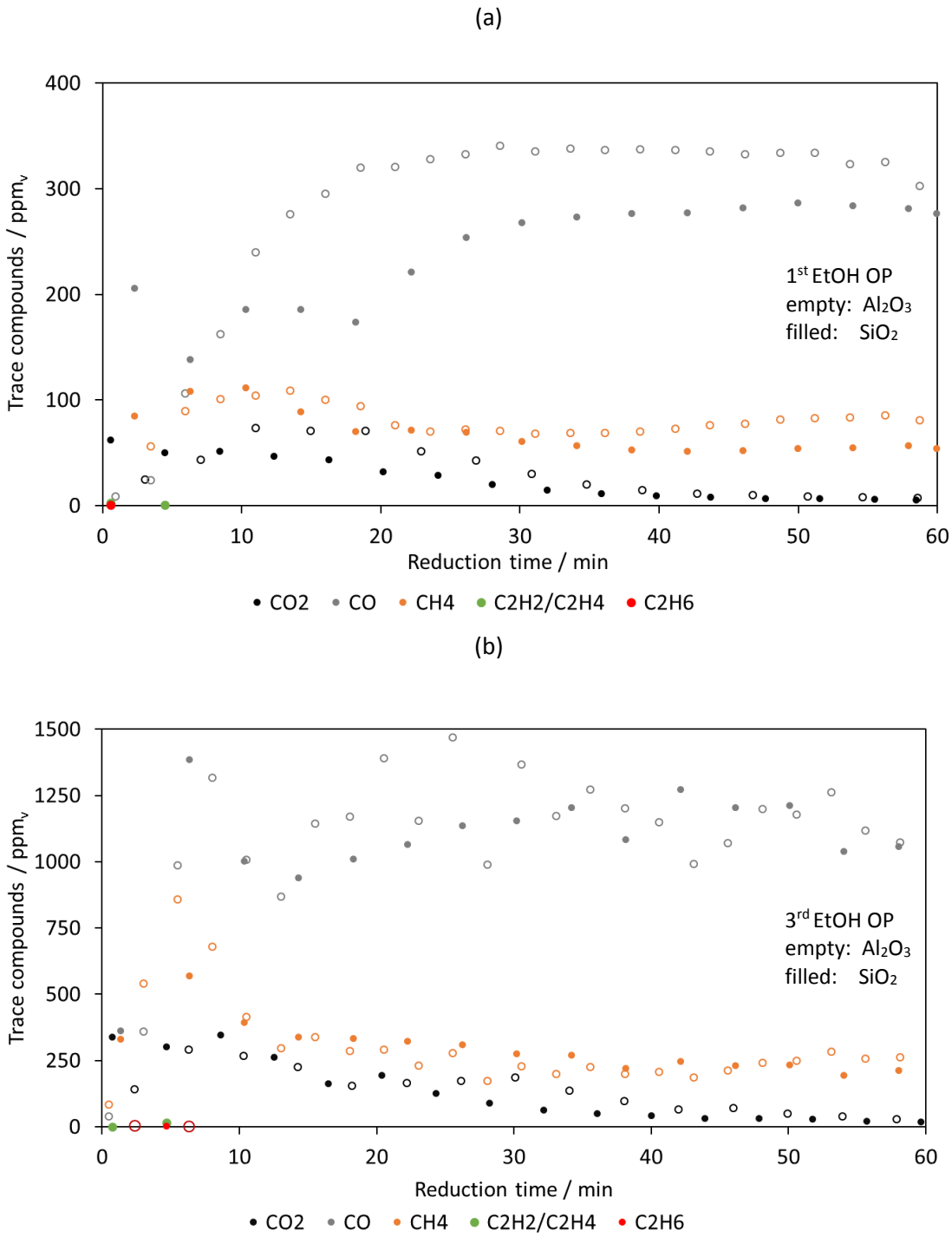

Figure 7-7: Trace compounds during reduction with ethanol over Al_2O_3 and over SiO_2 as inert material. 1st ethanol OP (average value cycles 13-16 for experiments with ethanol over Al_2O_3 and 9-12 for experiments with SiO_2) (a). 3rd ethanol OP (average value cycles 31-32 for experiments with ethanol over Al_2O_3 and 16-18 for experiments with SiO_2) (b).

7.4.2 Steam oxidation

Total impurities during oxidation for both inert materials are listed in Table 7-3. Total amount of impurities for the first cycle with Al_2O_3 was smaller than for the first cycle over SiO_2. But already after the third cycle total carbon impurities overtook the total impurity amount from the equivalent cycle with SiO_2. Total amount of impurities did not increase when SiO_2 was used as inert material. These results suggest that only little carbon was accumulated during those cycles.

Higher hydrocarbons as C_2H_2/C_2H_4 were detected during oxidation. Those compounds were unlikely to be formed at given conditions. Additionally, a pressure drop in the feed line of the piston pump was noticed, which is most likely the result of evaporation of liquid ethanol from the feed line. Implying that those impurities are product of the evaporated ethanol, arising C_2H_2/C_2H_4 impurities were neglected.

Table 7-3: Total impurities for consecutive cycles over Al_2O_3 and SiO_2 as inert material

			CO_2	**CO**	**CH_4**	**C_{tot}**
		Cycles	**ppm_v (H_2 based)**			
Al_2O_3	1st cycle	33	34	16	0	50
	3rd cycle	35	69	225	0	294
SiO_2	1st cycle	16	58	129	14	200
	3rd cycle	18	73	110	20	203

Figure 7-8 (a) shows the produced H_2 and impurities for consecutive cycles of the 3rd ethanol OP over SiO_2. The first oxidation after reducing with ethanol (cycle 16) is presented in dashed lines and empty dots and the third (cycle 18) in solid lines and filled dots. Results hint that only little carbon accumulation took place with ongoing number of cycles as deviation in the measured values was smaller than if Al_2O_3 was used. CO value for cycle 18 was higher than the one from the cycle 16, but values for CO_2 did not equally increase. This fact suggests that only little carbon accumulation took place when the reformation was performed over SiO_2 as inert material. During both cycles methane was not detected continuously.

The first cycles with ethanol over Al_2O_3 (dashed lines and empty spots) and over SiO_2 (continuous lines and filled spots) are shown in Figure 7-8 (b). Impurities for CO and CO_2 were constantly higher when SiO_2 was used as inert material. Noteworthy is the high CO_2 value at the beginning of the cycle with SiO_2. It was much higher than for Al_2O_3, but has not increased after three performed cycles (as already discussed and shown in (a)). The impurities during the third cycle of reduction with ethanol in the feed according to the 3rd OP are presented in (c). Results over Al_2O_3 as inert material are presented in dotted lines and empty spots and results over SiO_2 are presented in continuous lines and filled spots. As already discussed it seemed that carbon did accumulate over Al_2O_3. Therefore, the amount of CO and CO_2 at the beginning of oxidation were much higher than when SiO_2 was used. After the first few minutes

impurities over SiO_2 as inert material were slightly higher. Further evidence of carbon accumulation on Al_2O_3 is the increase of impurities from cycle 33 to cycle 35. Although amount for CO and CO_2 alternated for cycles 16 and 18 when using SiO_2 the total amount of impurities did not change.

(a)

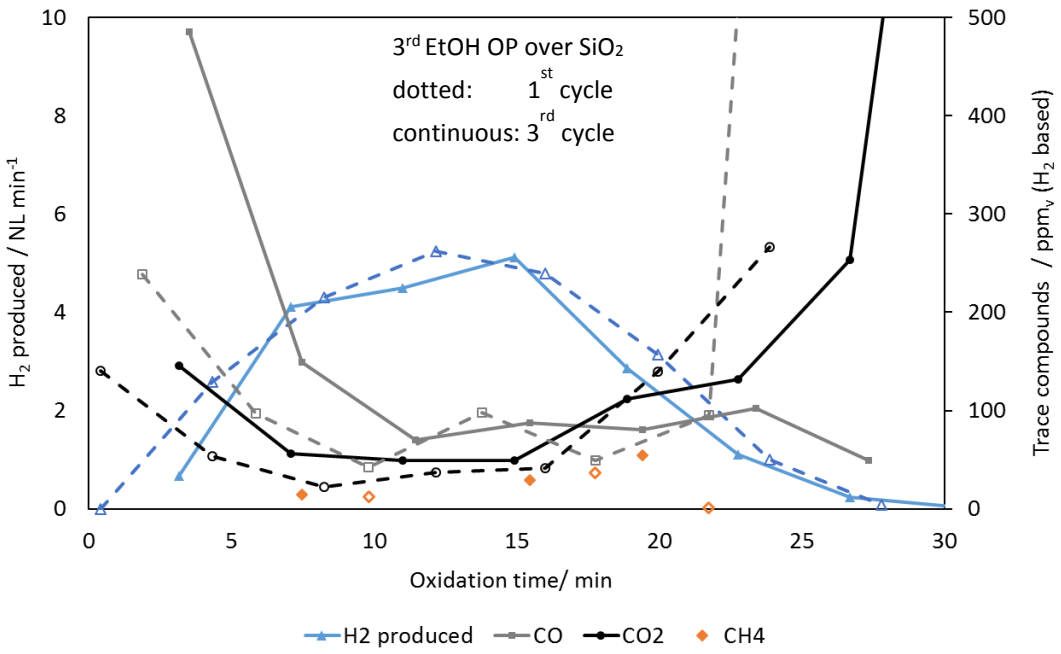

(b)

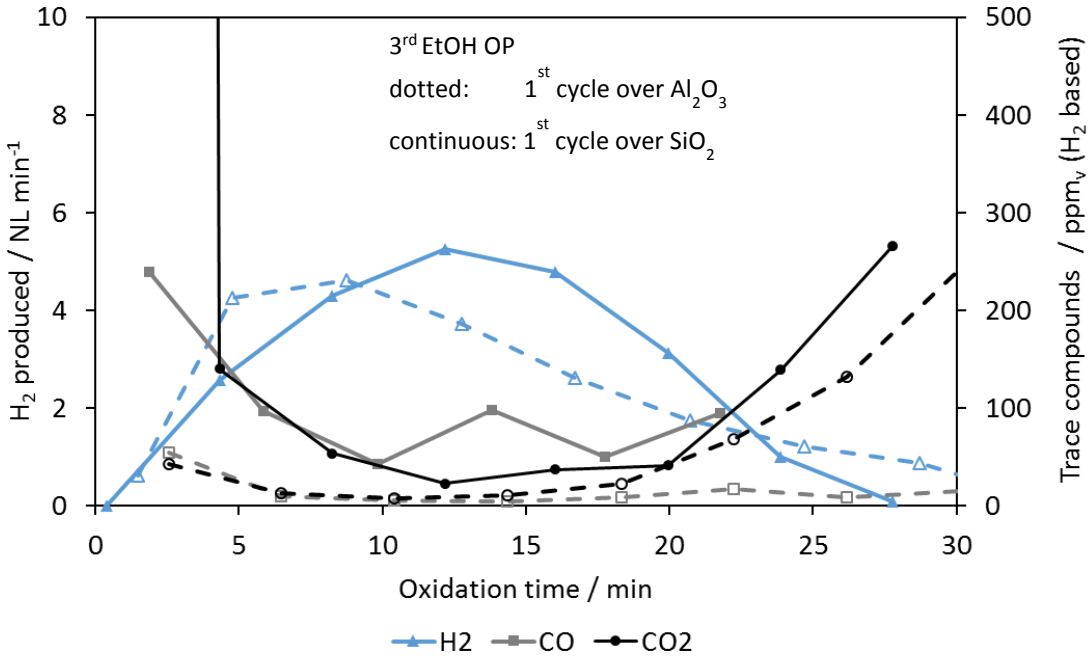

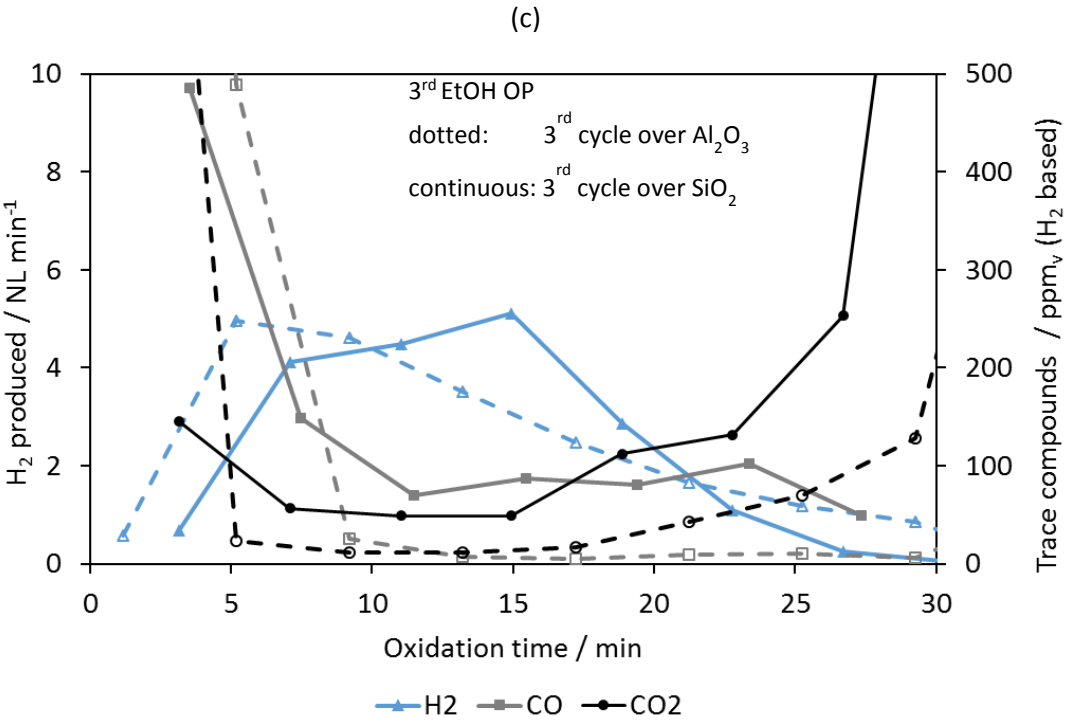

Figure 7-8: Produced H_2 and impurities for cycle 16 und 18 over SiO_2 (a). Comparison of impurities during oxidation of the first cycle over Al_2O_3 (cycle 33) and over SiO_2 (cycle 16) (b) and comparison of impurities during oxidation of the third cycle over Al_2O_3 (cycle 35) and over SiO_2 (cycle 18) (c).

To obtain a better knowledge of the long time performance of the inert materials more experiments are required. From this point of knowledge SiO_2 should be preferred as inert material for ethanol feed, as it seems to guarantee a constant performance.

If the respective third consecutive cycles over Al_2O_3 and SiO_2, where total amount of impurities are comparable, are considered, a different behaviour of carbon oxide impurities can be observed. When Al_2O_3 was used as inert material carbon oxide impurities were high at the beginning and low during the remaining oxidation phase. This suggests that most of the carbon was reoxidised immediately in the presence of steam. On the other hand, did the use of SiO_2 result in a more continuous contamination of the hydrogen stream during the whole oxidation phase.

As reoxidation of the deposited carbon seem to behave differently depending in the used inert material results hint that different type of carbon accumulation took place. Carbon deposition may be influenced by several factors such as acidity of the inert material or porosity. More experiments are required to gain a better insight of the nature of carbon deposition.

7.4.3 Reduction without steam

Three cycles were performed with 96% pure ethanol and no additional steam in the reductive gas. In order to compare the results with those from experiments where S/C ratio was predefined by the feed mixture to 1.4, the amount of conveyed ethanol was kept constant.

Figure 7-9 shows detected impurities during reduction with S/C=1.4 for the 1st ethanol OP in empty dots. Impurities detected during reduction with the equivalent amount of ethanol but no steam in the feed are marked by filled dots. For both cases C_2 compounds were detected only at the beginning of the reduction. As measurement fluctuations for values of CO and CO_2 was greater than the difference between the experiments no statement could be done for those impurities. CH_4 on the other hand seemed to be influenced when no water was present in the feed mixture as values are slightly lower. It may be result of incomplete reforming as no water was present to promote reformation reaction. Nonetheless all impurities aimed towards the same equilibrium level independently if steam was present.

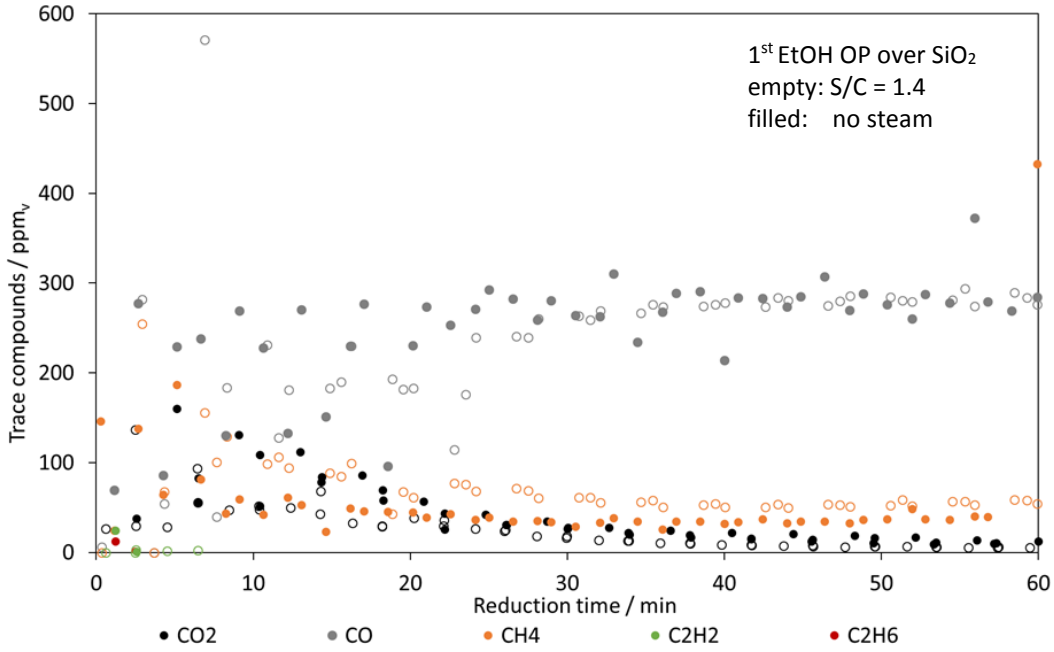

Figure 7-9: Impurities during reduction with S/C=1.4 (cycles 10-12) and with 96mol% ethanol (cycles 19-20).

Analysis of oxidation after reducing without steam was compared to reduction with S/C =1.4. Produced hydrogen and detected impurities for both cases are shown in Figure 7-10. Cycles with a molar S/C ratio equal to 1.4 are presented by dotted lines and empty spots, while cycles where no steam was added during reduction are presented by continuous lines and filled spots. Note that scaling for trace compounds on the secondary axis is logarithmic. Detected methane was not considered as it is no product of reoxidation of coke. Impurity values if reduction took place with pure ethanol were higher throughout the whole oxidation time. Noteworthy is that the first measured values for CO and CO_2 without steam were higher by several order of magnitudes. This leaded to the conclusion that more coke was formed and deposited when no steam was added during reduction phase. This is consistent with thermodynamic calculations of ESR from literature.

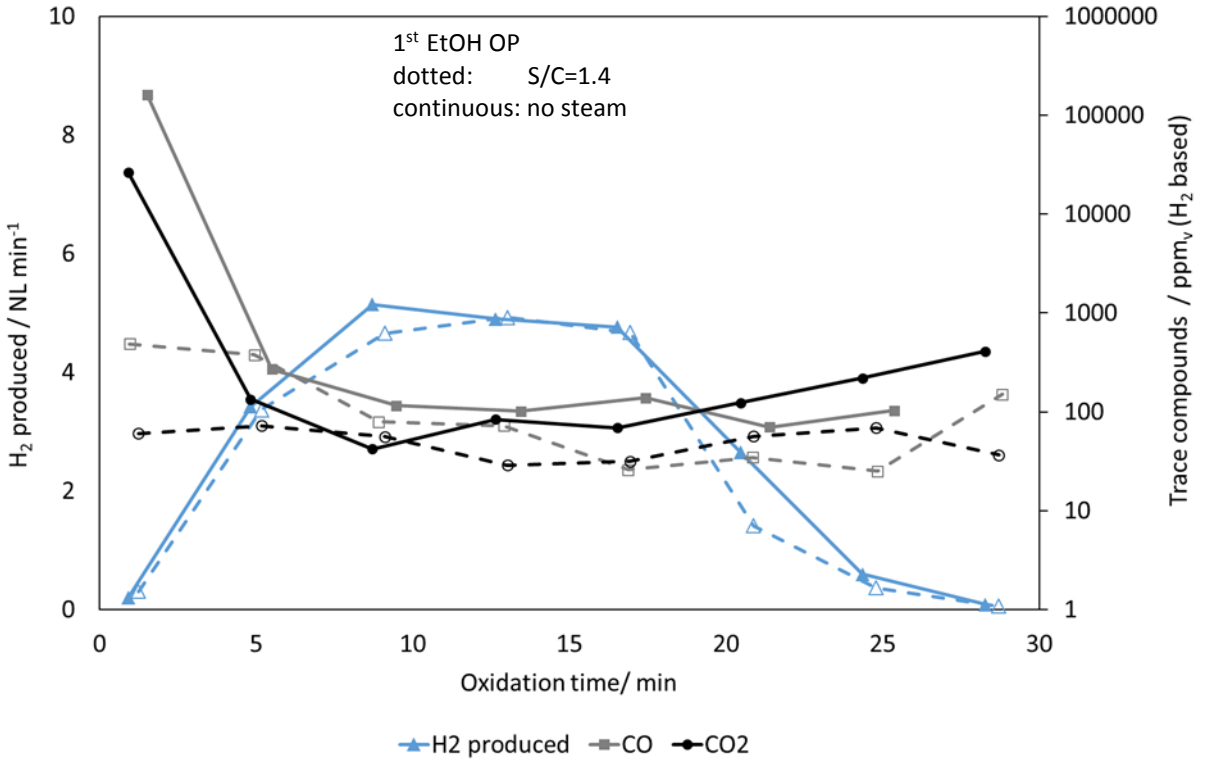

Figure 7-10: Produced H_2 and impurities for 1st ethanol OP during oxidation phase (average cycles 13-14) and for oxidation phase after reduction without steam (average cycles 19-21).

8 Results for addition of aromatic compounds to the reductive gas – model compound: Toluene

Toluene consists of a CH_3 group attached to a benzene ring. As it is not soluble in aqueous solutions the liquid was conveyed directly into the reactor by the piston pump. No water was supplied for experiments with toluene in the reductive feed. Experimental setup version 3 and SiO_2 as inert material were used.

8.1 Theory of toluene reformation

Gasification of biomass does not only result in syngas but also in a high amount of by-products such as tars and fly ashes. Especially tars, which are a complex mixture of condensable organics – mainly aromatic hydrocarbons - seriously affect process operation as they easily condense resulting in fouling and plugging of the equipment. Therefore, tar removal has a great economic interest. [40] [54]

Chunshan Li et. al. [55] investigated catalytic steam reforming of toluene in a fixed-bed reactor. Product composition is reported to be a result of various parallel reactions and highly influenced by operation parameters, used catalysts and S/C ratio. Reactions taking place during reformation are steam- and dry reforming (Equations (8-1) to (8-3)), hydrodealkylation (Equation (8-4)) as well as already discussed reaction mechanisms like water-gas shift, steam methane reforming and other decomposition reactions which lead to coke formation. No formation of benzene, but high amount of coke is reported by Josuinkas et. al. [56] when using NiO as catalyst for toluene reformation. Zou et. al. [54] investigated catalytic cracking of toluene over hematite. At temperatures of 800°C they report toluene conversions in the range of 50-99%. They furthermore report the catalytic activity of hematite is affected by reaction time and reaction temperature. Decrease of one of those factors did result in higher coke formation. Carbon formation might also be influenced by the consumption of lattice oxygen in the cracking reactions.

$$C_7H_8 + 7\,H_2O \rightarrow 7\,CO + 11H_2 \qquad \Delta H_{800°C} = 927.2\ kJ\ mol^{-1} \tag{8-1}$$

$$C_7H_8 + 14\,H_2O \rightarrow 7\,CO_2 + 18H_2 \qquad \Delta H_{800°C} = 688.5\ kJ\ mol^{-1} \tag{8-2}$$

$$C_7H_8 + 7\,CO_2 \rightarrow 14\,CO + 4H_2 \qquad \Delta H_{800°C} = 1166.0\ kJ\ mol^{-1} \tag{8-3}$$

$$C_7H_8 + H_2 \rightarrow C_6H_6 + CH_4 \qquad \Delta H_{800°C} = -50.9\ kJ\ mol^{-1} \tag{8-4}$$

8.2 Toluene operation points

Literature reports up to 2000 mg m-3 of total aromatics to be present in biogas (see Table 4-1). Although especially for syngas from biomass gasification toluene concentration can expected to be lower, OP with relatively high amount of toluene were chosen to gain a better

insight on the influences of aromatic compounds. Concentration of OP was 1000 mg m^{-3} and 2000 mg m^{-3} of toluene. Ppm level matched the level for the 1st and 2nd ethanol OP respectively. Table 8-1 gives an overview of toluene OP.

Table 8-1: Toluene operation points

	NL_{H2} min^{-1}	mL $_{Toluene}$ min^{-1}	mg $_{Toluene}$ m^{-3}_{BG}	ppm
1st Toluene OP	15	0.0086	1000	243
2nd Toluene OP	15	0.0175	2000	486

8.3 Observations during experiments with toluene

A high pressure drop of the piston pump was observed during oxidation phase. Therefore, it was concluded that toluene evaporated from the inlet pipe. Not to falsify oxidation analysis, the inlet pipe had to be withdrawn after every reduction phase.

A two-phase region was clearly distinguished in the condensate after cycling with toluene in the feed (left picture Figure 8-1). Besides an aqueous phase a small amount of non-water soluble organic phase was found. GC-MS analysis of the organic phase revealed toluene to be the only component. Clearly not all toluene was reformed, but as quantitative analysis of the organic phase was not possible, conversion rate of toluene could not be calculated.

After performing the last cycle, the reactor was cooled down and opened. The part above the toluene inlet pipe was found to be covered by a whitish film (right picture in Figure 8-1). These may be remains of evaporated toluene which was not conveyed through the reactor. Therefore, it could not be assured that the pre-defined amount of toluene was really present in the feed gas.

The first layer of SiO_2 on was found clean white with no visible staining, which could have been attributed to carbon deposition.

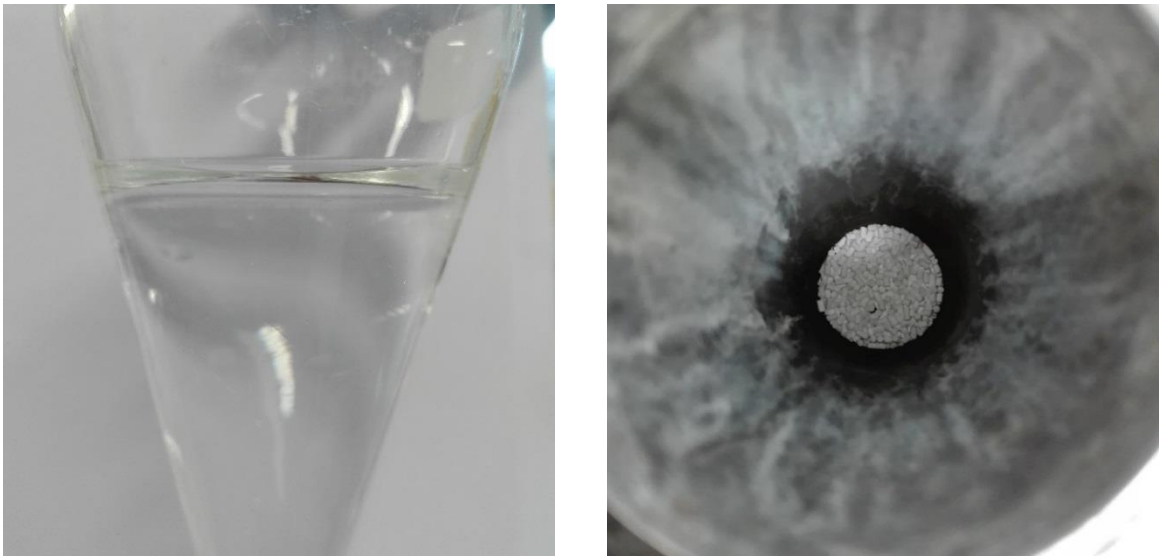

Figure 8-1: Picture of condensate during reduction with toluene (left) and opened reactor inlet after cycles with toluene (right)

8.4 Reduction

Methane, carbon dioxide and carbon monoxide were the only detected trace gases during reduction with hydrogen and toluene. Figure 8-2 shows the off gas analysis during reduction for the 1st and 2nd toluene OP. Measurement for the 1st OP are marked by blank spots, while values for the 2nd OP are marked by filled spots. As already observed during experiments with other model compounds carbon monoxide had the highest concentration of impurities in the off gas. Carbon dioxide was found to have the lowest concentration while methane concentration levelled in between. Impurity concentration for all components from the 2nd OP were more than double than those from the 1st OP.

As no water was added during reduction the occurrence of steam reforming reactions (Equations (8-1) and (8-2) is unlikely. The presence of methane is hint that hydrodealkylation reactions of toluene took place (Equation (8-4)). CO and CO_2 can result from further methane decomposition. Dry reforming of toluene (Equation (8-3)) might have taken place as some amount of CO_2 was present.

A different gas composition could be expected if water is fed during reduction, as that would result in higher toluene conversion due to steam reforming and additional SMR.

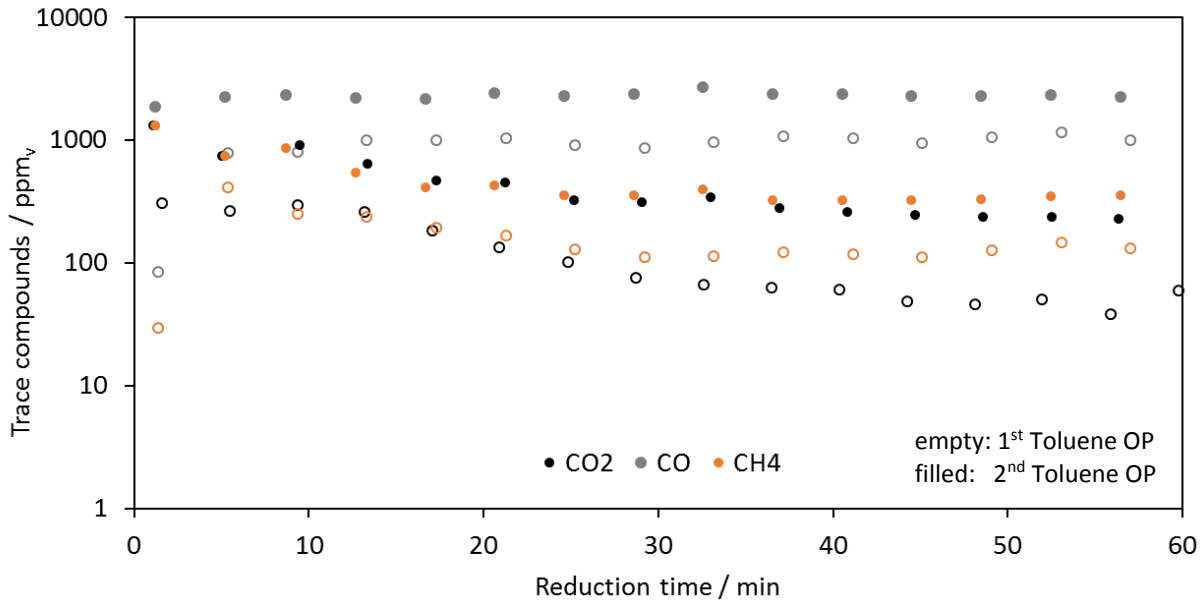

Figure 8-2: Off gas analysis during reduction of 1st and 2nd toluene OP over SiO_2, average for cycles 22-24 and 25-26

8.5 Steam Oxidation

During steam oxidation methane was only detected during oxidation of cycle 25 and is most likely to origin from a reductive gas remain. Carbon oxides were allocated to reoxidation of carbon settlements. Two consecutive cycles with reduction according to the 2nd toluene OP were compared and an increase of impurities was observed (

Table 8-2). Before cycle 25 an air oxidation was performed to eliminate all impurities from previous cycles. While no carbon accumulation over SiO_2 was observed during experiments with ethanol in the reductive feed, the level for all impurities increased already after two cycles in the presence of toluene. The highest increase of impurity level was observed for CO_2, with an increase of 146%. As CO_2 is a main product from reoxidation of carbon settlements it was concluded that a significant amount of carbon was accumulated even after one cycle. This is in accordance with reports from literature where coke formation during toluene refining was observed.

Table 8-2: Increase of produced H_2 impurity for consecutive cycles with toluene in the reductive gas.

		2nd Toluene OP		
	Cycle	25	26	increase
CO_2	ppm_v (H_2 based)	26	63	146%
CO	ppm_v (H_2 based)	42	63	50%
total	ppm_v (H_2 based)	70	127	80%

Figure 8-3 shows the produced hydrogen and the arising impurities based on the amount of produced hydrogen during oxidation of cycle 25 and 26. Cycle 25 is presented by continuous lines and filled spots and cycle 26 by dotted lines and empty spots.

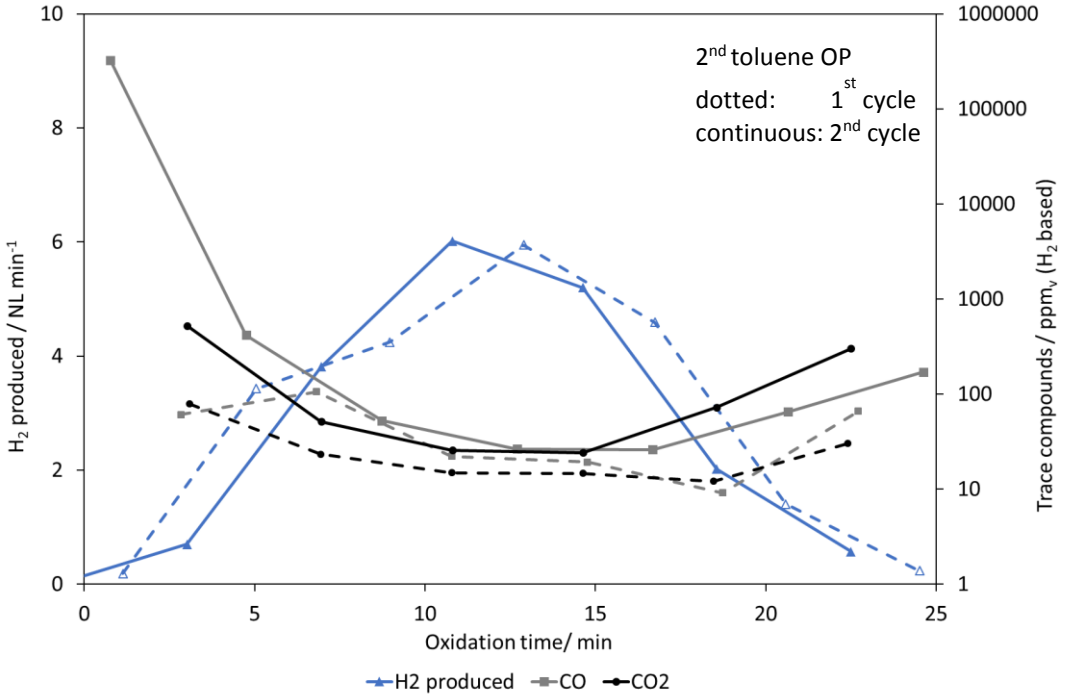

Figure 8-3: Produced H_2 and impurities during oxidation of consecutive cycles 25 and 25. Reduction according 2nd toluene OP.

In Table 8-3 impurity amount for cycles after reduction with ethanol and toluene are presented. Both were the third consecutive cycles where reduction took place according to the 1st ethanol and toluene OP respectively. During both reductions no steam was added and concentration of trace compounds within the reductive feed gas based on the feed hydrogen stream was kept constant (243 ppm_v). Even if methane impurities are neglected the amount of impurities arising during cycles with ethanol were significantly higher than when toluene was added. This could be due to incomplete toluene conversion.

Table 8-3: Impurities for third consecutive cycles after reduction according to the 1st ethanol and toluene OP.

1st OP		**Toluene**	**Ethanol**
Cycle		24	21
CO_2	ppm_v (H_2 based)	32	109
CO	ppm_v (H_2 based)	97	449
CH_4	ppm_v (H_2 based)	0	16
total	ppm_v (H_2 based)	129	575

8.6 Air Oxidation

Air oxidation was performed after cycle 26 in order to prove that carbon did accumulate during reduction with toluene in the reductive feed stream. After steam oxidation the reactor was purged for 15 minutes by pure nitrogen before 5.9 NL min^{-1} of air were introduced for one hour in the reactor. As soon as oxidation phase did stop and hence no more steam was added, no carbon monoxide was detected. Carbon dioxide outflow diminished during purging from 0.12 NmL min^{-1} to 0.03 NmL min^{-1} as remains formed during oxidation were slowly flushed out. As soon as air was introduced in the reactor CO_2 outflow increased to 3.55 NmL min^{-1}. After a maximum of CO_2 outflow at the first measurement of the GC it rapidly decreased and reached 0.45 NmL min^{-1} after 10 minutes. Over the remaining period of air oxidation, the CO_2 outflow reached the level before the air oxidation phase. Figure 8-4 illustrates the CO_2 outflow in NmL during purging and air oxidation. Starting time of air oxidation is marked by a green dotted line. The sudden increase of CO_2 as soon as air was added is a clear evidence for carbon deposition. This carbon was not reoxidised during steam oxidation and hence carbon consecutively accumulates. CO was not detected at any point of the air oxidation phase. This leads to the conclusion that during steam oxidation CO results as product from incomplete reoxidation according to Equation (3-8), while in presence of oxygen all carbon depositions are completely oxidised to CO_2.

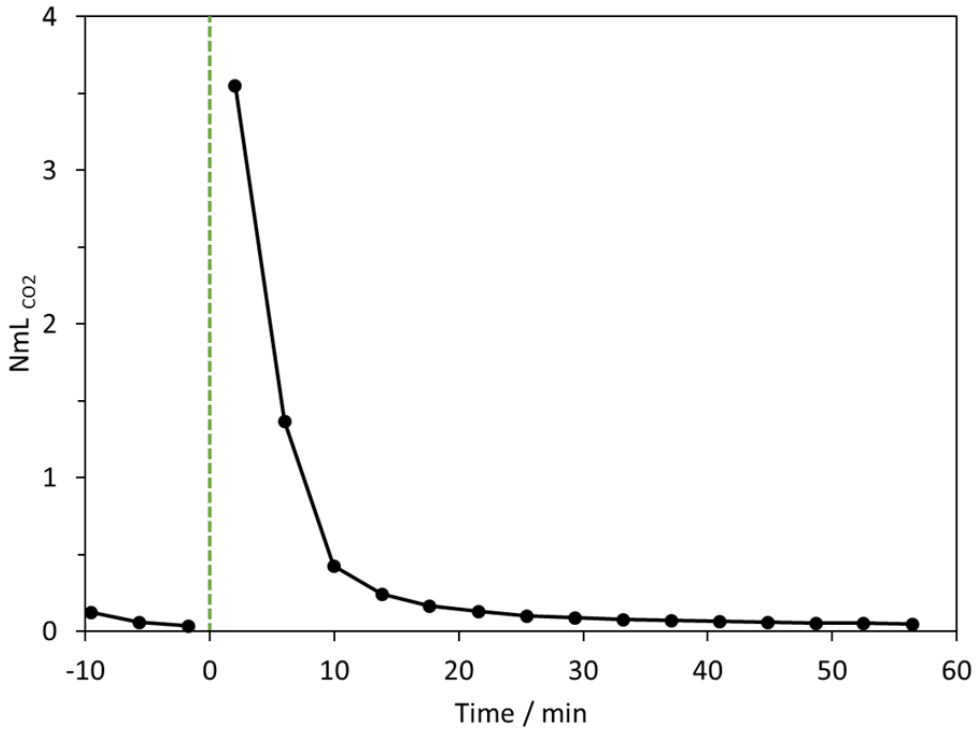

Figure 8-4: CO_2 outflow during air oxidation

9 Summary, conclusion and way forward

The Reformer Steam Iron Cycle (RESC) offers a carbon neutral production method for decentralised medium scale hydrogen production. An iron oxygen carrier is cyclically reduced by syngas and reoxidised by steam. As long as solid carbon formation during the reduction step is avoided, pure pressurized hydrogen can be obtained.

The use of syngases from different types of renewables was investigated. Therefore model compounds, which represent typical trace gases from biogas or gasified biomass, were added to the reaction system during the reduction step. Methane and propane were selected as model compounds for acyclic hydrocarbons, ethanol was to be substitutional for organic alcohols and toluene to represent cyclic hydrocarbons.

A fixed bed reactor was used. By switching between oxidizing and reducing gases a cyclic repetition of the process steps was possible. The idle reactor temperature was 830°C and the reaction took place at ambient pressure. Reduction was performed with 15 NL min^{-1} of hydrogen and S/C ratio of 1.4.

Hydrogen production during oxidation behaved like a ‘bell shape curve’. The amount of produced hydrogen heavily depended on the degree of reduction which in turn was influenced by the amount of steam of the reduction phase. Carbon oxides as well as hydrocarbons were detected during oxidation. Hydrocarbons were attributed to incomplete reactor purging as they were not expected to form under given conditions. Carbon oxide impurities were attributed to reoxidation of elemental carbon depositions formed during reduction.

Increasing methane content in the reductive gas from 2 to 10 vol% resulted in an increase of hydrogen contamination from 100 to 300 ppm_v. The addition of 2.5 and 5 vol% of propane during reduction resulted in a contamination of the produced hydrogen of 450 and 500 ppm_v respectively. The share of carbon oxide impurities accounted for 50 to 90% of total impurities. Reactor evacuation and longer reactor purging had positive effects on the quality of the produced hydrogen as hydrocarbons could be effectively removed. Doubling purging time after reduction resulted in 25% less impurities. By overnight purging 100% of all hydrocarbons were removed, while evacuation of the reactor resulted in a hydrocarbon removal of 60-90%. Carbon oxide impurities were not significantly affected by any of those means.

An increase of impurities with ongoing number of cycles related to carbon accumulation was not observed for gaseous trace compounds. The addition of ethanol to the reductive gas did result in a progressive decrease of the hydrogen quality as carbon was accumulated with ongoing number of cycles with Al_2O_3 as inert material. As acidic sites promote carbon formation on the surface, SiO_2 was investigated as inert material for its less acidic nature. The use of SiO_2 resulted in a smaller increase of progressive contamination and a constant

hydrogen quality for experiments with ethanol. Carbon accumulation was observed even for SiO_2 as inert material when toluene was present in the reductive feed. Intermediate air oxidation could prevent accumulation of carbon with ongoing number of cycles and allowed a constant hydrogen quality.

To simulate hydrogen storage with the RESC the reactor was stored for a time period of approximately 70 hours in reduced state before steam oxidation. An increased amount of CO_2 during oxidation was observed after storage. This was attributed to carbon formation as result of hydrocarbon cracking during storage time.

For the present experimental setup, the greatest field for improvement was identified to be in the off gas analysis. A time lag between system and gas analysis was observed, which could be overcome by reducing the distance from the gas analysis and the reactor outlet.

To predict the influence of the use of syngas from renewables for the hydrogen production with the RESC process more detailed investigations with traces of hydrogen sulphide, siloxanes or halogens are necessary.

10 References

[1] J. (Clean A. F. Burston, “Why hydrogen could be the future of green energy.” [Online]. Available: https://www.weforum.org/agenda/2018/05/this-forgotten-element-could-be-the-key-to-our-green-energy-future-heres-why?fbclid=IwAR1wy9CodW6MjfXsGo_7vUw68VvWIWCh2kXnYy6sWd5x7kcypu8s-H1fz0I. [Accessed: 06-Jan-2019].

[2] T. J. L. Jochen, *Wasserstoff und Brennstoffzelle*, 2. Auflage. 2017.

[3] G. Voitic *et al.*, *Chapter 10 - Hydrogen Production*. Elsevier Inc., 2018.

[4] S. Mitsushima and V. Hacker, *Role of Hydrogen Energy Carriers*. Elsevier Inc., 2018.

[5] International Energy Agency, “Energy Technology Analysis Prospects for Hydrogen and Fuel Cells: Complete Edition,” *SourceOECD Energy*, p. i-256, 2005.

[6] K. Mazloomi and C. Gomes, “Hydrogen as an energy carrier: Prospects and challenges,” *Renew. Sustain. Energy Rev.*, vol. 16, no. 5, pp. 3024–3033, 2012.

[7] Council Hydrogen, “Hydrogen scaling up : A sustainable pathway for the global energy transition,” *Hydrog. Counc.*, no. November, p. 80, 2017.

[8] M. Balat, “Potential importance of hydrogen as a future solution to environmental and transportation problems,” *Int. J. Hydrogen Energy*, vol. 33, no. 15, pp. 4013–4029, 2008.

[9] N. Armaroli and V. Balzani, “The hydrogen issue,” *ChemSusChem*, vol. 4, no. 1, pp. 21–36, 2011.

[10] H. Boerrigter and R. Rauch, “Review of applications of gases from biomass gasification,” *ECN Biomass, Coal Environ. …*, no. June, p. 33, 2006.

[11] M. Voldsund, K. Jordal, and R. Anantharaman, “Hydrogen production with CO2capture,” *Int. J. Hydrogen Energy*, vol. 41, no. 9, pp. 4969–4992, 2016.

[12] S. Mitsushima, B. Gollas, and V. Hacker, *Introduction*. Elsevier Inc., 2018.

[13] M. Luo *et al.*, “Review of hydrogen production using chemical-looping technology,” *Renew. Sustain. Energy Rev.*, vol. 81, no. June 2017, pp. 3186–3214, 2018.

[14] M. Bodner, J. Senn, and V. Hacker, *Chapter 7 - Degradation Mechanisms and Their Lifetime*. Elsevier Inc., 2018.

[15] S. M. Mousavi Ehteshami and S. H. Chan, “Techno-Economic Study of Hydrogen Production via Steam Reforming of Methanol, Ethanol, and Diesel,” *Energy Technol. Policy*, vol. 1, no. 1, pp. 15–22, 2014.

[16] International Energy Agency (IEA), “Technology Roadmap: Hydrogen and fuel cells,” *SpringerReference*, 2015.

[17] A. Sanna, “Advanced Biofuels from Thermochemical Processing of Sustainable Biomass in Europe,” *Bioenergy Res.*, vol. 7, no. 1, pp. 36–47, 2014.

[18] A. Arregi, M. Amutio, G. Lopez, J. Bilbao, and M. Olazar, “Evaluation of thermochemical routes for hydrogen production from biomass: A review,” *Energy Convers. Manag.*, vol. 165, no. January, pp. 696–719, 2018.

[19] M. R. Allen, A. Braithwaite, and C. C. Hills, “Trace Organic Compounds in Landfill Gas at Seven U.K. Waste Disposal Sites,” *Environ. Sci. Technol.*, vol. 31, no. 4, pp. 1054–1061, 1997.

[20] F. Hilaire, E. Basset, R. Bayard, M. Gallardo, D. Thiebaut, and J. Vial, “Comprehensive two-dimensional gas chromatography for biogas and biomethane analysis,” *J. Chromatogr. A*, vol. 1524, pp. 222–232, 2017.

[21] M. Arnold, *Reduction and monitoring of biogas trace compounds*, no. 2496. 2009.

[22] “https://www.energy.gov/eere/fuelcells/hydrogen-production.” .

[23] A. Haryanto, S. Fernando, N. Murali, and S. Adhikari, “Current Status of Hydrogen Production Techniques by Steam Reforming of Ethanol: A Review,” vol. 19, no. 5, pp. 2098–2106, 2005.

[24] P. Brea, J. A. Delgado, V. I. Águeda, and M. A. Uguina, “Comparison between MOF UTSA-16 and BPL activated carbon in hydrogen purification by PSA,” *Chem. Eng. J.*, vol. 355, no. August 2018, pp. 279–289, 2019.

[25] G. Bagnato, A. Iulianelli, A. Sanna, and A. Basile, “Glycerol production and transformation: A critical review with particular emphasis on glycerol reforming reaction for producing hydrogen in conventional and membrane reactors,” *Membranes (Basel).*, vol. 7, no. 2, 2017.

[26] R. W. Breault, Ed., *Handbook of Chemical Looping Technology*. WILEY-VCH.

[27] A. Nandy, C. Loha, S. Gu, P. Sarkar, M. K. Karmakar, and P. K. Chatterjee, “Present status and overview of Chemical Looping Combustion technology,” *Renew. Sustain. Energy Rev.*, vol. 59, pp. 597–619, 2016.

[28] E. Jerndal, T. Mattisson, A. Lyngfelt, C. Combustion, and O. After, “Thermal analysis of chemical-looping combustion,” no. September, 2006.

[29] G. Voitic and V. Hacker, “Recent advancements in chemical looping water splitting for the production of hydrogen,” *RSC Adv.*, vol. 6, no. 100, pp. 98267–98296, 2016.

[30] S. Bock, R. Zacharias, and V. Hacker, “High purity hydrogen production with a 10kWthRESC prototype system,” *Energy Convers. Manag.*, vol. 172, no. May, pp. 418–427, 2018.

[31] V. Hacker *et al.*, “Hydrogen production by steam-iron process,” *J. Power Sources*, vol. 86, no. 1, pp. 531–535, 2000.

[32] V. Hacker *et al.*, “Usage of biomass gas for fuel cells by the SIR process,” *J. Power Sources*, vol. 71, no. 1–2, pp. 226–230, 1998.

[33] V. Hacker, “A novel process for stationary hydrogen production: The reformer sponge iron cycle (RESC),” *J. Power Sources*, vol. 118, no. 1–2, pp. 311–314, 2003.

[34] S. Nestl, G. Voitic, M. Lammer, B. Marius, J. Wagner, and V. Hacker, “The production of pure pressurised hydrogen by the reformer-steam iron process in a fi xed bed reactor system,” *J. Power Sources*, vol. 280, pp. 57–65, 2015.

[35] O. Almpanis-lekkas, B. Weiss, and W. Wukovits, “Modelling of an ironmaking melter gasi fi er unit operation with multicomponent / multiphase equilibrium calculations,” *J. Clean. Prod.*, vol. 111, pp. 161–171, 2016.

[36] S. Nestl, “Biogas reforming and the steam iron process for the production of pressurised hydrogen,” no. September, p. 134, 2015.

[37] S. Nestl, G. Voitic, R. Zacharias, S. Bock, and V. Hacker, “High-Purity Hydrogen Production with the Reformer Steam Iron Cycle,” *Energy Technol.*, vol. 6, no. 3, pp. 563–569, 2018.

[38] M. Thaler and V. Hacker, “Storage and separation of hydrogen with the metal steam process,” *Int. J. Hydrogen Energy*, vol. 37, no. 3, pp. 2800–2806, 2011.

[39] G. Voitic *et al.*, “High purity pressurised hydrogen production from syngas by the steam-iron process,” *RSC Adv.*, vol. 6, no. 58, pp. 53533–53541, 2016.

[40] Z. Wang *et al.*, “Chemical looping reforming of toluene as a biomass tar model compound over two types of oxygen carriers: 2CuO-2NiO/Al2O3and CaFe2O4,” *Fuel*, vol. 222, no. February, pp. 375–384, 2018.

[41] S. Rasi, A. Veijanen, and J. Rintala, “Trace compounds of biogas from different biogas production plants,” *Energy*, vol. 32, no. 8, pp. 1375–1380, 2007.

[42] S. Rasi, *Biogas Composition and Upgrading to Biomethane Saija Rasi Biogas Composition and Upgrading to Biomethane*. 2009.

[43] S. Rasi, J. Läntelä, and J. Rintala, “Trace compounds affecting biogas energy utilisation - A review,” *Energy Convers. Manag.*, vol. 52, no. 12, pp. 3369–3375, 2011.

[44] G. Voitic and V. Hacker, “Recent advancements in chemical looping water splitting for the production of hydrogen,” *RSC Adv.*, vol. 6, no. 100, pp. 98267–98296, 2016.

[45] G. Voitic, S. Nestl, M. Lammer, J. Wagner, and V. Hacker, “Pressurized hydrogen production by fixed-bed chemical looping,” *Appl. Energy*, vol. 157, pp. 399–407, 2015.

[46] K. Svoboda, A. Siewiorek, D. Baxter, J. Rogut, and M. Pohořelý, “Thermodynamic possibilities and constraints for pure hydrogen production by a nickel and cobalt-based chemical looping process at lower temperatures,” *Energy Convers. Manag.*, vol. 49, no. 2, pp. 221–231, 2008.

[47] B. . A. Baker and S. G. D., “Alloy Selection for Environments Which Promote Metal Dusting,” *Corros. 2002*, no. Paper No. 00257.

[48] B. A. Baker, G. D. Smith, V. W. Hartmann, L. E. Shoemaker, and S. A. McCoy, “Nickel-Base Material Solutions to Metal Dusting Problems,” *Corros. 2002*, no. Paper No. 02394, pp. 1–16, 2002.

[49] J. C. Nava Paz and H. J. Grabke, “Metal dusting,” *Oxid. Met.*, vol. 39, no. 5–6, pp. 437–456, 1993.

[50] G. Rabenstein and V. Hacker, “Hydrogen for fuel cells from ethanol by steam-reforming, partial-oxidation and combined auto-thermal reforming: A thermodynamic analysis,” *J. Power Sources*, vol. 185, no. 2, pp. 1293–1304, 2008.

[51] V. Subramani and C. Song, “Advances in catalysis and processes for hydrogen production from ethanol reforming,” *Catalysis*, pp. 65–106, 2015.

[52] J. Llorca, P. R. de la Piscina, J. Sales, and N. Homs, “Direct Production of Hydrogen from Ethanolic Aqueous Solutions over Oxide Catalysts.,” *R. Soc. Chem.*, pp. 641–642, 2001.

[53] S. Cavallaro, V. Chiodo, S. Freni, N. Mondello, and F. Frusteri, “Performance of Rh/Al2O3catalyst in the steam reforming of ethanol: H2production for MCFC,” *Appl. Catal. A Gen.*, vol. 249, no. 1, pp. 119–128, 2003.

[54] X. Zou, T. Chen, H. Liu, P. Zhang, D. Chen, and C. Zhu, “Catalytic cracking of toluene over

hematite derived from thermally treated natural limonite," *Fuel*, vol. 177, pp. 180–189, 2016.

[55] C. Li, D. Hirabayashi, and K. Suzuki, "Development of new nickel based catalyst for biomass tar steam reforming producing H2-rich syngas," *Fuel Process. Technol.*, vol. 90, no. 6, pp. 790–796, 2009.

[56] F. M. Josuinkas, C. P. B. Quitete, N. F. P. Ribeiro, and M. M. V. M. Souza, "Steam reforming of model gasification tar compounds over nickel catalysts prepared from hydrotalcite precursors," *Fuel Process. Technol.*, vol. 121, pp. 76–82, 2014.

[57] H. Xie, E. Weitz, and K. R. Poeppelmeier, "Materials for Clean H2 Production from Bioethanol Reforming Thermodynamics for Ethanol Steam Reforming (SR) Rh-supported Catalysts," pp. 2–6, 2016.

11 Appendix

11.1 List of Abbreviations, terms and symbols

AW	Agricultural waste
AR	Air Reactor
BG	Biogas
CLC	Chemical Looping Combustion
CLH	Chemical Looping Hydrogen
EDX	Energy dispersive X-ray spectroscopy
ESR	Ethanol steam reforming
EJ	Exajoule = 10^{18} J
FC	Fuel cell
FCEV	fuel cell electric vehicle
FR	Fuel Reactor
GC	Gas chromatograph
GC-MS	Gas chromatography coupled with mass spectroscopy
HC	Hydrocarbons
LM	Light microscopy
LPG	Liquefied petroleum gas
MFC	Mass flow controller
S/C	Molar steam-to-carbon ratio
MSW	Municipal solid waste
OP	Operation point
OC	Oxygen carrier
POX	Partial oxidation
PSD	Particle Size distribution
PEFC	Polymer Electrolyte Fuel Cells
PtH_2	Power-to-Hydrogen
SEM	Scanning electron microscopy
SMR	Steam methane reforming
TCD	Thermal conductivity detector
VOCs	Volatile organic compounds
vol%	Volume percentage
WGS	Water-gas shift
wt%	Weight percentage

11.2 List of Figures

11.3 List of Tables

11.4 Supplementary data

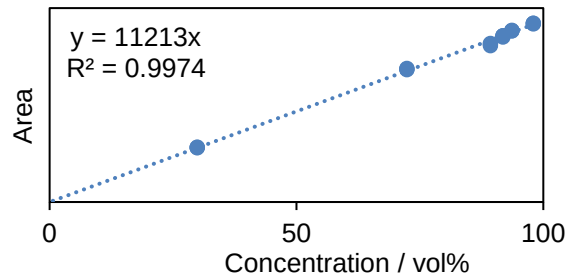

Figure 11-1: Calibration H_2

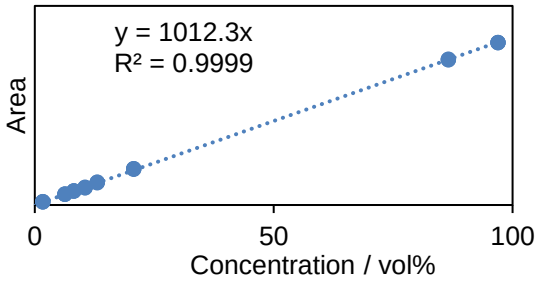

Figure 11-2: Calibration N_2

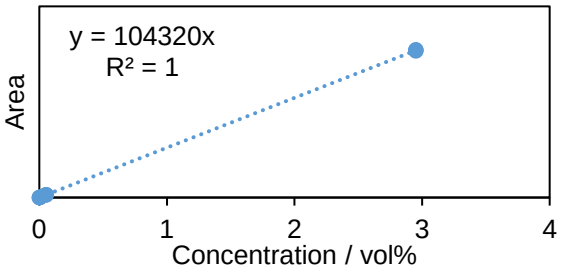

Figure 11-3: Calibration CO_2

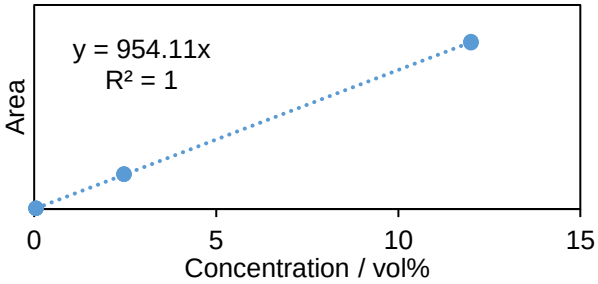

Figure 11-4: Calibration CO

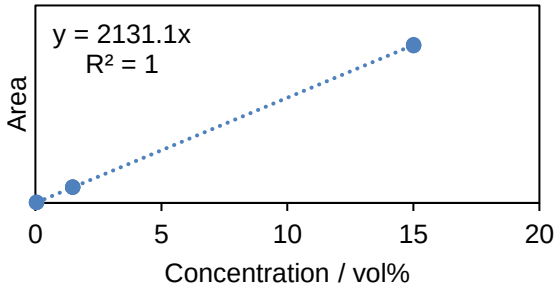

Figure 11-6: Calibration CH_4

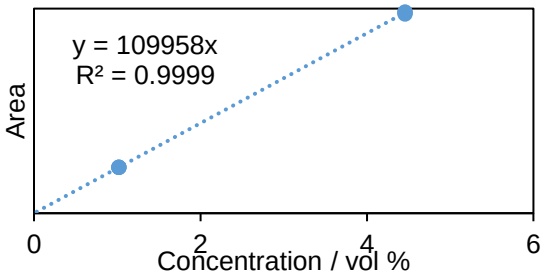

Figure 11-7: Calibration C_2H_6

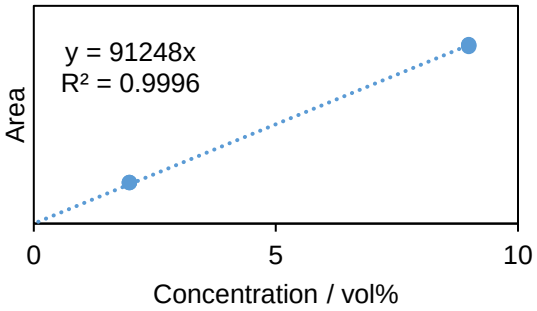

Figure 11-5: Calibration C_2H_4 & C_2H_2

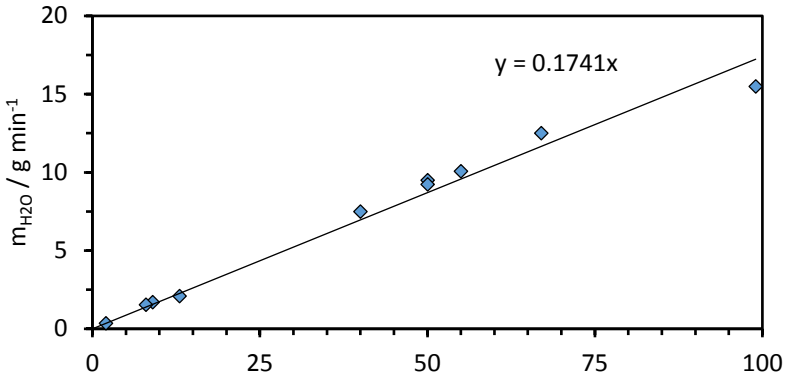

Figure 11-8: Calibration peristaltic pump (Ismatec Reglo Analog MS 2/12)

Table 11-1: PSD of a sample of 3283 metal oxygen carrier particles after calcination

		Maximum particle size / mm														
		<0.5	0.75	1	1.25	1.5	1.75	2	2.25	2.5	2.75	3	3.25	3.5	3.75	>4
q_0	%	2	9	18	21	18	13	9	5	3	1	0	0	0	0	0
Q_0	%	2	11	29	50	68	82	90	95	98	99	100	100	100	100	100
q_3	%	0	1	4	9	15	17	17	15	12	5	2	1	0	0	1
Q_3	%	0	1	5	14	29	46	63	78	90	95	98	99	99	99	100

Table 11-2: Calculation of mass change during cycles for methane experiments

$$m_{Fe2O3} = m_{oxygen\ carrier} * (1 - m_{support\ material})$$

$$m_{Fe2O3} = 501g * (1 - 20\%) = 400.8g$$

$$m_{Fe3O4} = m_{Fe2O3} * \frac{2 * (3M_{Fe} + 4M_O)}{3 * (2M_{Fe} + 3M_O)}$$

$$m_{Fe3O4} = 400.8g * \frac{2 * (3 * 56 + 4 * 16)}{3 * (2 * 56 + 3 * 16)} = 387.4g$$

$$m_{Fe} = m_{Fe2O3} * \frac{2 * M_{Fe}}{(2M_{Fe} + 3M_O)}$$

$$m_{Fe} = 400.8g * \frac{2 * 56}{(2 * 56 + 3 * 16)} = 280.6g$$

$$\Delta m_{1st\ cycle} = m_{Fe2O3} - m_{Fe}$$

$$\Delta m_{1st\ cycle} = 400.8g - 280.6g = 120.2g$$

$$\Delta m_{cycle} = m_{Fe3O4} - m_{Fe}$$

$$\Delta m_{cycle} = 387.4g - 280.6g = 106.9g$$

$$\Delta m_{Air\ OX} = m_{Fe2O3} - m_{Fe3O4}$$

$$\Delta m_{Air\ OX} = 400.8g - 387.4g = 13.4g$$

Table 11-3: Cycles of methane experiments

cycle	Δm RED	Δm OX	Δm Air OX	Δm cycle	Relative OC conversion	Ox time	CH_4 OP	comment	CO_2	CO	CH_4	C_{tot}
	g	g	g	g		min			ppm_v (H_2 based)			
1	123.6	105.9		114.8	95%	25						
2	96.0	96.9		96.4	90%	23		cycles to reach stable conditions				
3	87.6	83.0		85.3	80%							
4	86.0	85.1		85.6	80%	20						
5	83.4	81.6		82.5	77%							
6	79.1	71.3		75.2	70%							
7	73.8	72.5		73.1	68%		1st	investigation long time storage	19	20	38	77
8	72.0	67.4		69.7	65%				43	11	0	54
9	72.3	71.8		72.0	67%		1st	impurity elimination with H_2 reduction	21	28	29	77
10	71.3	70.4		70.8	66%				26	18	31	74
11	77.2	76.8		77.0	72%				6	7	0	12
12	77.7	76.9		77.3	72%				3	7	0	9
13	73.7	71.3		72.5	68%		1st	influence air oxidation	30	31	34	96
14	69.1	69.4	14.9	84.3	79%				104	29	34	166
15	89.6	74.5		67.2	63%				99	27	18	143
16	71.7	68.2		69.9	65%		1st	influence air oxidation	141	30	28	198
17	66.4	66.8	15.7	82.5	77%				122	23	18	163
18	98.9	82.8		75.2	70%				30	1	0	31
19	76.1	75.9		76.0	71%				19	3	0	22
20	76.2	73.4		74.8	70%							
21	72.0	68.8		70.4	66%							
22	65.0	64.2		64.6	60%	20	1st		53	27	24	104
23	62.5	62.9		62.7	59%							
24	62.2	62.6		62.4	58%							
25	60.8	61.0		60.9	57%							
26	48.2	44.7		46.5	43%	15	2nd		155	25	44	224
27	41.3	43.0		42.1	39%							
28	46.8	46.1		46.5	43%							
29	44.3	45.3		44.8	42%							
30	48.4	41.8		45.1	42%	15	3rd		174	34	86	293
31	41.1	40.7		40.9	38%							
32	40.3	40.5		40.4	38%							
33	40.8	41.4		41.1	38%							
34	44.3	41.0		42.6	40%	15	3rd		126	14	12	153
35	39.7	39.0		39.4	37%							

36	39.0	39.5	11.8	51.3	48%			influence applied vacuum					
37	97.5	84.1		79.0	74%	20							
38	78.2	74.8		76.5	72%								
39	69.1	69.6		69.3	65%			influence applied vacuum					
40	65.6	63.6		64.6	60%	20	1st		37	13	0	49	
41	62.9	63.2		63.1	59%								
42	45.5	42.6		44.1	41%			influence applied vacuum					
43	41.5	40.8		41.1	39%	15	3rd		114	8	11	133	
44	40.5	40.6		40.6	38%								
45	58.2			58.2	54%			60 min : 10% CH_4; S/C=1,4; 15 NL_{H2} min^{-1}; 240 min: 10% CH_4, S/C=1,4; 7,5NL_{H2} min^{-1}					

Table 11-4: Cycles of propane experiments

cycle	**Δm RED**	**Δm OX**	**Δm Cycle**	**Relative OC conversion**	**C_3H_8 OP**	**comment**	**CO_2**	**CO**	**CH_4**	**C_2H_4**	**C_2H_6**	**C_3H_8**	**C_{tot}**
	g	**g**	**g**				**ppm_v (H_2 based)**						
1	127.8	104.9	116.3	97%									
2	98.1	96.4	97.3	91%									
3	87.5	86.2	86.9	81%		cycles to reach stable conditions							
4	79.3	83.5	81.4	76%									
5	85.7	83.6	84.6	79%									
6	84.2	83.2	83.7	78%									
7	82.6	81.8	82.2	77%									
8	82.1	78.4	80.3	75%									
9	65.5	64.1	64.8	61%	1st		274	121	38	7	0	2	442
10	58.4	58.2	58.3	54%									
11	61.0	58.6	59.8	56%	1st	Influence weekend storage	210	38	5	2	0	1	256
12	61.6	59.8	60.7	57%	1st	Influence extended purging time	142	37	0	0	0	0	179
13	61.5	60.6	61.1	57%	1st	Influence applied vacuum	252	130	12	1	0	1	396
14	58.5	58.7	58.6	55%									
15	59.0	58.5	58.8	55%									
16	52.3	51.9	52.1	49%	2nd		194	236	37	32	1	13	513
17	51.4	50.9	51.1	48%									
18	54.5	54.0	54.3	51%									

19	50.3	49.4	49.8	47%	2nd	Influence weekend storage	211	53	5	3	0	2	273
20	51.9	50.2	51.0	48%									
21	57.8	42.0	49.9	47%									
22	49.6	48.2	48.9	46%	2nd	Influence extended purging time (overnight)	114	59	0	0	0	0	173
23	49.8	48.7	49.3	46%									
24	50.1	49.4	49.8	46%	2nd	Influence applied vacuum	264	150	12	1	0	5	432
25	48.7	48.4	48.5	45%									
26	48.1	47.6	47.9	45%									
27	48.6	47.5	48.1	45%	2nd	influence extended purging time (30 min)	219	118	35	8	1	7	387
28	47.4	47.0	47.2	44%									
29	47.7	48.4	48.1	45%									
30	45.7	44.6	45.2	42%	2nd	influence extended purging time (1h)	400	568	17	5	0	4	994
31	49.0	49.3	49.1	46%									

Table 11-5: Calculation of conversion factor from GC 3000 to GC Fusion for C_2H_4 quantity

	N2	**C_2H_4**
	%	**ppm**
GC 3000	7.20	1427
GC Fusion	7.15	4690
	Conversion factor	**3.29**

Table 11-6: Cycles of ethanol experiments over Al_2O_3 as inert material

cycle	Δm RED	Δm OX	Δm Air OX	Δm cycle	Relative OC conversion	Ethanol OP	CO_2	CO	CH_4	C_{tot}
	g	g	g	g				ppm_v (H_2 based)		
1	131.0	104.9		118.0	98%					
2	99.8	98.5		99.2	93%					
3	92.1	90.8		91.5	85%					
4	85.6	83.0		84.3	79%					
5	84.6	83.6		84.1	79%					
6	83.1	83.3		83.2	78%					
7	83.1	79.8		81.4	76%					
8	83.4	81.8		82.6	77%					
9	82.6	81.2		81.9	76%					
10	N/V	N/V								
11	N/V	N/V								
12	83.3	79.9		81.6	76%					
13	82.6	81.1		81.9	76%					
14	79.2	79.0		79.1	74%	1st Ethanol OP	10	9	1	20
15	80.1	79.1		79.6	74%					
16	78.9	77.7		78.3	73%					
17	80.6	79.0		79.8	74%					
18	77.9	69.5		73.7	69%					
19	77.6	76.9		77.3	72%					
20	76.9	75.6		76.3	71%	3rd Ethanol OP	32	93	1	126
21	67.8	73.0		70.4	66%					
22	75.5	91.7	16.10	83.6	78%					
23	92.4	77.8		85.1	79%					
24	77.4	78.9		78.1	73%	2nd Ethanol OP	56	24	0	80
25	77.4	72.5		74.9	70%					
26	75.1	73.3		74.2	69%					
27	73.5	67.6		70.6	66%					
28	68.9	81.1		75.0	70%					
29	76.1	76.1		76.1	71%					
30	78.1	74.3		76.2	71%					
31	75.7	74.8		75.3	70%	3rd Ethanol OP	115	150	0	271
32	74.7	72.3	14.70	73.5	69%					
33	81.3	73.4		77.4	72%		34	16	0	50
34	74.8	72.1		73.4	69%		30	38	0	68
35	72.7	70.4		71.6	67%	3rd Ethanol OP	69	225	0	294
36	71.6	70.5	13.90	71.0	66%		114	80	0	193
38	75.6	71.0	12.80	73.3	68%		16	11	0	28
39	83.8	69.9		76.8	72%		16	9	0	24

Table 11-7: Cycles of experiments with SiO_2 as inert material

cycle	Δm RED	Δm OX	Δm Air OX	Δm cycle	Relative OC conversion	OP	CO_2	CO	CH_4	C_{tot}
	g	g	g	g				ppm$_v$ (H_2 based)		
1	97.7	104		100.9	84%					
2	90.6	92.6		91.6	86%					
3	82.1	84.6		83.4	78%					
4	80.0	77.8		78.9	74%					
5	80.9	80.6		80.8	75%					
6	78.9	79.4		79.2	74%					
7	77.4	76.5		76.9	72%					
8	76.9	74.3		75.6	71%					
9	77.5	78.1		77.8	73%					
10	78.3	78.9		78.6	73%	1st Ethanol OP	29	224	13	265
11	78.6	78.7		78.7	73%		32	70	27	129
12	79.4	77.7		78.6	73%		42	392	16	450
13	77.1	78.8		77.9	73%	1st Ethanol OP	73	163	17	253
14	78.3	78.4		78.4	73%		9	171	9	229
15	77.2	72.4		74.8	70%					
16	77.7	77.0		77.4	72%	3rd Ethanol OP	58	129	14	200
17	77.0	75.8		76.4	71%		161	1005	21	1187
18	75.5	74.8	14.3	75.2	70%		73	110	20	203
19	100.1	83.7		91.9	86%	1st Ethanol OP no water	127	321	17	464
20	79.1	80.9		80.0	75%		56	114	10	180
21	76.2	75.1	17.2	75.7	71%		109	449	16	575
22	102.9	85.4		94.2	88%	1st Toluene OP	312	97	0	129.2
23	71.1	71.3		71.2	67%					
24	72.8	71.3	16.6	72.1	67%					
25	105.3	83.6		94.5	88%	2nd Toluene OP	256	42	3	70
26	71.9	68.7	16.7	70.3	66%		63	63	0	127